
**Laser excitation of 8-eV electronic
states in Th^+ : A first pillar
of the electronic bridge toward
excitation of the Th-229 nucleus**

Von der Fakultät für Mathematik und Physik der
Gottfried Wilhelm Leibniz Universität Hannover

zur Erlangung des Grades

Doktor der Naturwissenschaften
Dr. rer. nat.

genehmigte Dissertation

von

Óscar-Andrey Herrera-Sancho
geboren am 31. August 1979 in San José, Costa Rica

2012

Referent: PD Dr. Ekkehard Peik
Korreferent: Prof. Dr. Ernst Rasel
Tag der Promotion: 23.11.2012

Abstract

The possibility to realize a nuclear clock based on the optical magnetic dipole transition from the ground state to the low-energy isomeric state in the ^{229}Th nucleus has motivated experiments and proposals toward highly accurate clocks with trapped ions and highly stable optical frequency standards with Th-doped solids. These systems hold great promise to open a field of research in the borderland between atomic and nuclear physics, which will enable highly sensitive tests of postulates from fundamental physics and also will allow us to coherently excite and control nuclear states, opening a wonderful and intriguing new field in physics. A major experimental obstacle that has to be overcome before any precision spectroscopy can be performed with this system is however the insufficient knowledge on the exact transition energy. The best experimental result so far is an indirect determination from γ -spectroscopy with a relative uncertainty of about 6%. To facilitate the search for the nuclear transition within a wide uncertainty range around 8 eV, we investigate two-photon excitation in the dense electronic level structure of Th^+ , which enables the nuclear excitation via a resonantly enhanced inverse electronic bridge process.

Experiments on one- and two-photon laser excitation of buffer gas cooled $^{232}\text{Th}^+$ ions in a radio-frequency ion trap are reported in this thesis. The strongest resonance line at 402 nm from the $(6d^27s)J=3/2$ ground state to the $(6d7s7p)J=5/2$ state is driven as the first excitation step. Using nanosecond laser pulses in the 250-nm wavelength range for the second step of a two-photon excitation, we have observed seven previously unknown levels in the unexplored region of the electronic level structure around 8 eV. This investigation shows that the Th^+ ion seems to be well suited for the search of the isomer transition because both, theory and experimental results, agree on the density of strong transitions in the expected range of the nuclear resonance relevant for electronic bridge excitation.

We also investigate the interaction of the nanosecond pulsed Ti:sapphire laser with the ions ensemble and observe resonantly enhanced multi-photon ionization $\text{Th}^+ \rightarrow \text{Th}^{2+}$ and the photodissociation of molecular ions with Th^+ . The latter results in several hours of continuous laser interrogation of the Th^+ ion cloud and may therefore be very useful for future attempts on the search for direct optical detection of the isomeric state transition in the ^{229}Th nucleus, since to perform experiments with the radioactive isotope, a minimal amount of substance is required for trap loading.

keywords: Th-229, nuclear spectroscopy, ion trap, electronic bridge

Zusammenfassung

Der optische magnetische Dipol-Übergang vom Grundzustand des ^{229}Th Atomkerns zu einem nieder-energetischen isomeren Zustand verspricht die Möglichkeit zur Entwicklung von hochpräzisen Uhren auf Basis von gefangenen Ionen sowie von hochstabilen optischen Frequenzstandards auf Basis von Thorium-dotierten Kristallen. Diese Systeme versprechen die kohärente Anregung und Kontrolle von Kernzuständen und eröffnen ein hochinteressantes neues Forschungsgebiet im Grenzbereich von Atom- und Kernphysik. Zunächst gilt es allerdings ein großes Hindernis zu überwinden: Die Übergangsenergie des Thorium-Kerns ist nur mit unzureichender Genauigkeit bekannt. Das bisher beste experimentelle Ergebnis wurde mit Hilfe einer indirekten γ -Spektroskopie gewonnen und weist eine relative Unsicherheit von etwa 6% auf. Um eine erfolgversprechende Suche in dem großen sich ergebenden Unsicherheitsbereich um 8 eV zu ermöglichen, haben wir zwei-Photonen-Übergänge zu hochliegenden elektronischen Zuständen des Th^+ -Ions untersucht. Die Anregung eines geeigneten Zustands kann dann wiederum durch einen umgekehrten elektronischen Brückenprozess eine Anregung des Atomkerns bewirken.

In dieser Arbeit werden die Ergebnisse von Ein- und Zwei-Photonen-Anregung von Puffergas-gekühlten $^{232}\text{Th}^+$ -Ionen in einer Radiofrequenz-Ionenfalle präsentiert. Dabei wird im ersten Schritt der stärkste Übergang vom $(6d^27s)J=3/2$ Grundzustand in den $(6d7s7p)J=5/2$ Zustand angeregt. Der zweite Anregungsschritt erfolgt dann mit Hilfe von ns-Pulsen im Wellenlängenbereich um 250 nm. Wir konnten so sieben bisher unbekannte Energieniveaus im unerforschten Bereich um 8 eV beobachten. Diese belegen die theoretisch vorhergesagte hohe Dichte von starken elektronischen Übergängen und bestätigen damit die Eignung des Th^+ -Ions für eine Anregung des isomeren Kernzustands mit Hilfe eines elektronischen Brückenprozesses.

Weiterhin haben wir die Wechselwirkung des ns-gepulsten Titan-Saphir-Lasers mit dem Ensemble von Th^+ -Ionen untersucht und dabei sowohl resonant überhöhte Mehr-Photonen-Ionisation von Th^+ zu Th^{2+} als auch Photodissoziation von Molekular-Ionen beobachtet. Der letztgenannte Prozess verlängert die mögliche Beobachtungsdauer der Ionenwolke beträchtlich, auf einen Zeitraum von mehreren Stunden. Die ist für die Suche nach dem angeregten Kernzustand von großem Nutzen, da sich die benötigte Menge des radioaktiven Isotops ^{229}Th so minimieren lässt.

Schlagworte: Th-229, Kernspektroskopie, Ionenfallen, Photodissoziation, elektronische Brückenprozesse

Contents

1	Introduction	1
2	Concepts for laser excitation of the low-lying level in the ^{229}Th nucleus	3
2.1	The ground-state doublet of ^{229}Th	3
2.2	Search for the isomeric state transition in the ^{229}Th nucleus	8
2.3	Perspectives and applications of the isomeric $^{229\text{m}}\text{Th}$ nuclear state	14
3	Experimental apparatus	16
3.1	The linear Paul trap	16
3.2	Vacuum and buffer gas system	17
3.3	Production of Th^+ ions	19
3.4	Lasers used for spectroscopy of trapped $^{232}\text{Th}^+$ ions	20
3.5	Main resonance transitions studied and fluorescence detection	23
4	Single-wavelength laser excitation of $^{232}\text{Th}^+$ ions	26
4.1	Introduction	26
4.2	Ground state transitions: first excitation step	27
4.3	Excitation of the $0_{3/2}-24\,874_{5/2}$ transition at 402 nm	29
4.4	Effective 4-level model for collisional quenching and repumping	36
4.5	Quenching rates and population of the $24\,874_{5/2}$ level	40
5	Two-photon laser excitation of trapped $^{232}\text{Th}^+$ ions	46
5.1	Introduction	46
5.2	Two-photon laser excitation using ECDLs in continuous excitation	47
5.3	Two-photon laser excitation with nanosecond pulsed Ti:sapphire laser	52
5.4	Multi-photon ionization in trapped Th^+ ions	67
6	Formation and photodissociation of molecular ions with Th^+	72
6.1	Chemical reactions of trapped Th^+ ions	72
6.2	Photodissociation of molecular ions with Th^+	74
6.3	Secular frequency excitation of molecular ions	77
7	Conclusion and outlook	81

Bibliography

84

1 Introduction

Thorium was discovered at the beginning of the nineteenth century by the Swedish chemist Jöns Jakob Berzelius who named this chemical element in honor of the Nordic god of thunder: Thor. At the end of the same century and motivated by the announcement of the X-rays by the German physicist Wilhelm Röntgen, Henri Becquerel showed that uranium emitted “radiation” without an external source of energy and so, the term radioactivity was introduced by Marie Skłodowska-Curie who had also shown the radioactivity of thorium [1]. In those exciting years for physics the electron was also discovered, indicating that the atom has an internal structure [2]. Ten years passed by until the nuclear nature of the atom was demonstrated in the Rutherford scattering experiment [3, 4] and afterward atomic and nuclear physics have been continuously in a rapid development.

Excitation energies in the electron shell and in the nucleus are noticeably separated by several orders of magnitude. The former has typical excitation energy values in the order of a few electron volt, whereas the energy values of the latter are several kilo-electron volt or mega-electron volt. Therefore very different sources of excitation and detection are used nowadays for these two major fields of modern physics. Until now, a field of research in the borderland between atomic and nuclear physics has not been able to develop due to the above. A way to overcome this problem would be to find an unusual nucleus where the excitation energy of its low-lying nuclear state is in the order of magnitude of those in the electron shell.

In the mid-1970s the first indications of the existence of a low-lying nuclear state in ^{229}Th with an energy lower than 100 eV were obtained by Kroger and Reich [5] by means of spectroscopy of the γ -radiation emitted following the α -particle decay of ^{233}U . In the following thirty years, the upper bound on the energy of the first excited level was gradually reduced, until in 2007 the best experimental result so far was obtained: $E(^{229\text{m}}\text{Th}) = 7.8(5)$ eV via an indirect determination [6, 7]. This excitation energy corresponds to an excited state in the ^{229}Th nucleus connected with the ground state by a magnetic-dipole transition in the vacuum-ultraviolet at about 160 nm wavelength.

Since the nuclear $^{229\text{g}}\text{Th} \leftrightarrow ^{229\text{m}}\text{Th}$ transition frequency in ^{229}Th is accessible by frequency upconversion of narrow-bandwidth laser sources and since it can be less sensitive to external perturbations than transition frequencies of the electron shell, this transition was proposed as the basis of an optical nuclear clock of high precision [8]. Experiments toward an optical nuclear clock are now pursued worldwide with different approaches [9–12]. A major experimental obstacle that has

to be overcome before any precision spectroscopy can be performed is however the insufficient knowledge on the exact transition energy. Because of the wide present uncertainty range for the nuclear transition energy, further investigations are needed in order to establish a direct optical excitation and detection of the nuclear $^{229\text{g}}\text{Th} \leftrightarrow ^{229\text{m}}\text{Th}$ transition.

In order to achieve excitation of the ^{229}Th nucleus with the use of available laser sources by taking advantage of the dense electronic level structure of Th^+ , a two-photon inverse electronic bridge process in singly ionized ^{229}Th was proposed [13]. In an intuitive picture, the electronic bridge process uses the electron shell as a resonant antenna that enhances the coupling of the nucleus to the laser radiation. This method possesses the additional advantage of not requiring a VUV laser because the energy of 7.8 (5)eV [160(10) nm] is provided to the electron shell via a two-photon laser excitation.

This thesis is an effort toward direct observation of the unusually low-lying level in the ^{229}Th nucleus, which will enable highly sensitive tests of postulates from fundamental physics and will also allow us to coherently excite and control atomic nuclear states, opening a wonderful and intriguing new field in physics. As it will be shown in Chapter 4, laser excitation of the strongest resonance line of Th^+ at 402 nm from the $(6d^27s)J = 3/2$ ground state with the $(6d7s7p)J = 5/2$ state at $24\,874\text{ cm}^{-1}$ with trapped buffer cooled ions was accomplished. In order to increase the population in the excited state, collisional quenching of metastable states with different buffer gases and repumping with additional lasers was employed. The experimental results were compared with a rate equation model, in which we approximated the dense Th^+ level system up to the $24\,874\text{ cm}^{-1}$ level by a four-level system. A two-photon laser excitation through the latter intermediate state is described in Chapter 5. Since in continuous excitation only a small fraction of ions (less than 10^{-4}) can be transferred to the excited state via the intermediate state, we established and studied nanosecond pulsed optical excitation. Seven previously unknown levels in the unexplored region of the electronic level structure of the Th^+ ion above $60\,000\text{ cm}^{-1}$ (7.44 eV) have been observed. The characterization of the highly excited electronic states allowed us to study the resonantly enhanced multi-photon ionization $\text{Th}^+ \rightarrow \text{Th}^{2+}$ when the Ti:sapphire laser excited an upper state with high peak intensities. Photodissociation of thorium-containing molecular ions induced by the Ti:sapphire laser in the 250-nm wavelength range is described in Chapter 6. While otherwise the formation of molecular ions limited the storage time of the highly reactive Th^+ to several minutes, efficient photodissociation allowed us to observe that the 402-nm fluorescence signal decays only by $\approx 10\%$ in several hours of continuous interrogation of the Th^+ ensemble. The latter results in a tremendous advantage for the future attempts in direct optical excitation and detection of the $^{229\text{g}}\text{Th} \leftrightarrow ^{229\text{m}}\text{Th}$ transition in the ^{229}Th nucleus, since to perform experiments with the radioactive isotope, a minimal amount of substance is required for trap loading.

2 Concepts for laser excitation of the low-lying level in the ^{229}Th nucleus

2.1 The ground-state doublet of ^{229}Th

It has been inferred from γ -spectroscopy of ^{229}Th that this nucleus possesses an isomeric state at an energy of only a few eV above the ground state, establishing the lowest excitation energy that is known in nuclear physics. ^{229}Th is part of the decay chain of ^{233}U and undergoes α -decay with a half-life of approximately 7880 years. Since its discovery by Kroger and Reich in 1976 [5], the existence of the low-lying metastable nuclear state ($3/2^+$ [631] Nilsson state) has been well-established experimentally [14–17] and different groups have attempted to measure its energy [18, 19]. The most recent experimental value for the ^{229}Th isomer energy is 7.8(5) eV [6, 7], which is an order of magnitude lower than the next known low-energy level at 76.5 eV in ^{235}U [20].

Figure 2.1 summarizes the relevant spectroscopic information that is presently available. The representation of the nuclear levels is based on the nuclear shell model proposed by S. G. Nilsson which defines the shape of the nucleus in an elliptical deformed oscillator potential [21]. The set of quantum numbers known as Nilsson classification can be written as $\Omega^\pi[N, n_z, \Lambda]$, where Ω is the projection of the single-particle angular momentum (j) onto the symmetry axis, π is the parity, N is the principal quantum number of the major shell, n_z is the number of nodes in the wave function along the symmetry axis, and Λ is the projection of the orbital angular momentum.

The unusually low excitation energy in the ^{229}Th nucleus has stimulated a number of proposals for studies of the effects of atomic electrons on the nuclear transition (see Refs. [24, 25] and references therein). This can be expected to be especially pronounced here since the energy of the nuclear transition between the isomeric $^{229\text{m}}\text{Th}$ state and the ground $^{229\text{g}}\text{Th}$ state is in the same range as that of excited states of the outer-shell electrons.

However, the nuclear transition $^{229\text{g}}\text{Th} \leftrightarrow ^{229\text{m}}\text{Th}$ depicted in Figure 2.1 has never been directly observed. In the late 1990s, after the experimental result of 3.5 eV from γ -spectroscopy had been published, two incorrect observations of an optical

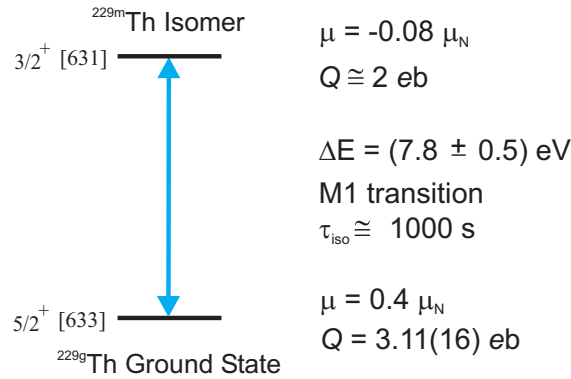


Figure 2.1: The lowest nuclear levels of ^{229}Th [7] with their nuclear spin and Nilsson state classifications [5, 21], radiative lifetime τ_{iso} for the magnetic dipole transition, the magnetic moments μ in nuclear magnetons [22], and the quadrupole moment Q of the ground state [9] and excited state [23].

signal from the decay of the isomer were reported by two groups [26, 27], but it was soon clarified by different researchers that the observed spontaneous ultraviolet luminescence was luminescence induced by the background of α -radiation [28, 29] in the air that surrounds the radioactive ^{233}U sample. It was until 2007 when a group at Lawrence Livermore National Laboratory reported the value that is presently accepted. They used a high resolution γ -spectrometer (x-ray microcalorimeter spectrometer with an experimental energy resolution of 26 eV FWHM) and resolved two decay cascades very precisely [6]. The main advantage in this case was the use of a detector with an energy resolution about ten times higher than in previous experiments.

Figure 2.2 shows the lower-lying nuclear level scheme of ^{229}Th used in Ref. [6]. In this case, the 71.82 keV state, populated in the α -decay of ^{233}U , decays with closely spaced γ -ray doublets to the ground state via interband and intraband transitions (with energies 29.39 keV and 42.43 keV, see green circles in Fig. 2.2) and to the isomeric state via intraband transitions (with energies 42.63 keV and 29.18 keV, see purple circles in Fig. 2.2). Therefore, by energy conservation one obtains the relation: $71.82 \text{ keV} = 42.63 \text{ keV} + 29.18 \text{ keV} + E(^{229\text{m}}\text{Th}) = 29.39 \text{ keV} + 42.43 \text{ keV}$, where $E(^{229\text{m}}\text{Th})$ is the energy of the low-lying metastable state in the ^{229}Th nucleus. As it can be seen, the energy differences of the doublets are about 200 eV, which is out of the experimental resolution in previous experiments (see Ref. [16]).

In these experiments were not resolved the interband M1 transition of the 29.19 keV state to the ground state (see black dashed line in Fig. 2.2) and the interband E2 transition of the 42.43 keV state to the $^{229\text{m}}\text{Th}$ state (see red dashed line in Fig. 2.2). Due to a possible perturbation of the lineshapes by these unresolved transitions, a correction to the measured value had to be taken into account. The contribution

of the unobserved transition of the 29.19 keV state to the ground state can be estimated from the interband branching ratio of the 71.82 keV state to the 42.43 keV state, and the scaling of E_γ^3 for the M1 γ -ray transition rates. The use of the branching ratio of 1/13 yields a correction of +0.6 eV [6]. The other correction was estimated in Ref [7] with the use of the rotational model parameters, which describe the electromagnetic transition strengths of intraband and interband γ -ray decays. Using this model they estimated a correction of +0.2 eV.

Therefore the value nowadays accepted for the isomeric state is:

$$E(^{229\text{m}}\text{Th}) = [7.0(5) + 0.6 + 0.2] \text{ eV} = 7.8(5) \text{ eV} , \quad (2.1)$$

corresponding to an excited state in the ^{229}Th nucleus connected with the ground state by a magnetic-dipole transition in the vacuum-ultraviolet at about 160 nm wavelength. Radiation at this wavelength is not transmitted through air. This explains why all prior experimental attempts for a direct observation had not been successful. Because this value is the result of an indirect measurement, further investigations are needed in order to establish a direct optical detection of the nuclear $^{229\text{g}}\text{Th} \leftrightarrow ^{229\text{m}}\text{Th}$ transition.

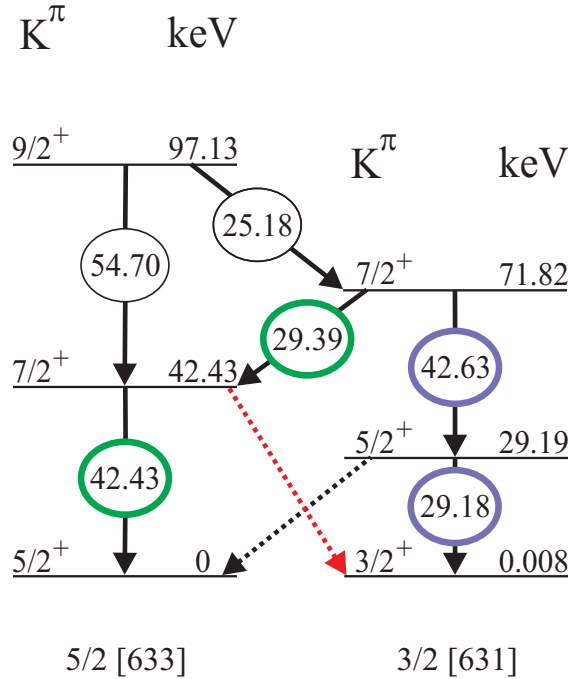


Figure 2.2: Partial level scheme of the ^{229}Th nucleus showing the doublets (green and blue) after the γ -decay of the 71.82 keV state investigated in Ref. [6]. The rotational bands (K^π) are labeled by the Nilsson asymptotic quantum numbers.

The estimates for the radiative lifetime of the isomeric state $^{229\text{m}}\text{Th}$ vary between a few minutes and several days; see Refs. [16, 30]. Ref. [19] reports the reduced probability $B(M1)=0.025 \mu_N^2$ by means of quasiparticle-plus-phonon model calculations, which connect the $^{229\text{m}}\text{Th}$ isomer state and the $^{229\text{g}}\text{Th}$ ground state. From the relation $T_{1/2} = 10.95/[E_\gamma^3 B(M1)]$, the estimated lifetime expressed in hours of the $^{229\text{g}}\text{Th} \leftrightarrow ^{229\text{m}}\text{Th}$ transition can be obtained. If we assume that $E_\gamma = 7.8(5)$ eV then the lifetime will be 3300_{-550}^{+750} s. In addition, the lifetime depends on the availability of other decay channels that can shorten the lifetime significantly [31, 32].

In 2003, the pioneering work of Peik and Tamm proposed an application of this transition for the unusually low-lying level of the ^{229}Th nucleus. They suggested using this transition as the basis of an optical nuclear clock of high precision since it is accessible by frequency upconversion of narrow-bandwidth laser sources [8]. Also, this nuclear transition can be less sensitive to external perturbations than transition frequencies of the electron shell because the characteristic nuclear dimensions are small compared to the atomic dimension. However, as described above, the most accurate value of the nuclear transition wavelength is about 160(10) nm. Due to its large uncertainty, further investigations are therefore needed in order to enable a direct optical observation of the isomeric state of ^{229}Th by means of optical spectroscopy, and to gradually increase the spectroscopic resolution to the suitable level for an optical nuclear clock.

Experiments toward an optical nuclear clock are now pursued worldwide with different approaches. Originally, the triply charged ^{229}Th ion was proposed as a well suited candidate due to its simple level scheme characterized by a single valence electron [8]. In fact, it has a three-level Λ system, allowing fluorescence detection and laser cooling. Indeed in 2010, the group at Georgia Tech demonstrated experimentally laser cooling in triply ionized thorium, this being the first time that a multiply charged ion was laser cooled [33]. Previously, the lifetime of the excited states was estimated in Ref. [34]. Recently in 2011, the same experimental group made a tremendous advance toward optical excitation of the unusually low-lying isomer in the ^{229}Th nucleus. To clearly resolve all optical transitions, this group demonstrated sympathetic cooling of $^{229}\text{Th}^{3+}$ by $^{232}\text{Th}^{3+}$. They deduced the nuclear quadrupole moment Q by measuring the optical transition frequencies between the hyperfine levels in the four-lowest states in $^{229}\text{Th}^{3+}$. They found the value of $Q=3.11(16)$ eb¹ which can be compared with results previously obtained by means of electromagnetic excitation of an electrodeless discharge tube ($Q=4.6$ eb) [35], Fourier spectroscopy ($Q=4.3(9)$ eb) [36], and Coulomb excitation of states in ^{229}Th using 17.0-MeV $^4\text{He}^{2+}$ ions ($Q=3.149(32)$ eb) [37].

Furthermore, in the original proposal in 2003, the excitation of the nuclear transition $^{229\text{g}}\text{Th} \leftrightarrow ^{229\text{m}}\text{Th}$ was also proposed to be performed in a doped transparent

¹the barn, 1 b = 10^{-28} m²

crystal at the nuclear resonance wavelength [8]. This approach has the advantage of addressing densities as high as 10^{14} ^{229}Th nuclei/cm³.

This scheme will require none of the complex experimental techniques for ion trapping, and would allow a broadband search with a synchrotron or free-electron laser source. Another difficulty is the requirement of growing the ^{229}Th -doped crystal, which is a complex task, while working with a radioactive isotope. Nevertheless, this technique seems to be promising for an initial localization of the frequency of the isomer transition. Experiments toward a direct observation of the nuclear transition by interrogating ^{229}Th , using this approach, are being investigated in three different groups worldwide (see Refs. [10–12]).

In addition, a collaboration between the University of Mainz (Germany) and Jyväskylä (Finland) is aiming at the identification of the low-lying 7.8 eV isomer by measuring the nuclear ground state ^{229g}Th hyperfine structure and the isomer state ^{229m}Th hyperfine structure with recoil ions from a ^{233}U source. It is assumed that the recoil ions contain an isomer fraction of about 2%. Recently, the first group reported resonance ionization spectroscopy (RIS) inside a gas cell for the identification of a suitable three-step resonance ionization scheme for neutral thorium [38] and also reported, for the first time, the ground-state hyperfine structure of neutral ^{229}Th by means of RIS [39]. Almost in parallel, the group at Jyväskylä reported on the extraction of a low-energy beam of $^{229}\text{Th}^+$ with a production efficiency of 1.6% by using an α -decay recoil source of ^{233}U mounted in a gas cell [40]. This efficiency translates into a usable $^{229}\text{Th}^+$ ion yield of $\approx 2400\text{ s}^{-1}$ and to increase the $^{229}\text{Th}^+$ ion yield from the recoil nuclei, this group aims to use RIS by accessing the remaining neutral ^{229}Th fraction. In principle, this joint group will attempt collinear laser experiments on both the ground state ^{229g}Th and the isomeric state ^{229m}Th of singly charged ^{229}Th .

An experimental realization of the former approaches has the additional difficulty that the ^{229}Th isotope is not available in a metallic form. This isotope is radioactive with a half-life of 7880 years. The ^{229}Th isotope is part of the Neptunium series [41], which arises as a result of the α -decay of ^{233}U , and can only be extracted from ^{233}U in the form of a thorium compound, e.g. $^{229}\text{Th}(\text{NO}_3)_4$. All thorium isotopes decay via either α or β radiation. With a half-life of more than 1.4×10^{10} years (considered relatively stable), only the naturally occurring ^{232}Th isotope can be found in a metallic form. Therefore, this isotope is widely used in test experiments because of its easy handling and lower price. In the ion trapping experiments, see below, this isotope is also used in all preparatory experiments before using the radioactive isotope.

2.2 Search for the isomeric state transition in the ^{229}Th nucleus

2.2.1 Choosing a proper atomic charge state

In principle, any charge state should exhibit the nuclear $^{229\text{g}}\text{Th} \leftrightarrow ^{229\text{m}}\text{Th}$ transition, including neutral Th, Th^+ , Th^{2+} and Th^{3+} . In the following, we will summarize the most important features of each charge state for a proper selection of the most suitable candidate for the search of the isomeric state transition in the ^{229}Th nucleus. The singly ionized thorium will be presented separately in the next subsection since we conducted all the investigations described in this thesis with this ion.

Firstly, let us consider the case of neutral thorium, which has an ionization energy (IE) of 6.08 eV, that is significantly lower than the nuclear transition energy of 7.8(5) eV. Hence, the isomeric state $^{229\text{m}}\text{Th}$ can decay into the ground state $^{229\text{g}}\text{Th}$ as a result of internal conversion. Internal conversion is the release of the nuclear excitation energy by ejection of an electron from the electron shell. This effect is a second-order process in respect of the electromagnetic interaction (see for example Ref. [24] for further details). The release of an electron from the electron shell would cause the change of the charge state in neutral thorium resulting in a complete change in the electronic structure. This is not a desired situation for spectroscopy of the nuclear $^{229\text{g}}\text{Th} \leftrightarrow ^{229\text{m}}\text{Th}$ transition.

In the case of doubly ionized Th, and of all higher charged ions, the IE exceeds the isomeric nuclear energy. Therefore the decay via internal conversion is not possible in the mentioned ions. The electronic energy level structure of Th^{2+} has been extensively studied using spark discharges at high currents, and the spectral lines have been measured with a spectrograph from 50 nm to 1070 nm (see Refs. [42, 43]). It is worth noting that this electronic structure has a gap of configurations between 6.9 eV and 8.6 eV. As will be explained below, electronic states around the actual nuclear energy range will increase the excitation rate to the isomeric state and, if a suitable electronic transition frequency happens to be very close to the nuclear transition, a larger excitation rate can be expected due to an inverse electronic bridge process [44]. Therefore, the Th^{2+} ion is not well suited for investigations through such an electronic bridge process, which can resonantly enhance the excitation of the ^{229}Th nuclear resonance.

Finally, in the case of triply ionized Th, its level scheme is characterized by a single valence electron and also energy levels up to the $165\,059\text{ cm}^{-1}$ state can be found in the Refs. [45, 46]. As was mentioned before, this ion has a three-level Λ system, allowing fluorescence detection and laser cooling [33]. The three lowest electronic transitions in Th^{3+} can be easily driven with semiconductor diode lasers. A disadvantage of the electronic energy level structure in Th^{3+} for the

search of the isomeric state transition is that its spectrum is not too dense so that a strong enhancement from an electronic bridge process is unlikely. Actually, this was pointed out by an investigation of Porsev and Flambaum in Ref. [44]. For the realization of high-precision nuclear clock, however, Th^{3+} is the most promising charge state.

When the valence electron is entirely considered in the metastable state $7s\ ^2\text{S}_{1/2}$ of the Th^{3+} ion, the electronic bridge process probability is approximately 10^3 times larger than when the valence electron is in the ground state ($5f\ ^2\text{F}_{5/2}$) [44]. Therefore the search strategy for the nuclear transition may be as follows: The $7s$ state must be populated via optical pumping of the electric-quadrupole $6d\ ^2\text{D}_{3/2} - 7s\ ^2\text{S}_{1/2}$ transition at 717.5 nm. The radiative decay of this state is electric-dipole forbidden and its lifetime can be estimated to be of the order of 1 s. Then, the $7s\ ^2\text{S}_{1/2} - 7p\ ^2\text{P}_{1/2}$ transition should be excited with radiation at 269.5 nm providing a total energy of ≈ 7.5 eV to the ensemble of trapped $^{229}\text{Th}^{3+}$ ions. The latter implies that the searching for the isomeric transition in Th^{3+} will be through an inverse two-photon electronic bridge process from the $7p\ ^2\text{P}_{1/2}$ state to states ranging from 215 nm to 780 nm (i.e. from the $7p\ ^2\text{P}_{3/2}$ state to the $8s\ ^2\text{S}_{1/2}$ state). However, it is possible to generate such laser wavelengths from available laser sources; the low probability of this process in Th^{3+} makes the searching of the nuclear isomeric state with higher precision rather complicated at this stage.

2.2.2 The electronic energy level structure in Th^+

The electronic energy level system of Th^+ is very complex (see Fig. 2.3) and is well known only up to an excitation energy of about 7.3 eV. The 32 odd-parity energy levels above 7.3 eV, mentioned as unpublished in Ref [47], were not included in Fig. 2.3 because the values have not been published elsewhere. The classified energy levels in Th^+ belong to the lowest 15 configurations of the three valence electrons. More than 400 energy levels have been identified [48] and the wavelengths of about 14 000 lines have been tabulated [49]. In addition to the lack of information on energy levels above 7.3 eV in Th^+ , there is also an absence of information on radiative lifetimes and branching ratios of higher-lying states. Until now, only twenty-three radiative lifetimes of levels and partial branching ratios are reported between the energy range of $18\,214\text{ cm}^{-1}$ (2.3 eV) and $32\,957\text{ cm}^{-1}$ (4.1 eV) (see Ref. [50]).

Recent relativistic Hartree-Fock calculations indicate an exponential increase of the energy level density toward the IE in Th^+ of 11.9 eV [51]. In this study, it was predicted that approximately 40 even-parity states with total angular momentum $J=3/2$ are in the present uncertainty range of the nuclear transition energy. This result is very promising since the higher the density of states, the higher may be the probability of resonance situation with the isomeric state of the ^{229}Th nucleus [44].

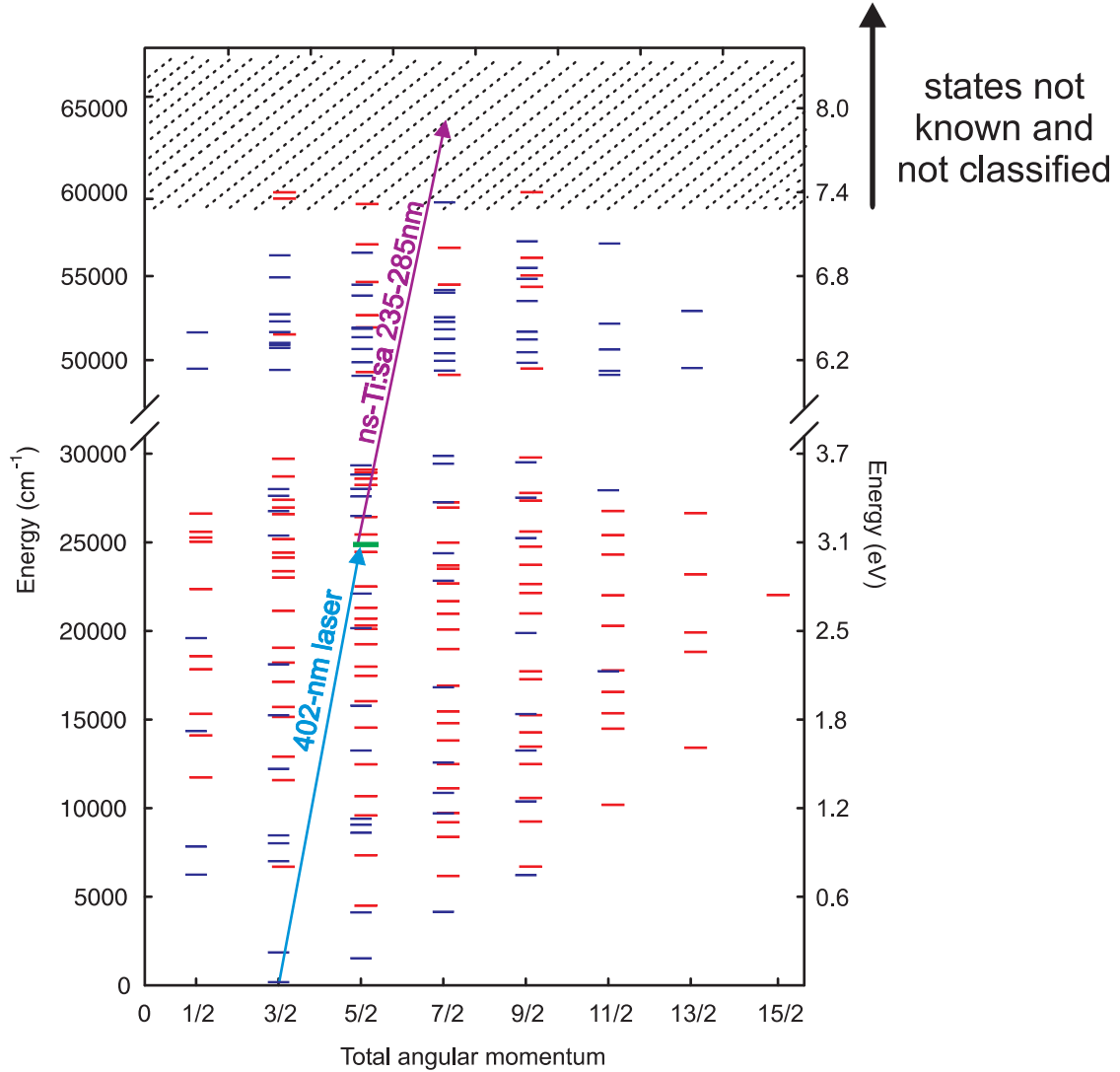


Figure 2.3: Electronic energy level structure (classified levels, Ref. [48]) of Th^+ showing two-photon excitation through the intermediate state at 24874 cm^{-1} to accomplish laser excitation of unknown higher-lying states around 8 eV . The intermediate state at 24874 cm^{-1} is highlighted with green color. *Odd (even)* parity is represented by red (blue) color. The hatched area corresponds to the present 1σ uncertainty range for the nuclear transition energy in ^{229}Th . The *odd* levels are slightly shifted horizontally for visual purpose.

In order to achieve excitation of the ^{229}Th nucleus with the use of available laser sources by taking the advantage of the dense electronic level structure of Th^+ , a two-photon inverse electronic bridge process in singly ionized ^{229}Th was proposed [13]. The electronic bridge process uses the electron shell as a resonant antenna that enhances the coupling of the nuclear transition to the laser radiation. This method possesses the additional advantage of not requiring a VUV laser because the energy of 7.8 (5)eV [160(10) nm] is provided to the electron shell via a two-photon laser excitation. The latter prevents the experimental effort that tunable VUV laser radiation has to be generated and transmitted in a vacuum apparatus (or oxygen-free atmosphere) since photons with a wavelength shorter than 180 nm are absorbed by oxygen. Figure 2.3 shows the dense electronic energy level structure in Th^+ , along with the two laser photons to accomplish laser excitation of unknown higher-lying states around 8 eV (see Chapter 5).

2.2.3 Two-photon inverse electronic bridge process in singly ionized ^{229}Th

Radiative transitions in nuclei are generally impeded by the small size of the nucleus in comparison to the wavelength of the radiation, especially for higher multipole orders. The term “electronic bridge”, where the atomic shell is used as a mediator for the depopulation of the isomeric state in a nucleus, was introduced as the enhancement of γ -decay rates through the excitation of shell electrons to higher-lying bound states [52]. This effect is a third-order process in respect of the electromagnetic interaction. The inverse process, i.e. inverse electronic bridge, is also known as nuclear excitation by electron transition (NEET) and transfer of energy by electrons from nuclei (TEEN). Morita [53] introduced this term as a mechanism where the nuclear ground state is excited to the higher energy level by receiving the excess energy of the electronic state by means of electromagnetic interactions between nucleus and electrons.

The apparent experimental realization was carried out in 1985 when the excitation of the isomeric state of ^{93}Nb at 30.7 keV was reported [54]. Furthermore the nuclear transition in ^{197}Au at 80.9 keV was also demonstrated [55] via monochromatic x-rays of synchrotron radiation. In the above experiments, the main decay channel of the isomer transition is internal conversion and the probability of a de-excitation of the nucleus via an electronic bridge process is very small ($\approx 10^{-6}$ [30]). However, the observation of the electronic bridge process in a “pure” form (e.g. by means of laser excitation), and not against the background of the internal conversion signal, is at this point pending.

In order to search for the excitation of the isomeric $^{229g}\text{Th} \leftrightarrow ^{229m}\text{Th}$ transition via an inverse electronic bridge process in Th^+ , we proposed to excite the electron shell by two laser photons whose sum frequency corresponds to the nuclear tran-

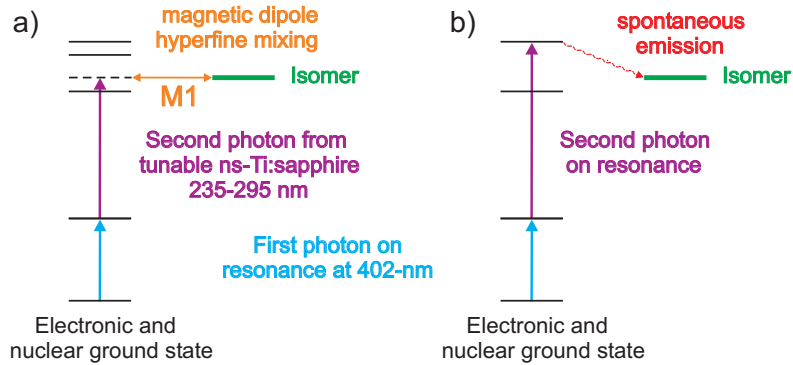


Figure 2.4: Schematic of the electronic energy levels with nuclear ground state (black line) and isomeric state (green line). (a) The second photon excites a virtual state (dashed line) which is resonant with the isomeric state via an inverse electronic bridge process. (b) The second photon can also be in resonance with a real higher-lying state, which releases its energy via spontaneous emission and thus, providing enough energy to excite the isomer transition.

sition frequency. In the case of pronounced coupling between the electron shell and the nucleus, hyperfine-induced mixing of the isomeric state and the electronic energy levels allows electric-dipole transitions between them [see Fig. 2.4(a)]. In our experiment, we use for the first excitation step a continuous laser tuned to the strongest tabulated line of the Th^+ emission spectrum at 402 nm, which connects the $(6d^27s)J=3/2$ ground state with the $(6d7s7p)J=5/2$ state at $24\,874\text{ cm}^{-1}$. For the second excitation step, we use nanosecond laser pulses in the 250-nm wavelength range for a two-photon excitation of unknown high-lying states of Th^+ around 8 eV (see Fig. 2.3 and Fig. 2.4).

The latter process was analyzed quantitatively by Porsev *et al.* [13] (along with previously calculated high-lying even-parity states [56]) who found that a $^{229}\text{Th}^+$ ion can be excited to the isomeric state with a probability in the range of at least $W_{\text{EB}}^{\text{in}} \approx 10\text{ s}^{-1}$. This calculation was carried out by using a combination of configuration-interaction and many-body perturbation theory and obviously depends on many parameters. The mentioned $W_{\text{EB}}^{\text{in}}$ value was obtained assuming a laser source for the second excitation step with a pulse energy of 10 mJ, a spectral width of $\Delta\omega = 2\pi \times 3\text{ GHz}$, a repetition rate of 30 Hz, and a laser beam spot of dimensions $0.1 \times 0.1\text{ mm}^2$. It was also assumed that a 100% population of the state at $24\,874\text{ cm}^{-1}$ can be achieved. If the total excitation energy provided from the two laser photons is very close to the isomeric $^{229\text{g}}\text{Th} \leftrightarrow ^{229\text{m}}\text{Th}$ transition, a significantly enhancement in $W_{\text{EB}}^{\text{in}}$ can be expected. Therefore, for the search of the isomeric transition in the ^{229}Th nucleus, the Th^+ ion is the most promising

candidate since it has the highest density of states in the expected range of the nuclear transition.

While the high density of electronic energy levels in Th^+ increases the probability for a strong resonance enhancement of electronic bridge processes leading to excitation of the ^{229}Th nucleus, it also possesses an experimental problem: Laser excitation of an ensemble of atoms from the ground state to a definite excited state is often inefficient for a multilevel system such as Th^+ , because spontaneous decay leads to the accumulation of population in metastable levels that are decoupled from the laser. If the number of metastable levels is not too high, additional repumper lasers may be applied for reexcitation from each of those states. Otherwise, atoms in metastable states can be returned to the ground state by inelastic quenching collisions with a buffer gas. The latter approach has already been utilized for laser spectroscopy of Th^+ ions: In order to determine the nuclear charge radii of the isotopes ^{227}Th to ^{230}Th and ^{232}Th , isotope shifts and hyperfine splittings have been recorded in one- and two-photon laser excitation to levels at $17\,122\text{ cm}^{-1}$ and $34\,544\text{ cm}^{-1}$ using Th^+ ions in a radio-frequency trap in the presence of helium and hydrogen buffer gases [57, 58].

2.2.4 Detection of the nuclear transition

In our approach laser excitation of the isomeric $^{229g}\text{Th} \leftrightarrow ^{229m}\text{Th}$ transition could be detected in three possible scenarios. The first detection-scenario is assuming a long-lived radiative lifetime of the isomer. In this case, one could monitor the laser-induced fluorescence signal resulting from excitation of the $(6d^27s) \leftrightarrow (6d7s7p)$ transition by making use of the differences between the hyperfine structure characteristics of electronic transitions in $^{229g}\text{Th}^+$ and $^{229m}\text{Th}^+$ [8]. Therefore, returning to Fig 2.4, if the second photon happens to be in resonance with the isomeric state in the ^{229}Th nucleus, the nuclear moments and nuclear spin will change. The latter will cause a change of the hyperfine splittings of the energy levels in the electronic shell, e.g. the $(6d^27s) \leftrightarrow (6d7s7p)$ transition, will thus be out of resonance and the laser-induced fluorescence intensity might change. This method is similar to the electron shelving scheme for detection of metastable states in the electronic energy levels of a single trapped ion [59, 60] and is also used in high-resolution laser spectroscopy of trapped ions [61].

The second detection-scenario, applicable for shorter radiative lifetime of the isomer, is the γ -ray emission of the excited ^{229}Th nucleus in the optical range called the “nuclear light” [25]. As described above, the ^{229}Th nucleus possesses an excited state at an energy of only 7.8(5) eV, connected with the ground state by a magnetic-dipole transition in the vacuum-ultraviolet at about 160(10) nm wavelength. Therefore the spontaneous emission of “nuclear light” from the isomeric state to the ground state can be detected with the use of a photomultiplier with

a suitable spectral sensitivity range. The latter must be mounted in an evacuated housing (or oxygen-free atmosphere) to avoid the absorption of photons by oxygen.

The third detection-scenario, and probably the most relevant for experiments with Th^+ , is the decay of the excited ^{229}Th nucleus via an electronic bridge process. In this case, the coupling between the electronic shell and the nucleus is assumed to be pronounced enough, allowing excitation of the nucleus through an inverse electronic bridge process and de-excitation of the nucleus by the inverse mechanism. In this case, the expected laser-induced fluorescence signal from the excited ^{229}Th nucleus would be the spontaneous emission of a characteristic photon cascade in the electron shell. Using either the second or third detection-scenario by means of a comparison of the fluorescence signals observed with $^{229}\text{Th}^+$ and $^{229\text{m}}\text{Th}^+$ with $^{232}\text{Th}^+$ the population of the isomeric nuclear level in $^{229}\text{Th}^+$ will be indicated.

2.3 Perspectives and applications of the isomeric $^{229\text{m}}\text{Th}$ nuclear state

Once the energy value of the $^{229\text{g}}\text{Th} \leftrightarrow ^{229\text{m}}\text{Th}$ transition is measured with higher accuracy, either in our system with Th^+ [62] or using one of the other approaches [9–12, 40], several perspectives and applications can be addressed. It is worth noting that the ability to manipulate a nuclear system at will with laser radiation offers innumerable intriguing possibilities. In the following, we will summarize the most relevant proposals with this nuclear transition and emphasize the possible realization of a high-accuracy frequency standard, since through the years the physical quantity frequency has always had a special status in physics.

Since the beginning of the year 2000 there were several pioneering proposals: Tkalya *et al.* suggested to investigate the dependence of the isomeric level half-life on different chemical surroundings [31, 32]. In 2003, Peik and Tamm proposed to use this nuclear transition as a way toward the next generation of optical clocks: “nuclear clock” [8]. Related to the previous, Flambaum *et al.* predicted that monitoring the frequency ratio of an atomic clock transition (e.g. Al^+) and the nuclear clock transition in the ^{229}Th nucleus, might establish the most sensitive test for a hypothetical temporal variation of the fundamental constants [63–65]. Recently in 2011, Tkalya suggested a nuclear γ -ray laser, i.e. population inversion where there are more excited than unexcited nuclei, by means of an ensemble of the $^{229\text{m}}\text{Th}$ isomeric nuclei in a host dielectric crystal [66]. Additionally, the interrogation of the isomeric $^{229\text{m}}\text{Th}$ nuclear state may be used as a qubit with extraordinary features in quantum computing.

The possible realization of a nuclear clock with high accuracy will open a new frontier in high-accuracy frequency metrology. For this purpose, a single trapped $^{229}\text{Th}^{3+}$ ion is expected to be an ideal system to take advantage of the unusually

low-lying level in the ^{229}Th nucleus. The advantage of the nuclear clock can be expected to be especially pronounced here since, compared to an atomic system, a nucleus may be exceptionally stable against external perturbations (because the characteristic nuclear dimensions are much smaller than the atomic dimension), and also because the nucleus is shielded by the atomic electrons. In the original proposal, the isomeric ^{229m}Th transition may be interrogated via the $^2S_{1/2}$ electronic state within both the ground state and the isomeric state. The latter in order to avoid the influence of the linear Zeeman effect, quadratic Stark effect and quadrupole shift [8]. Recently, using a clock transition composed of stretched states within the $5F_{5/2}$ electronic ground state of both nuclear ground state and the isomeric state was proposed [23]. This provides a large suppression of all external field clock shifts and simultaneously avoids the problem of having to use a metastable electronic state. The authors estimated that the performance of such a clock can achieve a level of 1×10^{-19} of fractional inaccuracy.

Definitely, to coherently excite and accurately measure the isomeric transition in a single trapped $^{229}\text{Th}^{3+}$ ion with optical radiation, several challenges will have to be addressed. First of all, the isomer $^{229g}\text{Th} \leftrightarrow ^{229m}\text{Th}$ transition energy must be determined with higher precision. Then, an ultrastable interrogation VUV laser will be used for the utilization of this nuclear transition, see e.g. Ref. [67]. When these experimental difficulties are overcome, we will be able to coherently control atomic nuclear states, opening a wonderful and intriguing new field in physics.

3 Experimental apparatus

This Chapter describes a summary of the experimental techniques and the experimental apparatus used throughout the thesis. At first, the linear Paul trap, the vacuum setup, and the buffer gas system are described. Afterward, the laser setup used for production of ions and laser spectroscopy of $^{232}\text{Th}^+$ ions are presented. Finally, we present the main resonance transitions studied in this thesis and the spectral sensitivity ranges for the different schemes of fluorescence detection.

3.1 The linear Paul trap

All the experiments conducted in this thesis employ a linear radio-frequency (rf) Paul trap of 160 mm in total length (see Fig. 3.1 (a)). The central section for storage of the ions is 20 mm long. The trap electrodes were machined from a CuBe alloy and were divided along their length into three sections which were held at different dc potentials. The ratio between the electrode radius (r_e) and the trapping area (r_o) was chosen to be $r_e/r_o \approx 1.143$, in agreement to the optimum rod size of $r_e/r_o \approx 1.147$ for a quadratic rf potential in the x - y plane [68]. For ion loading, a 1 mm metallic ^{232}Th sample¹ was placed between two electrodes near the end of the loading section (see Fig. 3.1 (b)). Figure 3.2 shows a photograph of the linear Paul trap.

Typically, a rf trap drive voltage in the range of 0.5-1 kV amplitude at a frequency of 2 MHz was used, produced by a function generator², power amplifier³ and a resonant transformer, corresponding to a Mathieu q parameter in the range of 0.2-0.4 (for a review see Ref. [69]). For these rf trap drive voltage range, the transverse secular frequency corresponds to 155–280 kHz and the pseudopotential depths to 15–44 eV. Unless otherwise indicated, the q parameter used throughout all experimental investigations was ≈ 0.35 . The end sections were kept at a dc potential of +40 V relative to the central section for axial confinement. The trap was mounted in the subsequently described vacuum system and pumped down to a pressure around 10^{-8} Pa.

¹Goodfellow, purity 99.5 % ^{232}Th

²Agilent, 33210A

³Telemeter Electronic, RF1100-20 amplifier

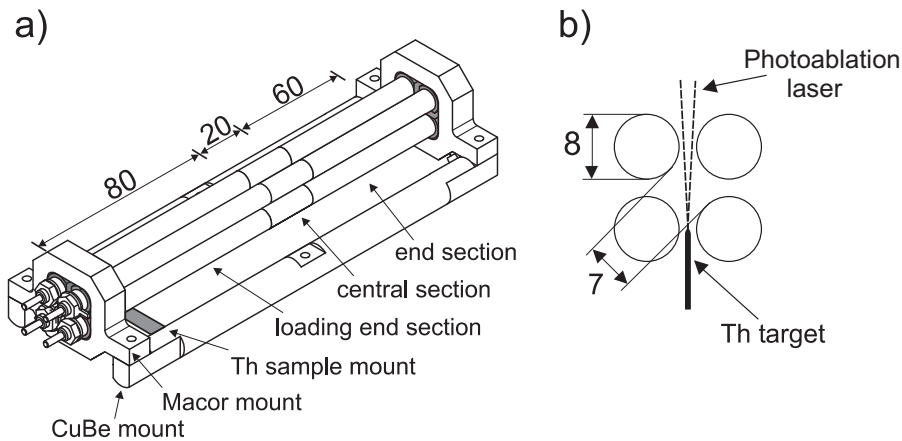


Figure 3.1: (a) drawing of the linear Paul trap used in the experiments. (b) cross section of the trap electrode arrangement and the position of the Th sample used for ion loading by photoablation with a nitrogen or Nd:YAG laser. Dimensions are in millimeters.

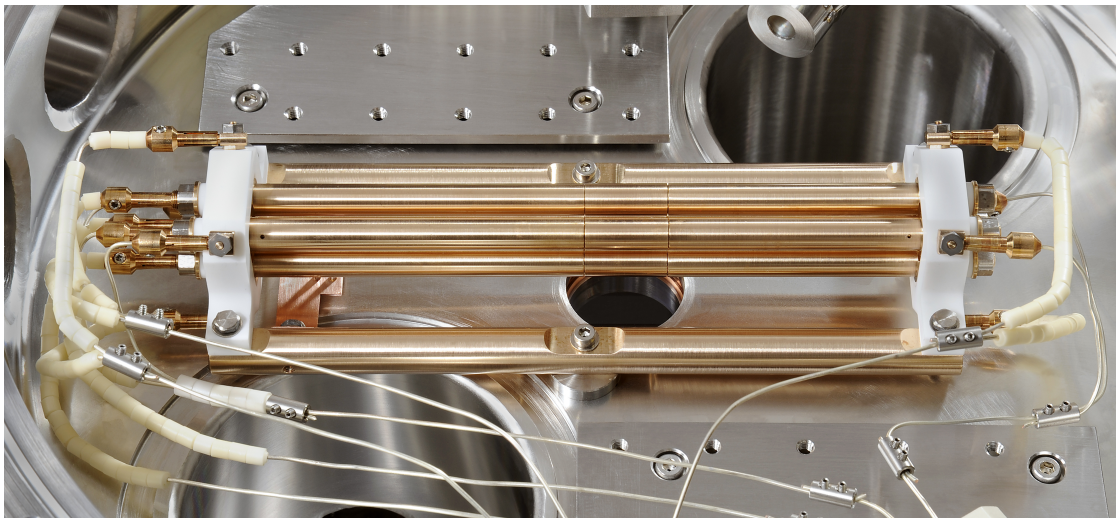


Figure 3.2: Photograph of the linear Paul trap showing the connections for rf drive voltage and the dc offset voltage applied to the segments.

3.2 Vacuum and buffer gas system

The vacuum chamber has an inner diameter of 325 mm with a height of 45 mm. The chamber⁴ is made from stainless steel with a very low permeability (residual permeability $\mu_r \leq 1.004$) to avoid magnetic field influences on the trap. This system was equipped with the following parts: two CF35 flanges along the trap axis were

⁴custom-made product, purchased from Reuter Technologies

installed with quartz Brewster angle viewports⁵ to pass linear polarized radiation. Three electrical CF35 feedthroughs provided the rf trap drive voltage, the dc offset voltage for segments of the linear Paul trap and for the Macor (glass-ceramics) shields. These shields (made of copper) were used to prevent charging of the ceramic due to the electron production by laser ablation (see below). Two additional CF35 flanges were equipped with a cold-cathode pressure gauge⁶ (used to monitor the buffer gas pressure) and a hot-cathode pressure gauge⁷ (used to monitor the residual gas pressure). Two CF35 flanges with CaF₂ windows⁸ are facing each other on the top and the bottom of the chamber for detection of fluorescence from the trapped Th⁺ ions. An additional fused silica window on the top of the chamber was used for the photoablation laser beam.

The previously described system was evacuated with a rotary-vane roughing pump⁹ (ultimate total pressure $\approx 10^{-1}$ Pa), a turbomolecular vacuum pump¹⁰ (base pressure: less than 10^{-8} Pa) and a non-evaporable getter¹¹ (NEG) pump. This system allows residual gas pressures lower than 10^{-8} Pa. After assembly, the chamber (together with the linear Paul trap) was heated to approximately 180 °C for a period of a few weeks while the partial pressure of water vapor in the chamber was monitored by a residual gas analyzer¹² (RGA). After baking, the base pressure was reduced below 10^{-8} Pa.

At high temperatures (10^4 K) the Th⁺ ions have a large Doppler width which leads to inefficient laser excitation resulting in a very small amount of fluorescence emission. In order to reduce the initial kinetic energy of the ions (created via a photoablation laser) and thus increase the fluorescence signal, we used buffer gas cooling. The buffer gas cooling also serves as a quenching mechanism as is pointed out in Section 4.3. The buffer gas system was built to provide a clean supply and a constant flux of the buffer gas into the chamber. This system was combined with the vacuum chamber as follows: Firstly, the buffer gas (declared purity: higher than 99.9999 %) was passed through a gas purifier¹³ (with a $0.003 \mu\text{m}$ grid-filter) and is stored in a 30 L reservoir with a pressure of about 2000 Pa. This buffer gas system was connected to the main chamber through a CF35 precision leak valve¹⁴. Independently of the main system, the buffer gas system was capable to pump down to a pressure below 10^{-6} Pa. The purity of the buffer gas inside of

⁵Bomco, B1254S

⁶Varian, Inverted Magnetron Gauge

⁷Varian, UHV-24p Nude Bayard-Alpert

⁸custom-made product, purchased from Trinos, Inc

⁹Varian, DS 302 rotary-vane pump

¹⁰Varian, Turbo-V 551 Navigator

¹¹CapaciTorr, D 400-2, ZrVFe alloy composition

¹²Dycor, LC Series

¹³Pure Gas Products, MC1-902FV

¹⁴Varian, 951-5100

the vacuum chamber was monitored by an RGA. A comprehensive overview of the vacuum system and the linear Paul trap is available in Ref. [70].

3.3 Production of Th⁺ ions

Throughout all experimental investigations, production of Th⁺ ions was carried out by photoablation. Here, we work in the characteristic regime when the laser pulse duration is longer than the time of electron-phonon interaction, i.e. thermal ablation. Above a certain laser intensity threshold (of the order of 10^8 W/cm²), the ablation layer thickness quickly reaches the range of 10 nm per laser pulse [71]. The resulting plume contains atoms, molecules, and clusters as well as electrons and ions, which leave the plume away from the target surface at velocities in the range of 10^4 m/s (see Ref. [72] and references therein). For production of ²³²Th⁺ ions by laser ablation, we used a nitrogen laser¹⁵ at a wavelength of 337 nm with a maximum pulse energy of ≈ 100 μ J, a pulse duration of 4 ns, and a maximum repetition rate of 20 Hz. The transverse multimode laser beam was focused to a spot of 100×150 μ m² to obtain a peak intensity of about 170 MW/cm² (which corresponds to a energy density of ≈ 0.7 J/cm²).

In order to investigate the suitability of the photoablation process for ion production and trapping, we carried out an experiment where the strongest tabulated resonance line at 402 nm in Th⁺ (see Section 4.3 and Fig. 3.5) was excited with radiation from an ECDL after creating ions via the photoablation laser. Figure 3.3 shows that laser ablation loading in this trap geometry is cumulative over several ablation shots before the ion number saturates. This figure also depicts axial confinement of the ²³²Th⁺ ions for two different dc voltages U_{EC} . As can be seen from Fig. 3.3, after 10 ablation pulses the linear Paul trap was filled and we estimated more than 10^5 of ²³²Th⁺ ions were loaded into the trap [72]. Here, helium buffer gas at a pressure of 0.2 Pa was used for collisional cooling and quenching of metastable states. A disadvantage of this method is the significantly high shot-to-shot fluctuation of the ion number, which causes the need for several adjustments of the beam position (i.e. one adjustment per five shots).

Alternatively, we used the fundamental radiation at 1064 nm of a lamp pumped Nd:YAG laser¹⁶. The maximum pulse energy of this system is 50 mJ with a pulse duration of 5 ns, and a maximum repetition rate of 10 Hz. The laser beam was focused to a spot of ≈ 430 μ m. The output pulse energy of this laser was controlled via the Q-switch delay. Typically the pulse energy was varied within 9–11 mJ, equivalent to an energy density of 1.3–1.6 J/cm². After 1–2 ablation pulses of the lamp pumped Nd:YAG laser we observed an ion number about two times higher

¹⁵Stanford Research Systems, NL-100

¹⁶Quantel, Ultra 50

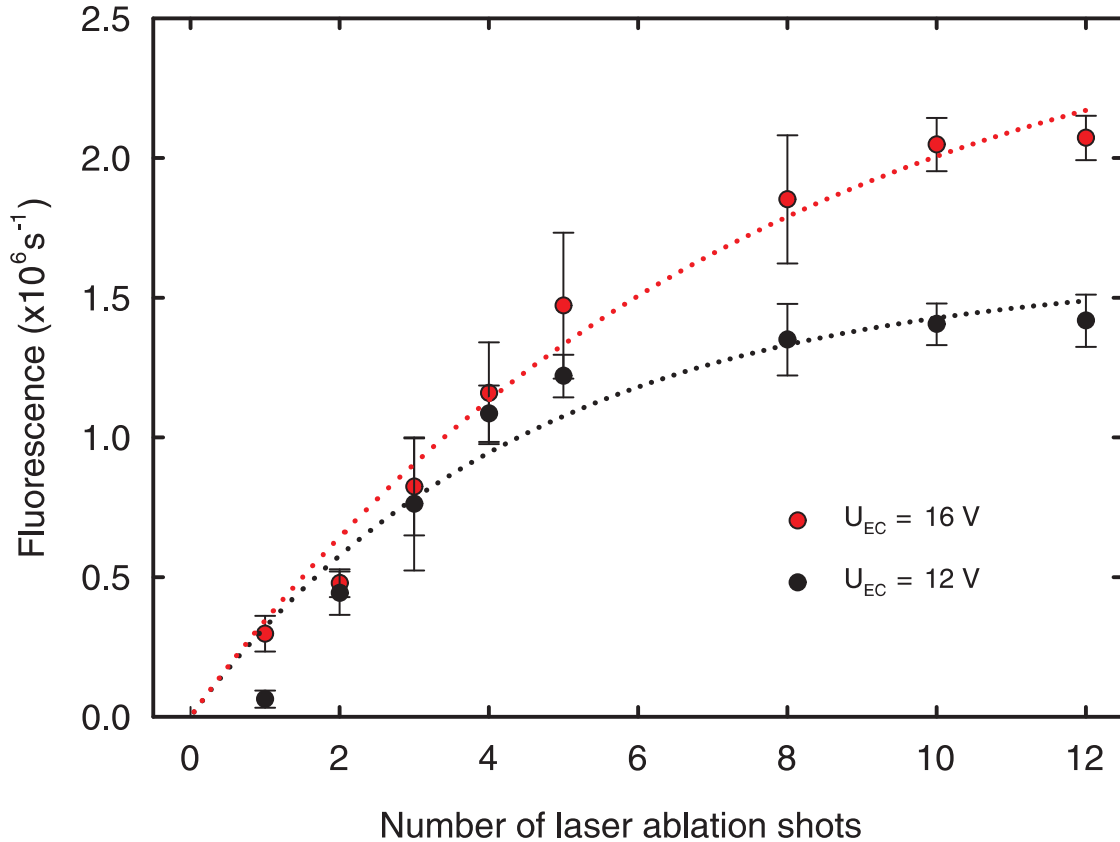


Figure 3.3: Fluorescence signal of stored $^{232}\text{Th}^+$ ions for multiple ablation pulses with different dc axial confinement voltages, showing cumulative loading of the trap. A nitrogen laser is used for loading the trap via photoablation. U_{EC} is the static voltage that is applied to all electrodes of the two outer sections for the axial confinement within the central section (see Fig. 3.1).

than with the nitrogen laser. Furthermore, the shot-to-shot fluctuations of the ion number are smaller for this system.

3.4 Lasers used for spectroscopy of trapped $^{232}\text{Th}^+$ ions

For different laser excitation schemes of $^{232}\text{Th}^+$ ions collisionally cooled by buffer gas, we use a combination of the following lasers (see Fig. 3.4): three extended-cavity diode lasers (ECDL), a picosecond pulsed Ti:sapphire laser, and a nanosecond pulsed Ti:sapphire laser. In this section, we will review the main features of them.

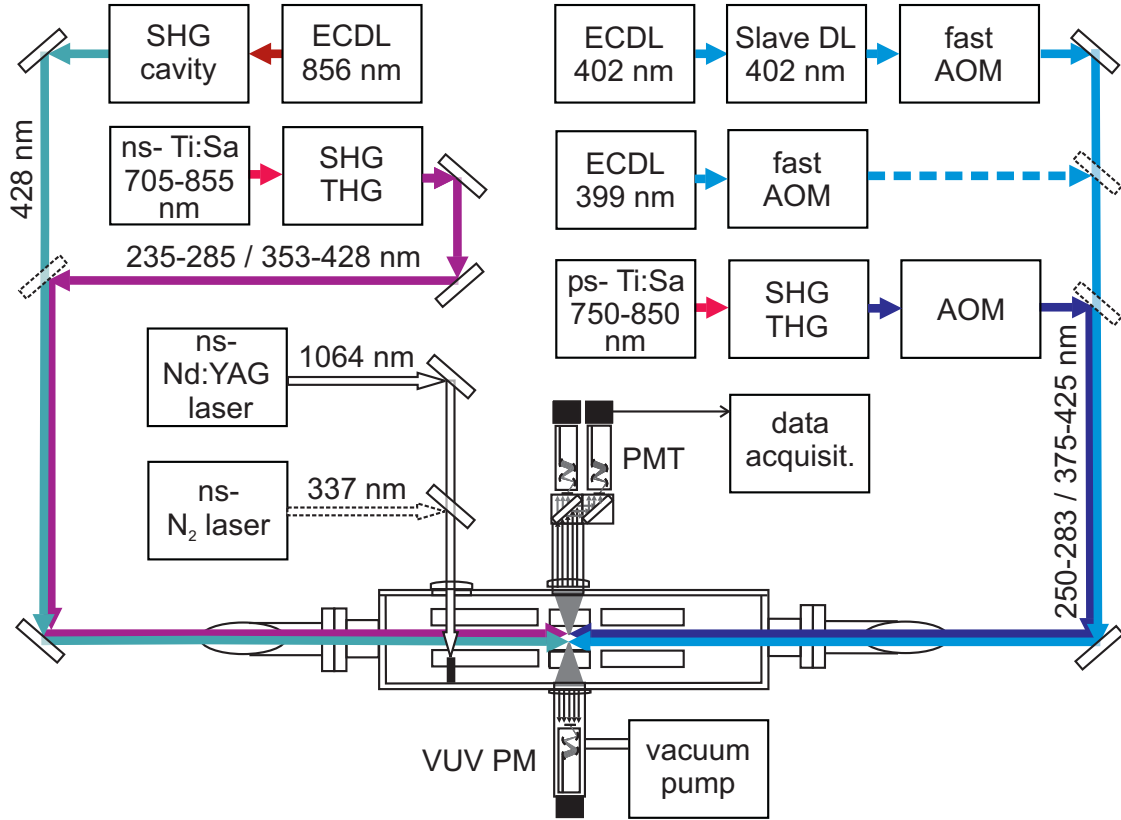


Figure 3.4: Experimental arrangement for laser excitation of trapped Th^+ . SHG: Second-harmonic generation, THG: third-harmonic generation. For further details see text.

Extended-cavity diode lasers

We used an ECDL¹⁷ tuned to the $0_{3/2}-24874_{5/2}$ transition at 402 nm (see also Fig. 3.5 for a partial level scheme of the thorium ion Th^+) with a typical average output power of 7 mW and a linewidth of a few hundred kHz. The wavelength was measured by a Fizeau-interferometer-based wavelength meter¹⁸. In order to obtain an intensity profile with a Gaussian shape and to minimize light scattering, the output of all the ECDLs used here was passed to the trap through polarization-maintaining single-mode fiber. Beam diameter in the trap was ≈ 1 mm. To scan over the atomic transition, the frequency of the ECDL was scanned via an external modulation voltage applied to a piezoelectric transducer (PZT) changing the cavity length.

In pulsed laser excitation (see Section 5.3) we used the laser injection-locking technique to obtain higher output power for the radiation at 402 nm. More than

¹⁷Toptica, DL 100

¹⁸Ångstrom HighFinesse Wavelength meter, WS-7

50 mW average output power was obtained using this system. Furthermore, the 402-nm radiation was amplitude-modulated to produce pulses using a fiber coupled acoustic-optical modulator (AOM)¹⁹ with a rise time of approximately 9 ns.

A similar ECDL, at about 399 nm wavelength was used to excite the $24874_{5/2}$ – $49960_{7/2}$ transition (see also Fig. 3.5) for two-photon laser excitation. In an investigation of possible first excitation steps from the ground state, this system was also used to excite the $0_{3/2}$ – $25027_{1/2}$ ground state transition at 399.5 nm. This transition was as well used for a partial classification of the total angular momentum J of the newly observed even-parity states around 8 eV (see Section 5.3.4).

The metastable level at $1521_{5/2}$ was depleted by a frequency-doubled ECDL producing light at a wavelength of 428 nm (see also Fig. 3.5). The ECDL at 856 nm was frequency-doubled using a PPKTP crystal in an external enhancement cavity. The incident average power at 856 nm was approximately 80 mW. The optical cavity was locked to the ECDL via the Pound-Drever-Hall technique. With this system we obtained more than 25 mW of radiation at 428 nm with less than 1 MHz linewidth.

Picosecond pulsed Ti:sapphire laser

For low-resolution spectroscopy over extended wavelength ranges, we used a tunable Kerr-lens modelocked Ti:sapphire laser²⁰ pumped by a solid-state laser²¹ at 532 nm with 8 W output power (see Fig. 3.4). This system produces pulses of about 3 ps duration and 90 MHz repetition rate. In our experiments, we tuned the output wavelength of this system in the range of 750–950 nm and in the corresponding second- and third-harmonic generation ranges (SHG and THG, respectively). The SHG and THG occurs via a single pass through non-linear crystals²². The fundamental output average power of this system was approximately 1 W. In the case of the second-harmonic and the third-harmonic radiation it was about 100 mW and 50 mW, respectively. The spectral linewidth of the second-harmonic radiation is approximately 0.25 nm (≈ 500 GHz). This laser was also used for two-photon excitation of the $24874_{5/2}$ – $49960_{7/2}$ transition and as a photodissociation laser (see Fig. 3.5 and Section 6.2, respectively). Additional extended repumping schemes, which maximize the population of the $24874_{5/2}$ state, were also studied with this system (see Section 4.5.2).

Nanosecond pulsed Ti:sapphire laser

In order to search for unknown atomic transitions from the $24874_{5/2}$ state to higher-lying states above the energy range of $60\,000\text{ cm}^{-1}$ (7.4 eV), we used a nanosecond pulsed Ti:sapphire laser²³ (see Fig. 3.4 and Fig. 3.5), pumped by a pulsed multimode system (which is diode pumped, solid state and Q-switched) at

¹⁹A-A Opto-electronic, MT200-B9-FIO

²⁰Coherent, Mira 900

²¹Coherent, Verdi V8

²²Photop, TP-2000B

²³Photonics Industries, TU-L

527 nm with 45 W output power²⁴, spectrally narrowed by an intracavity grating. This laser is ideally suited for this study since it has a narrower linewidth (in comparison with the picosecond pulsed Ti:sapphire laser) and also its peak power is in the kilo-Watt range. This system produces pulses of approximately 25 ns (FWHM) duration at a 1–4 kHz repetition rate. The fundamental output wavelength is tunable from 705 nm to 855 nm and in the corresponding second- and third-harmonic ranges. The typical average powers are 900 mW, 300 mW and 100 mW, for the outputs of fundamental, SHG and THG, respectively.

The free spectral range of the cavity of this laser system is given by $\text{FSR}=c/2L$, where c is the speed of light and L is the length of the cavity. For this laser, the length of the cavity is $L\approx 50$ cm, therefore one obtains $\text{FSR}\approx 600$ MHz. The fundamental output spectrum of the laser is determined by about 20 longitudinal modes separated by ≈ 600 MHz. Analyzed with a fast photodiode (bandwidth 1 GHz), the beat signal between the modes showed a linewidth in the range of a few 10 MHz (FWHM) for a time scale of 1–10 s. For shorter time scales, it is about one order of magnitude smaller. The fundamental wavelength was measured by the same wavelength meter as described before, where we estimated its wavelength readout accuracy in the order of 2 GHz limited by the high noise level induced by the pulsed laser [73]. The construction of the commercial nanosecond pulsed Ti:sapphire laser was modified with the installation of a PZT to the grating of the laser system, which allows fine tuneability of the fundamental laser frequency up to approximately 15 GHz. Bigger wavelength steps were controlled via a step motor attached to the grating.

3.5 Main resonance transitions studied and fluorescence detection

As it was mentioned already in Section 2.2.2, the electronic energy level structure in Th^+ is extremely complex. Since throughout all our experimental observations we investigated several excitation schemes in Th^+ , it is worth showing the complete resonance transitions investigated in trapped Th^+ ions collisionally cooled by buffer gas. The main resonance transitions studied in this thesis are shown in Figure 3.5. In the following we label states by their energy in cm^{-1} and their total angular momentum as shown in Fig. 3.5. Also, in this figure are displayed: the strongest transition in Th^+ at 402 nm (used as the first excitation step in Section 4.3), the repumping laser at 428 nm, and the transitions used for two-photon excitation (in cw excitation: 399 nm and in pulse excitation: 379 nm and hatched area). The hatched area in Fig. 3.5 corresponds to the energy range of search for states at

²⁴Photronics Industries, DM-527-30

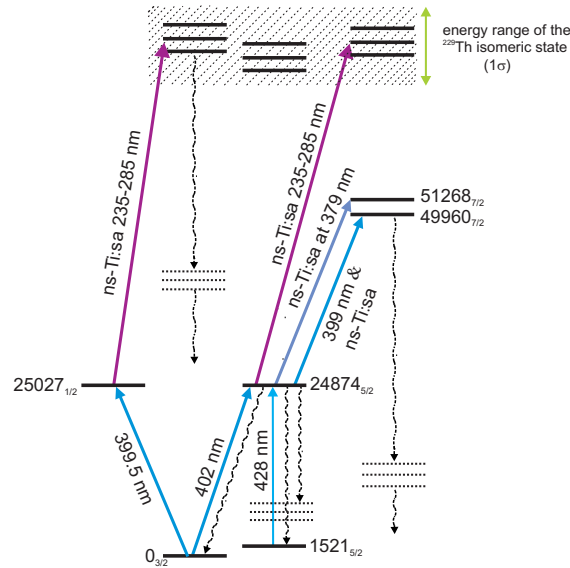


Figure 3.5: Partial level scheme of the thorium ion Th^+ showing the main resonance transitions studied in this thesis. The hatched area corresponds to the present 1σ uncertainty range for the nuclear transition energy in ^{229}Th . The level energies are given in cm^{-1} and the subscript denotes the total angular momentum.

higher excitation energies, which is the present 1σ uncertainty range for the nuclear transition energy in ^{229}Th .

The laser-induced fluorescence emission of the trapped Th^+ ions was detected with the use of photomultiplier tubes (PMT) in photon counting mode, as shown in Fig. 3.4. In total, we used three PMT with different spectral sensitivities. Two PMT²⁵ were employed for detecting the fluorescence signal from photons with wavelength larger than 200 nm. Another PMT²⁶ was used for observation of photons with wavelengths lower than 200 nm (see VUV PMT in Fig. 3.4). The latter was mounted in an evacuated housing at pressure below 3 Pa to avoid the absorption of photons by oxygen molecules and therefore allowing the detection of high energy photons.

With the aim of discriminating between the fluorescence emissions associated with one- and two-step excitations, a combination of spectral filters and a dichroic beam splitter separated the spectral sensitivity ranges of the PMT. Figure 3.6 shows the spectral sensitivity of the used filters together with the quantum efficiency of the PMT for observation of: fluorescence signals from the $0_{3/2}$ – $24\,874_{5/2}$ transition at 402 nm (a) and fluorescence signals from the $24\,874_{5/2}$ – $49\,960_{7/2}$ transition at 399 nm (b). Fluorescence signals from the $24\,874_{5/2}$ – $51\,268_{7/2}$ transition at 379 nm

²⁵Hamamatsu, R7459, sensitivity 160–650 nm and Hamamatsu, R6836, sensitivity 115–320 nm

²⁶Hamamatsu, R6835, sensitivity 115–200 nm

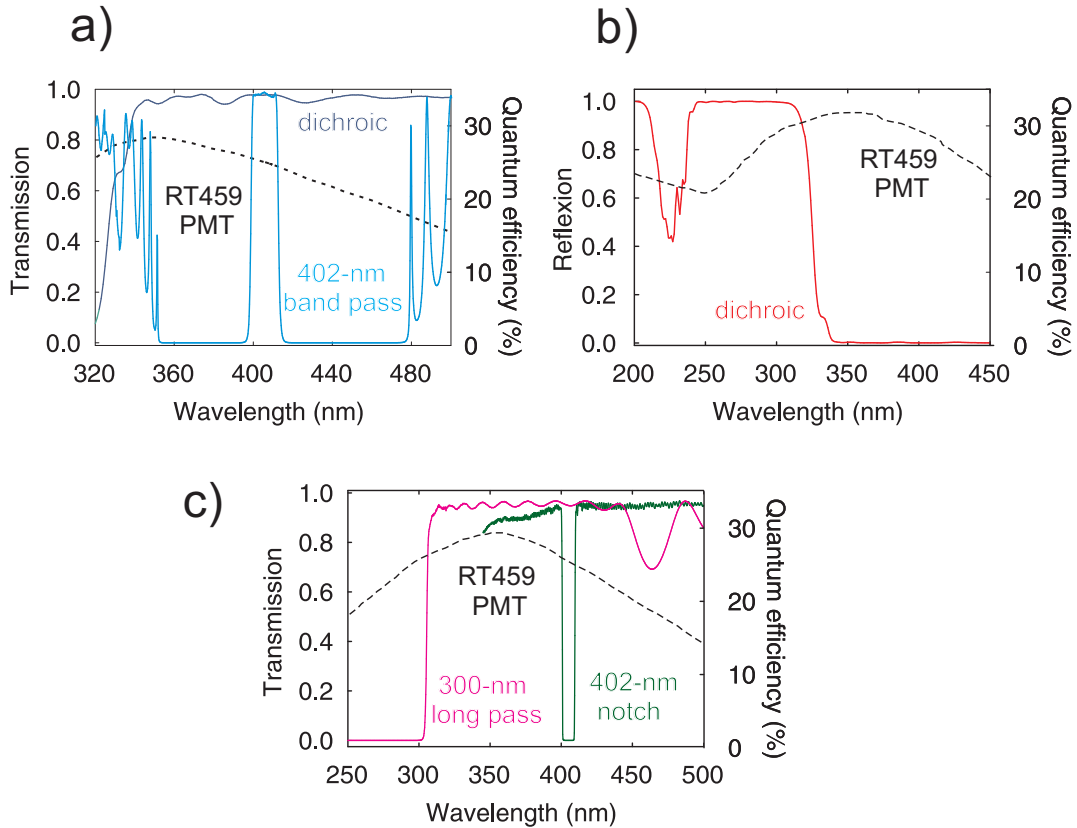


Figure 3.6: Spectral sensitivity ranges for the used filters, dichroic beam splitter and quantum efficiency of the PMT. (a) observation of fluorescence signals from the $0_{3/2}-24\,874_{5/2}$ transition, 402-nm selected. (b) observation of fluorescence signals from the $24\,874_{5/2}-49\,960_{7/2}$ transition. (c) observation of fluorescence signal of higher-lying states above the energy range of $60\,000\text{ cm}^{-1}$, 402-nm blocked.

were observed with the configuration shown in Fig. 3.6 (b). For the observation of the new levels above the energy range of $60\,000\text{ cm}^{-1}$, we used the configuration shown in Fig. 3.6 (a) for the fluorescence signal of the 402 nm level (without dichroic beam splitter and with a 300-nm long pass filter) when the 402-nm signal was selected and Fig. 3.6 (c) for fluorescence signal of the excited state when the 402-nm signal was blocked.

Data acquisition was accomplished with a LabVIEW program, which includes: a recording of the fluorescence signal in cw and pulsed excitation, monitoring of the laser wavelengths, control of the 402-nm laser PZT, control of the pulse durations and pulse delays, and the dc offset voltage for segments of the linear Paul trap.

4 Single-wavelength laser excitation of $^{232}\text{Th}^+$ ions

4.1 Introduction

Since our goal is to achieve resonant excitation of the ^{229}Th nucleus with the use of the photons from conventional laser sources, we carried out an investigation of possible first excitation steps from the ground state to states around 400 nm and 270 nm. As it was mentioned already in Section 2.2.3, the advantage of the two-photon excitation in the electron shell of the singly ionized ^{229}Th [13] is that the actual spectral interrogation wavelength for the nuclear transition shifts from the challenging range of 160(10) nm to the manageable range of 265(30) nm by using a transition around 400 nm as a first excitation step. If a transition around 270 nm is used as a first excitation step, the spectral interrogation wavelength shifts to the convenient range of 400(60) nm. The wavelength ranges nearby 400 nm and 270 nm for the first excitation step are important because it enables the use of commercially available tunable lasers with harmonic generation around 265(30) nm (e.g. third-harmonic generation of Ti:sapphire laser) and 400(60) nm (e.g. second-harmonic generation of dye laser) for the second excitation step. In addition, in previous experiments with a hollow-cathode discharges [48, 49], these wavelength ranges for the first excitation step show a dense region of transitions with high excitation intensity in Th^+ .

This chapter describes possible first excitation steps from the ground state to states near 400 nm and 270 nm of trapped, buffer gas cooled $^{232}\text{Th}^+$ ions. However, since we are pursuing observation of weak fluorescence signals from the second excitation step, we concentrated on the strongest transition at 402 nm in Th^+ as the first excitation step because the transition at 402 nm is more suitable than the transitions around 270 nm. As it was mentioned already in Section 2.2.2, the electronic energy level scheme of Th^+ is extremely complex (see Fig. 2.3). In terms of experimental realization it has the disadvantage that laser excitation of an ensemble of atoms from the ground state to a definite excited state is often inefficient for a multilevel system such as Th^+ because spontaneous decay leads to the accumulation of population in metastable levels that are decoupled from the laser. In this context and in order to maximize the population of atoms in the excited state, we studied collisional quenching of metastable states with helium,

argon and nitrogen buffer gases. Moreover, the effect of repumping laser excitation from the three lowest-lying metastable levels was measured. The experimental results were compared with a four-level rate equation model, which allowed us to deduce quenching rates for the buffer gases mentioned above. Finally, we estimated the amount of photons/s per ion detected in the strongest transition at 402 nm using nitrogen as a buffer gas.

4.2 Ground state transitions: first excitation step

In a research of suitable first excitation steps from the ground state, we performed laser excitation of trapped, buffer gas cooled $^{232}\text{Th}^+$ ions around 400 nm and 270 nm. These energy ranges are important because they make feasible the use of photons from commercial tunable sources for the second excitation step. Nevertheless, the range around 400 nm is more appealing because it enables the use of commercial cw extended-cavity diode lasers for the first excitation step. Also in this range, the strongest resonance line in Th^+ is reported at 402 nm [48, 49].

In this section, laser-induced fluorescence signals of $^{232}\text{Th}^+$ ions were detected by illuminating the trapped ion cloud by means of second-harmonic or third-harmonic radiation of a picosecond Ti:sapphire laser. The experimental setup used in this section is shown in Fig. 3.4, where the picosecond Ti:sapphire laser and the ECDL at 402 nm were employed for the optical excitation. In order to compensate variations in fluorescence strength caused by fluctuations of the number of loaded ions, the laser-induced fluorescence signal registered at each laser wavelength was normalized to the signal resulting from resonant cw diode-laser excitation of the 402-nm transition. The average excitation power were 10 mW and 1 mW for the harmonic generation of the picosecond Ti:sapphire laser and ECDL at 402 nm, respectively. The beam diameter in the trap was ≈ 1 mm for the two laser beams. Helium was used as a buffer gas at a pressure of 0.2 Pa.

Fig. 4.1 shows a typical excitation spectrum of electric-dipole transitions around 400 nm originating from the ground state. Here, we scanned the wavelength of the picosecond Ti:sapphire laser over a range of 12 nm, demonstrating the high density of levels for Th^+ in this range. In the presented figure, the line widths are determined by the spectral linewidth of the picosecond Ti:sapphire laser, in this situation approximately 0.25 nm (≈ 500 GHz). The transitions from the ground state depicted in Fig. 4.1 and their relative strengths are in agreement with the data tabulated in Ref. [48] for the studied scan range. The signal strength of each transition is mainly observed (using spectral filters, see Fig. 3.6) by monitoring the fluorescence emission of the spontaneous decay into the ground state.

In Fig. 4.2 the experimental data for laser excitation of trapped $^{232}\text{Th}^+$ ions by using the third-harmonic radiation of the picosecond Ti:sapphire laser are plotted. The four transitions displayed in Fig. 4.2 are transitions from the ground state to

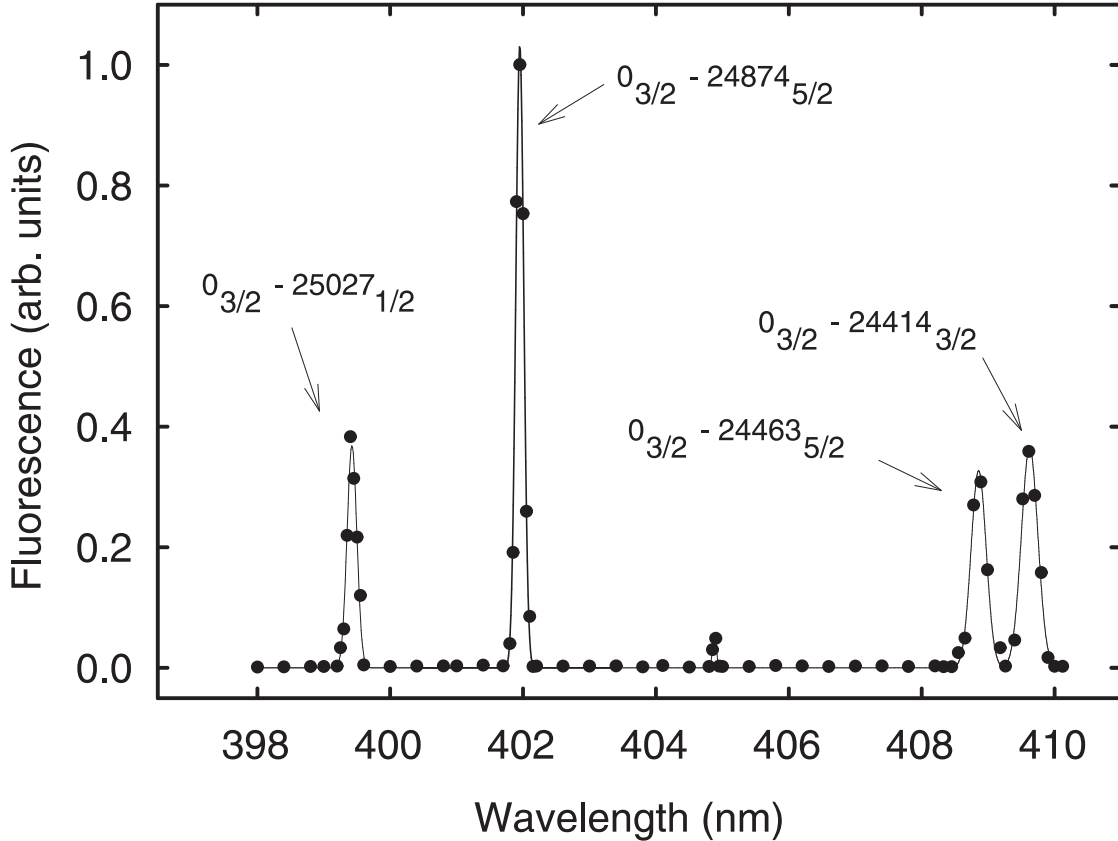


Figure 4.1: Excitation spectrum of trapped $^{232}\text{Th}^+$ ions, using the second-harmonic radiation of a modelocked picosecond Ti:sapphire laser.

higher-lying states of about 270 nm and their relative strengths are in agreement with the data tabulated in Ref. [48]. The spectrum was normalized taking into account the wavelength dependence for the quantum efficiency of the PMT. The level $37\ 130_{1/2}$ shown in Fig. 4.2 is one of the strongest tabulated energy levels in terms of fluorescence strength that can be excited by an electric dipole transition from the ground state.

In conclusion, we have shown laser excitation of trapped $^{232}\text{Th}^+$ ions collisionally cooled by helium buffer gas at 0.2 Pa pressure using a modelocked picosecond Ti:sapphire laser in the wavelength range around 400 nm and 270 nm. It can be clearly seen that the $0_{3/2}-24874_{5/2}$ transition at 402 nm is the strongest one in terms of fluorescence strength. Therefore, we have chosen this transition as our first excitation step. The next section discusses the aforementioned transition in more detail using excitation with an ECDL at 402 nm.

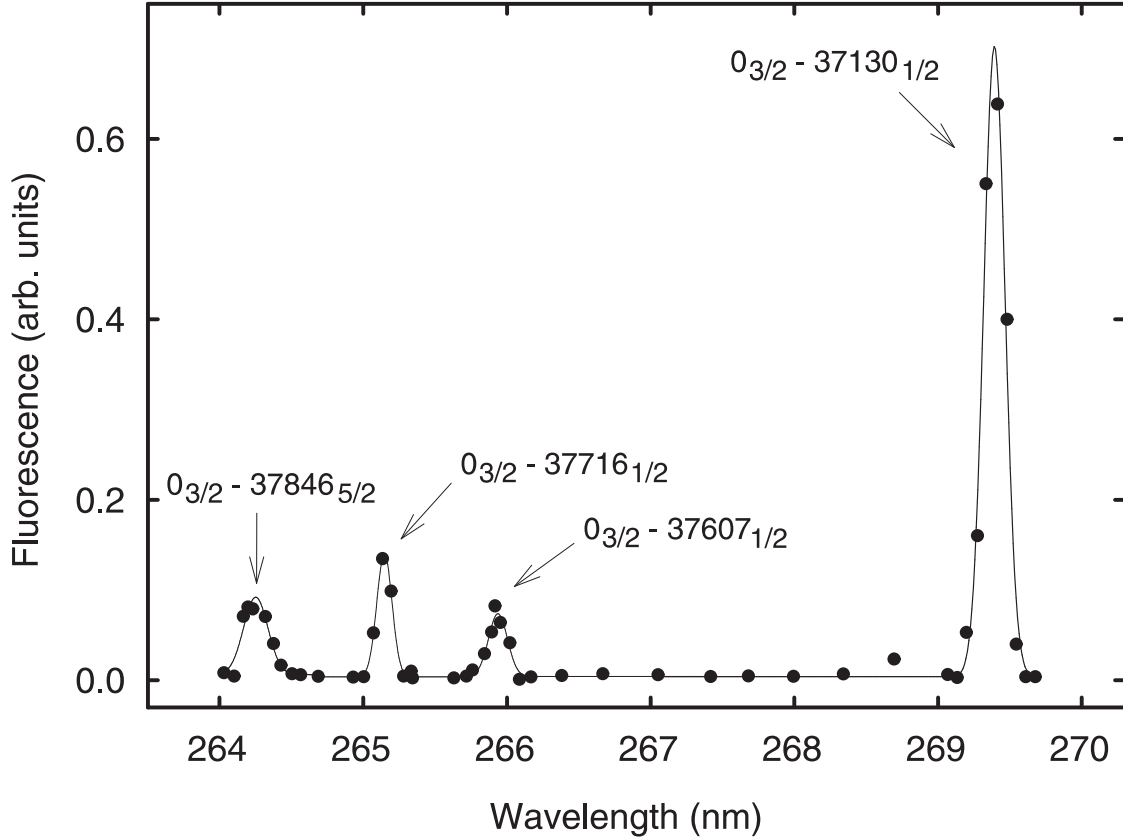


Figure 4.2: Excitation spectrum of trapped $^{232}\text{Th}^+$ ions, using the third-harmonic radiation of a modelocked picosecond Ti:sapphire laser.

4.3 Excitation of the $0_{3/2}-24874_{5/2}$ transition at 402 nm

In this section we investigated continuous laser excitation of the strongest tabulated and observed line of the Th^+ emission spectrum at 402 nm. This transition connects the $(6d^27s)J = 3/2$ ground state with the $(6d7s7p)J = 5/2$ state at 24874 cm^{-1} . The experimental arrangement used in this section is shown in Fig. 3.4, where laser excitation of this transition using a cw extended-cavity diode laser at 402 nm was carried out. Also, the fluorescence detection and the level scheme is described in Fig. 3.6 and Fig. 4.5.

The spectrum resulting from 402-nm cw laser excitation is shown in Fig. 4.3. In order to record the Doppler-broadened excitation spectrum of the ions we scanned the laser frequency over ± 1.5 GHz range and thus, a resonance spectrum with full width at half maximum (FWHM) of ≈ 700 MHz was observed using 0.2 Pa of helium buffer gas pressure. For helium pressures above 0.1 Pa the Doppler FWHM

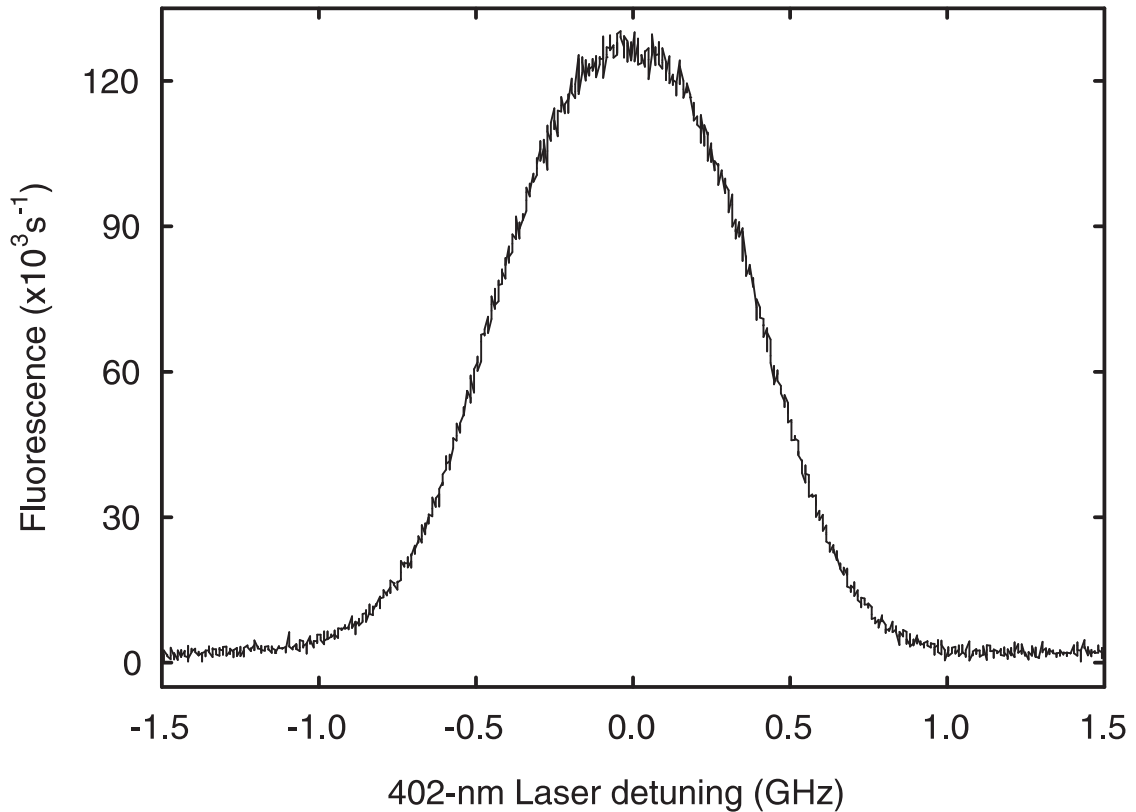


Figure 4.3: Excitation spectrum of trapped $^{232}\text{Th}^+$ ions, using cw output of an extended-cavity diode laser tuned to the $0_{3/2}-24874_{5/2}$ transition at 402 nm. The average excitation power is $50\ \mu\text{W}$. The signal strength is mainly ($\approx 94\%$) observed by detection of the fluorescence of the spontaneous decay into the ground state via an optical filter in front of the PMT, which selected the 402-nm signal.

of $\approx 700\ \text{MHz}$ indicates that the trapped ions were collisionally cooled to approximately $300\ \text{K}$ for motion along the trap axis. The lifetime of the $24874_{5/2}$ level is $\tau=23\ \text{ns}$ [74] and therefore its natural linewidth is given by $\Gamma_{402}=1/(2\pi\tau)\approx 7\ \text{MHz}$. For the other buffer gases studied here, collisional cooling to room temperature was achieved at pressures of $\approx 0.2\ \text{Pa}$ and $\approx 0.01\ \text{Pa}$, using argon or nitrogen, respectively. The storage times of the $^{232}\text{Th}^+$ ions was typically $300\ \text{s}$ allowing the measurement of the ion temperature in the equilibrium state.

Since in our case the collisions of Th^+ with the much lighter buffer gas will essentially result in viscous damping, which lowers the mean kinetic energy of the ions [75]. Also, as it is well known, collisional cooling becomes more effective for a lighter collisional partner [76], and thus we observed this behavior for the noble gases. In our experiment, when the $^{232}\text{Th}^+$ ion cloud is collisionally cooled by

helium buffer gas, we observed a faster fall of the ion temperature around $5 \cdot 10^{-2}$ Pa in comparison with argon. In contrast with helium and argon, we observed with nitrogen buffer gas a rapid decrease of the ion temperature about $5 \cdot 10^{-3}$ Pa. As will be described in Sec. 4.5, in comparison with helium, larger fluorescence signals were observed using argon or nitrogen buffer gas at 0.2 Pa pressure, because of the more efficient collisional quenching of metastable levels.

4.3.1 Doppler-free saturation spectroscopy of the $0_{3/2}-24874_{5/2}$ transition

In order to study broadening effects of the linewidth of the $0_{3/2}-24874_{5/2}$ transition, we investigated Doppler-free saturation spectroscopy of trapped $^{232}\text{Th}^+$ ions collisionally cooled by nitrogen buffer gas. This technique is particularly useful for finding narrow homogeneous lineshapes that are hidden inside the Doppler-broadened excitation spectra. The characteristic of the Doppler-free saturation spectroscopy is the existence of two counterpropagating laser beams in the ion cloud, one having a low intensity ($I \ll I_{sat}$) and the other with high intensity ($I \geq I_{sat}$), with I_{sat} the saturation intensity for the $0_{3/2}-24874_{5/2}$ transition (see Table 4.2 and Eq. 4.7). Now, when the two opposite direction beams are tuned close to resonance, they interact with the velocity group of atoms around $v \cong 0$ right in the line center, which is independent of first order Doppler shifts. This leads to a narrow feature in the Doppler-broadened excitation spectrum shown in Fig. 4.3. In this case, the narrow feature appearing in the line center of the spectrum corresponds to the so-called Lamb dip.

A typical Doppler-free saturation spectrum at the center of the Doppler-broadened excitation spectrum is shown in Fig. 4.4. Here, the extended-cavity diode laser at 402 nm was used to produce the two counterpropagating beams. Nitrogen was used as a buffer gas at a pressure of 0.2 Pa. We studied broadening mechanisms with trapped $^{232}\text{Th}^+$ ions to reach the natural linewidth of the $0_{3/2}-24874_{5/2}$ transition of ≈ 7 MHz. Among others, the broadening effects that were investigated were: variation of rf trap drive voltage amplitude, buffer gas pressure, saturation intensity, beam diameter (transit effect) and ion number. Table 4.1 summarizes the results. We are uncertain about the small range of variation of the parameters determining the broadening effects that we performed, however we assumed its linear dependence to extract additional information. We could not observe any dependence for different beam diameters of the 402-nm laser radiation. The minimum width observed was 26(2) MHz FWHM, definitely overshadowed by additional broadening. As can be seen from the Table 4.1, the dominant broadening mechanism can likely be attributed to a frequency modulation resulting from the driven micromotion of the ions in the trap. Here, the broadening effect due to the buffer gas can be neglected because the buffer gas pressure was confirmed by

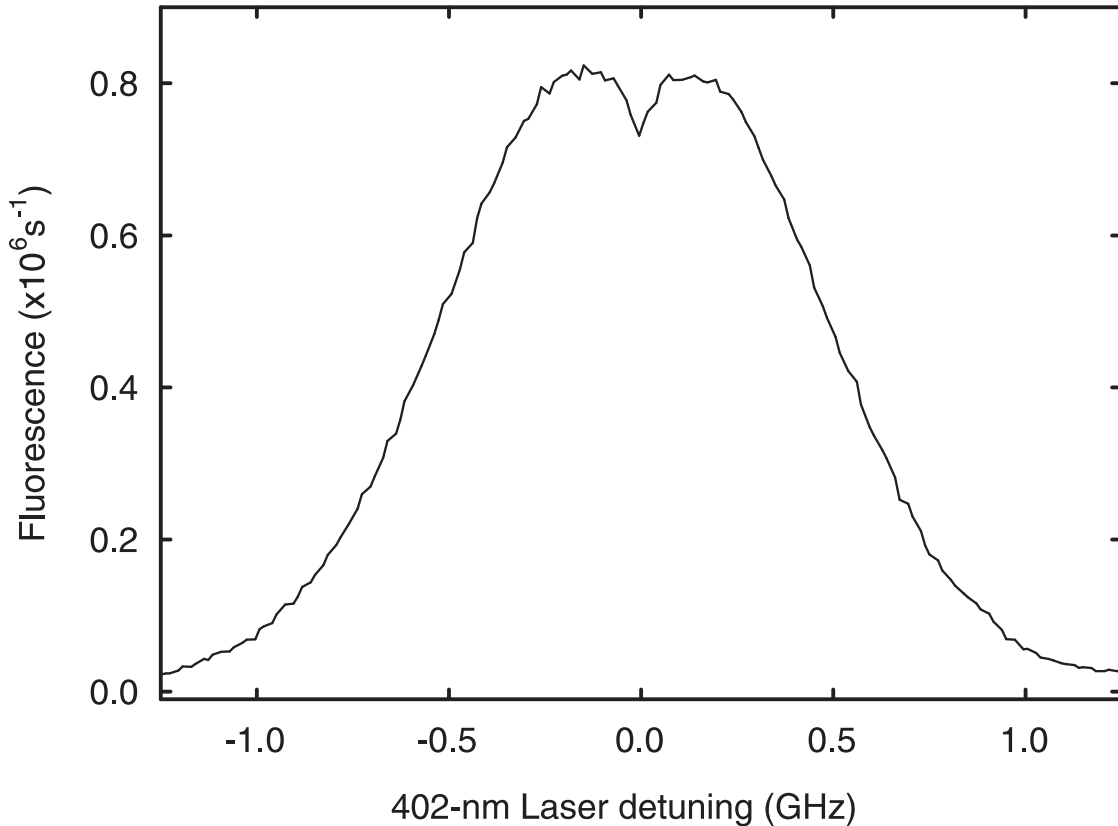


Figure 4.4: Doppler-free saturation spectrum at the center of the Doppler-broadened excitation spectrum of trapped $^{232}\text{Th}^+$ ions using two counterpropagating beams, derived from a single cw output of an extended-cavity diode laser tuned to the $0_{3/2}-24874_{5/2}$ transition. When the counterpropagating beam is blocked the experiments gives a simple Doppler-broadened excitation spectrum as shown in Fig. 4.3.

measuring the temperature of the ions and by direct measurement of the buffer gas via a cold-cathode gauge.

4.3.2 Population trapping in metastable levels

For all experimental conditions studied here, population trapping in low-lying metastable levels limits the obtainable population of the $24874_{5/2}$ state. As shown in Fig. 4.5 the excited $24874_{5/2}$ level spontaneously decays to twelve metastable states (the hatched area corresponds to a manifold of eleven metastable states). Atoms in metastable states can be returned to the ground state by inelastic collisions with a buffer gas. To obtain a significantly higher population in the excited level, we firstly describe the use of pulsed optical excitation in the millisecond

Table 4.1: Variation of the width of the Doppler-free saturation resonances for different broadening mechanisms. In order to determine the variation with the amount of ions, it was assumed that 10^6 ions loaded into the trap produce 10^6 photons s^{-1} fluorescence signal.

Broadening effect	slope variation	Units
Drive voltage amplitude	+29(7)	MHz kV^{-1}
Buffer gas	-189(38)	MHz Pa^{-1}
Saturation intensity	+0.20(8)	MHz $mW^{-1} cm^2$
Ion number	$+2.4(3) \cdot 10^{-6}$	MHz ion^{-1}

range. Afterward, we show population trapping in the $1521_{5/2}$ state, which can decay to the ground state through quenching collisions with buffer gas. In the last section, we describe the effect of repumping laser excitation from the lowest-lying metastable levels to achieve a higher population in the $24874_{5/2}$ level.

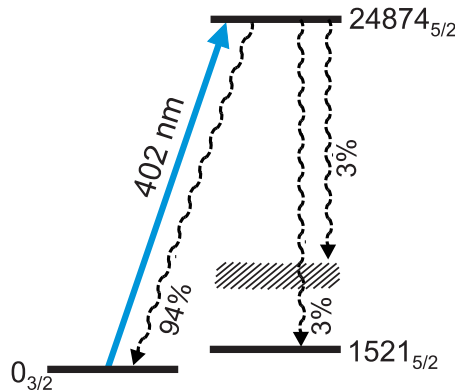


Figure 4.5: Partial level scheme of the thorium ion $^{232}Th^+$ showing the strongest transition from the ground state studied in this section and the lowest-lying metastable levels. The hatched area corresponds to a manifold of eleven metastable states and for the $24874_{5/2}$ level the spontaneous-decay branching fractions are indicated as given in Ref. [50].

Initially the population of the Th^+ ions is entirely in the ground state. In order to measure the fluorescence signal precisely when the $24874_{5/2}$ state is excited by the 402 nm radiation, we carried out pulse excitation with time resolved detection. In doing so, the extended-cavity diode laser at 402-nm was modulated using an acousto-optical modulator (AOM) with a rise time of approximately $1 \mu s$. The minimum pulse length used with this system was in the order of a few milliseconds and therefore was not limited by the rising time of the AOM. The average excitation power for the ECDL was 1 mW with a beam diameter of 1 mm. Helium was used as a buffer gas at a pressure of 0.2 Pa.

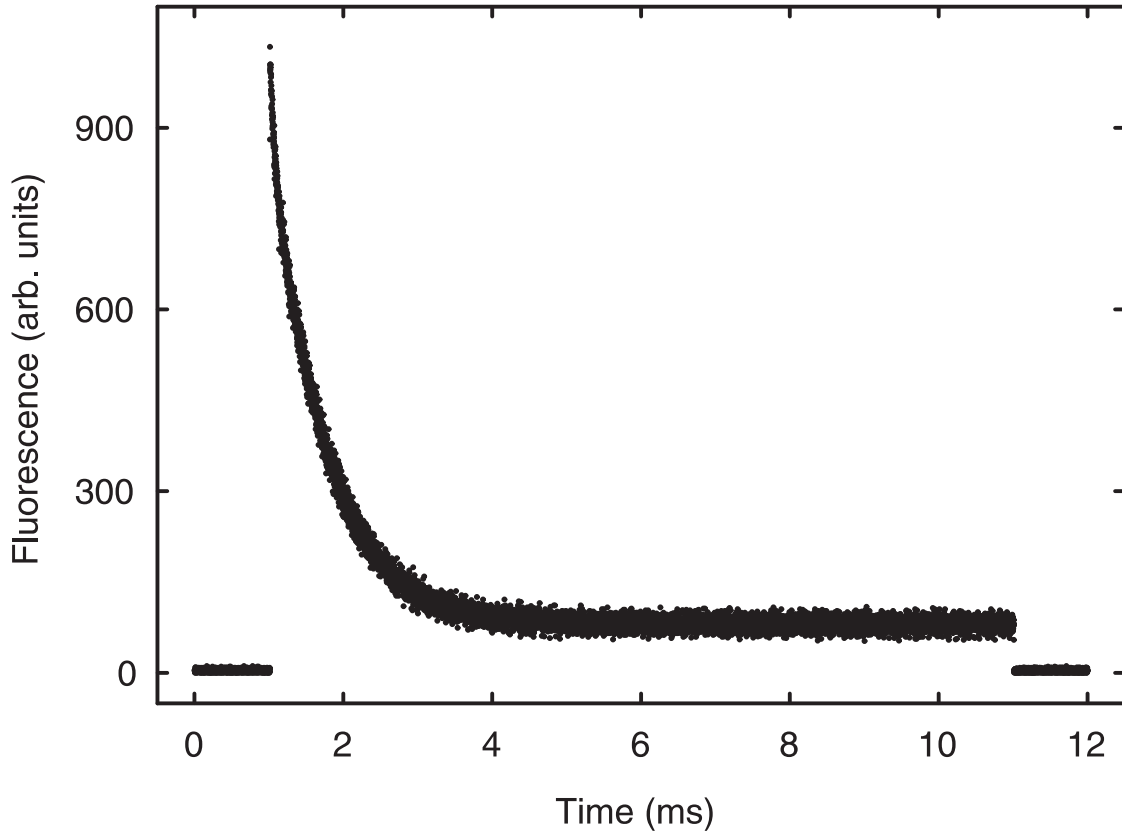


Figure 4.6: Laser-induced fluorescence signal of trapped $^{232}\text{Th}^+$ ions resulting from pulsed laser excitation of the $0_{3/2}-24874_{5/2}$ transition at 402 nm. The pulse length of the 402 nm light was 10 ms and was triggered at 1 ms time.

Figure 4.6 shows the laser-induced fluorescence signal of trapped $^{232}\text{Th}^+$ ions resulting from millisecond-pulsed laser excitation of the $0_{3/2}-24874_{5/2}$ transition at 402 nm. Here, background radiation scattered from the trap electrodes has been subtracted. As it can be clearly seen in Fig. 4.6, pumping into metastable states (see hatched area and $1521_{5/2}$ state in Fig. 4.5) occurs on the millisecond timescale. The exponential decay shown in Fig. 4.6 was dominated by two time constants in the range of a few 100 ns and 1 ms. The longer time constant might reflect the collision-induced population transfer between the various metastable levels (see below). The observed fast time constant cannot be directly associated with the spontaneous decay rates to metastable levels because also transit-time and saturation effects and the rise time of the AOM shutter are expected to strongly affect the temporal variation of the laser-induced fluorescence signal on this time scale.

In conclusion, we have obtained in a transient mode significantly higher population in the excited level by means of pulsed optical excitation in the millisecond range of the $0_{3/2}$ - $24874_{5/2}$ transition at 402 nm. By extrapolating the exponential portion of the curve (in Fig. 4.6) back to zero time, the initial fluorescence intensity was more than 20 times larger than the steady-state value obtained with 402 nm cw excitation, indicating that population trapping in low-lying metastable levels limits the time averaged obtainable population of the $24874_{5/2}$ state. In the next section, we measure the quenching rate of the $1521_{5/2}$ level via time-separated millisecond pulsed excitation with two ECDLs. This level is important because it has the highest branching fraction for decay from the $24874_{5/2}$ state (see Fig. 4.5).

4.3.3 Measured collisional quenching rate of the $1521_{5/2}$ state

In this section, we studied population trapping in the $1521_{5/2}$ level, which can decay to the ground state by means of collisional quenching with buffer gas. Using time-separated pulsed laser excitation in the millisecond range, we obtained the quenching rate of the $1521_{5/2}$ level, which is compared with the one predicted by our 4-level model subsequently described. We performed pulsed excitation with 402-nm laser and repumping excitation of the $1521_{5/2}$ - $24874_{5/2}$ transition at 428 nm. In order to control the switching pulses of the ECDLs, two AOMs with a rise time of approximately $1 \mu\text{s}$ were used. The average excitation power for the ECDLs were 1 mW and the beam diameters were ≈ 1 mm. Helium was used as a buffer gas.

To measure the quenching rate Γ_2 of the $1521_{5/2}$ level, after introducing the buffer gas at a given pressure, we analyzed the metastable state population decay in time by the following steps (also shown in Fig. 4.7). Firstly, the $1521_{5/2}$ level was populated via the $24874_{5/2}$ state during a 2-ms pulse of the ECDL at 402 nm. This pulse duration was long enough to populate the metastable state. Finally, after a variable time delay Δt , the remaining population of the $1521_{5/2}$ level was determined by applying a probe pulse from the 428-nm repumping laser and recording the time-integrated fluorescence signal at 402 nm. The 2-ms pulse of the repumping laser at 428 nm depopulated the metastable level through the $24874_{5/2}$ state, and therefore we were able to observe the spontaneous emission from the $24874_{5/2}$ state to the ground state at 402 nm. The stray light from the repumping laser was blocked using an optical filter in front of the PMT to avoid background signal. We varied Δt from 2 ms to 256 ms for the buffer gas pressures in the range of 0.01 Pa to 0.2 Pa. A similar method was used in Refs. [77, 78]. We observed an exponential decay of the fluorescence signal as a function of the time delay between the 402-nm and 428-nm excitation [see Fig. 4.8(a)] and a linear dependence of the decay rate on helium pressure of $63(3) \text{ s}^{-1} \text{ Pa}^{-1}$ [see Fig. 4.8(b)]. For a pressure of 0.2 Pa, we obtained $\Gamma_2 = 13(2) \text{ s}^{-1}$. In theory it is possible to infer the natural lifetime of the

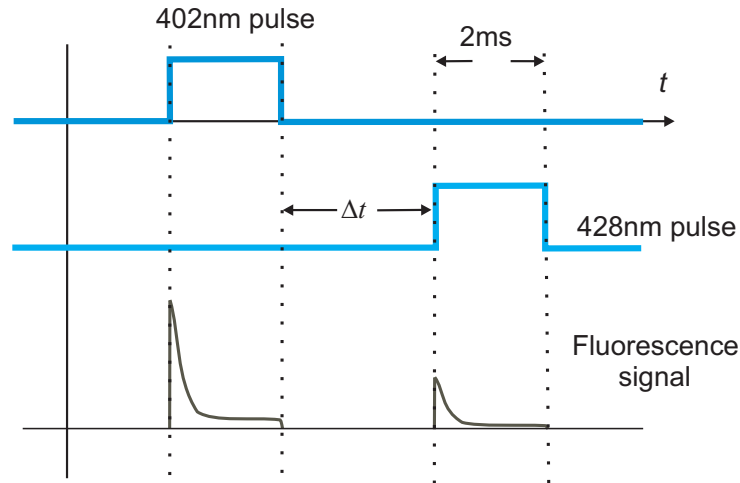


Figure 4.7: Time sequence of the 402-nm and 428-nm pulses during the measurements of the quenching rate Γ_2 of the $1521_{5/2}$ level. The time separation Δt between pulses was varied from 2 ms to 256 ms. Each set of data was normalized according to the signal obtained in the first pulse of the 402-nm laser in order to compensate the trap loading fluctuations. The measurement cycles were averaged 100 times.

$1521_{5/2}$ state (expected value of ≈ 15 s) by extrapolating the obtained curves to zero pressure. Nevertheless, since these measurements had a large uncertainty and were taken at relatively large pressures of helium buffer gas, extrapolation to zero pressure did not give a meaningful result.

4.4 Effective 4-level model for collisional quenching and repumping

In order to obtain an analytic description of the population and fluorescence signal, and to compare the previously obtained value of the quenching rate of the $1521_{5/2}$ level, we introduce a model where we approximate the dense Th^+ level system up to the $24874_{5/2}$ level by the four-level system shown in Fig. 4.9: the 402-nm transition from the ground state $|1\rangle$ to state $|3\rangle$ is driven with Rabi frequency Ω_1 , the metastable state $|2\rangle$ is depleted by 428-nm repumping light with Rabi frequency Ω_2 , and the manifold of eleven higher-lying metastable states is represented by a single level $|m\rangle$. In this approximation we assume that the state $|m\rangle$ is depleted only by quenching collisions. The upper state $|3\rangle$ radiatively decays into the states $|1\rangle$, $|2\rangle$ and $|m\rangle$ with rates γ_1 , γ_2 and γ_m . The sum of the three radiative decay rates, i.e. $\gamma = \gamma_1 + \gamma_2 + \gamma_m$, determines the radiative lifetime of the state $|3\rangle$ as $\tau = \frac{1}{\gamma}$. Due to the fact that the branching fractions for decay to the $1521_{5/2}$ level and for

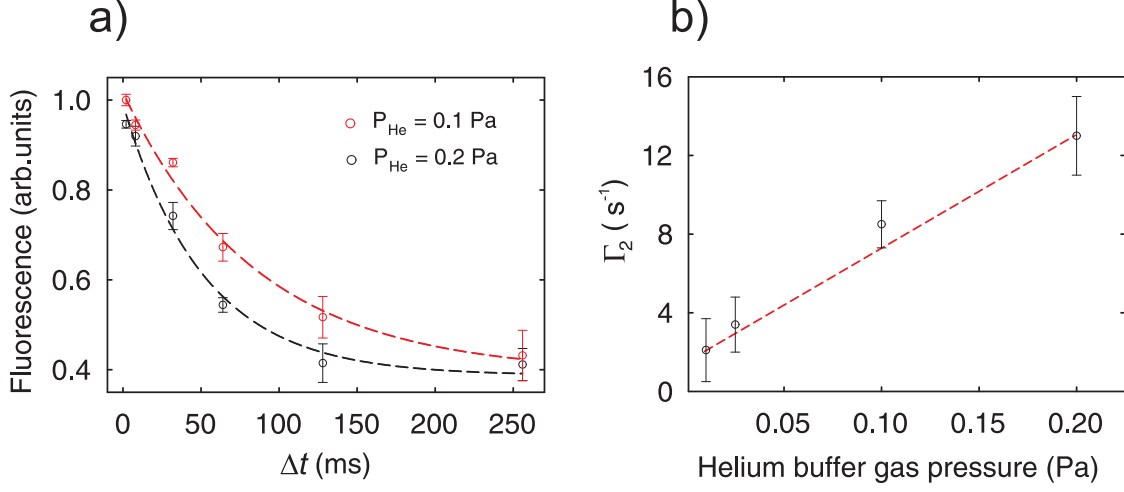


Figure 4.8: (a) $1521_{5/2}$ state population as a function of the time separation Δt between 402-nm and 428-nm pulses. The dashed lines are fits to an exponential decay. (b) measured quenching rate Γ_2 as a function of helium buffer gas pressure. The dashed line is a fit to a straight line.

decay to $|m\rangle$ are approximately equal (see Ref. [50]) we consider that $\gamma_1 = b\gamma$ and $\gamma_2 = \gamma_m = (1 - b)\frac{\gamma}{2}$, and $b = 0.94$ as the branching fraction for decay to the state $|1\rangle$. The populations of $|2\rangle$ and $|m\rangle$ can decay to the ground state through quenching collisions with buffer gas and the corresponding rates are denoted by Γ_2 and Γ_m .

Neglecting the light-induced coherence between states $|1\rangle$ and $|2\rangle$, the population distribution among the levels can be described by rate equations for the population probabilities p_i ($i = 1, 2, 3, m$). In the steady-state limit the rate equations of the four-level system shown in Fig. 4.9 can be expressed as:

$$\begin{aligned}
 -\gamma S_1 p_1 + \Gamma_2 p_2 + \gamma_1 p_3 + \gamma S_1 p_3 + \Gamma_m p_m &= 0, \\
 -\gamma S_2 p_2 - \Gamma_2 p_2 + \gamma_2 p_3 + \gamma S_2 p_3 &= 0, \\
 \gamma S_1 p_1 + \gamma S_2 p_2 - \gamma p_3 - (S_1 + S_2)\gamma p_3 &= 0, \\
 \gamma_m p_3 - \Gamma_m p_m &= 0,
 \end{aligned} \tag{4.1}$$

with the normalization condition $\sum p_i = 1$. Here S_j ($j = 1, 2$) are the saturation parameters for the transitions $|j\rangle - |3\rangle$. Assuming thermalization of velocities due to both, velocity-changing collisions and interaction with the trap potential, we approximate the optical pumping rates as:

$$\gamma S_j \approx 2\sqrt{\pi} \frac{\Omega_j'^2}{kv}, \tag{4.2}$$

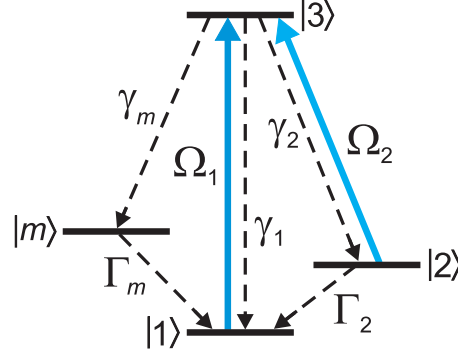


Figure 4.9: Energy level system considered in the rate equation model of Eq. 4.1. The levels $|1\rangle$, $|3\rangle$, $|2\rangle$, and $|m\rangle$ represent the ground state, the $24874_{5/2}$ and $1521_{5/2}$ levels, and a manifold of eleven metastable states, respectively (cf. Fig. 4.5). Ω_j ($j = 1, 2$) is the Rabi frequency to drive the state $|j\rangle$ to the state $|3\rangle$. The state $|3\rangle$ radiatively decays into the states $|1\rangle$, $|2\rangle$ and $|m\rangle$ with rates γ_1 , γ_2 and γ_m . Γ_k ($k = 2, m$) is the quenching rate of the state $|k\rangle$ to the ground state.

where kv is the Doppler width. In Eq. 4.2 we consider vanishing detunings from the transitions $|j\rangle - |3\rangle$. For linearly polarized laser fields, the effective Rabi frequencies Ω'_j are obtained by averaging over the Zeeman sublevels:

$$\Omega_j'^2 = \frac{(2J_j + 1)}{3(2J_j + 1)} \Omega_j^2, \quad (4.3)$$

where J_j is the total angular momentum of the level $|j\rangle$. For our case, the effective Rabi frequencies for the transitions $|1\rangle - |3\rangle$, $|2\rangle - |3\rangle$ are: $\Omega_1'^2 = \frac{1}{2}\Omega_1^2$ and $\Omega_2'^2 = \frac{1}{3}\Omega_2^2$, respectively.

To obtain an analytic solution of the rate equations 4.1, one achieves the population of state $|3\rangle$ as follows:

$$p_3 = [2G_2G_mS_1 + 2G_mS_1S_2] \times \{2G_2G_m + [(1-b)(G_2 + G_m) + 4G_2G_m]S_1 + [(1+b)G_m + 2G_2G_m]S_2 + [(1-b) + 6G_m]S_1S_2\}^{-1}, \quad (4.4)$$

where $G_k = \Gamma_k/\gamma$, ($k = 2, m$). The observed fluorescence rate is proportional to p_3 . If both optical excitations $|j\rangle - |3\rangle$ saturate the corresponding transitions, $S_1 \gg (1+b)G_2/(1-b)$ and $S_2 \gg (G_2 + G_m)$, the fluorescence rate is limited by the quenching relaxation of the state $|m\rangle$:

$$p_3 \approx \frac{2G_m}{1-b}. \quad (4.5)$$

In the absence of the repumping field ($S_2 = 0$), level $|2\rangle$ is depleted only by quenching collisions. In this case, the fluorescence rate is reduced and can be expressed as follows:

$$p_3 \approx \frac{2G_m}{1-b} \frac{G_2}{G_2 + G_m}. \quad (4.6)$$

According to Eq. 4.5 and Eq. 4.6, the fluorescence enhancement factor g due to repumping from level $|2\rangle$ obtained in the limit of high 402-nm and 428-nm laser powers is given by $g=1+\Gamma_m/\Gamma_2$.

Table 4.2: Values for the parameters used for numerical estimation of the quenching rates in Sec. 4.5. The intensity I is given in units of W/cm².

Parameter	Value
Lifetime of the state $ 3\rangle$	$\tau = 23$ ns
Natural linewidth of the state $ 3\rangle$	$\frac{1}{2\pi\tau} \approx 7$ MHz
Branching fraction for decay to state $ 2\rangle$	3×10^{-2}
Branching fraction for decay to state $ m\rangle$	3×10^{-2}
Saturation intensity for the state $ 3\rangle$	27.8 mW/cm ²
Saturation intensity for the state $ 2\rangle$	0.73 mW/cm ²
Doppler width of the $ 1\rangle - 3\rangle$ transition	$kv \approx 2\pi \times 360$ MHz
Effective Rabi frequency for the $ 1\rangle - 3\rangle$ transition	$\Omega'_1 \approx 2\pi \times 29$ MHz \sqrt{I}
Effective Rabi frequency for the $ 2\rangle - 3\rangle$ transition	$\Omega'_2 \approx 2\pi \times 4.8$ MHz \sqrt{I}
Optical pumping rate for the $ 1\rangle - 3\rangle$ transition	$\gamma S_1 \approx 2\pi \times 8.2$ MHz I
Optical pumping rate for the $ 2\rangle - 3\rangle$ transition	$\gamma S_2 \approx 2\pi \times 0.22$ MHz I

Based on the results of the model described above, in the next section we investigate the collisional quenching rates of the $1521_{5/2}$ level, which are populated during continuous excitation of the 402-nm $0_{3/2}-24874_{5/2}$ transition. For doing so, we use the experimental value and the estimated values presented in Table 4.2. Here, the saturation intensity for the 402-nm transition is defined as:

$$I_{sat} = \frac{2\pi\hbar c}{3\tau\lambda^3}, \quad (4.7)$$

where $\Omega^2 = I/I_{sat}\gamma^2$. The saturation intensity for the 428-nm transition is estimated based on the ratio of the branching fractions of the $0_{3/2}-24874_{5/2}$ and $1521_{5/2}-24874_{5/2}$ transitions, i.e. $0.94/0.03 \approx 31$, and the wavelength ratio is given by $(428.10 \text{ nm}/401.91 \text{ nm})^3 \approx 1.2$. Therefore a factor of 38 times between the two saturation intensities of the 402-nm and 428-nm transitions is plausible. The previous assumption is not rigorous since saturation in a 3-level system cannot be defined with a single parameter.

4.5 Quenching rates and population of the $24874_{5/2}$ level

In this section, collisional quenching rates of the $1521_{5/2}$ level and of the manifold of the other metastable levels, which are populated during continuous excitation of the $0_{3/2}$ - $24874_{5/2}$ transition at 402 nm, are reported. For the buffer gases helium, argon, and nitrogen we estimated the quenching rate coefficients applying the equations derived from the 4-level model described in Section 4.4. We studied the effect of additional repumping laser excitation from lowest-lying metastable levels. For all the buffer gases, the maximum reachable population in the $24874_{5/2}$ level with continuous laser excitation were determined.

4.5.1 Estimated collisional quenching rates of the $1521_{5/2}$ state

To estimate collisional quenching rates of the $1521_{5/2}$ level by using Eq. 4.4, we proceeded as follows. Trapped $^{232}\text{Th}^+$ ions collisionally cooled by helium buffer gas at 0.2-Pa pressure were continuously excited by 402-nm radiation tuned to the line center of the $0_{3/2}$ - $24874_{5/2}$ transition. Then, with a constant excitation power of the $0_{3/2}$ - $24874_{5/2}$ transition, the relative increase in the laser-induced fluorescence signal at 402 nm, which results from repumping excitation of the $1521_{5/2}$ - $24874_{5/2}$ transition at 428 nm, was measured. Fig. 4.10 shows the experimental observations. The measurements were obtained for two settings of the 402-nm laser power, which differ by a factor of ≈ 30 . It turns out that the laser-induced fluorescence signal at 402 nm was enhanced by up to a factor of nine at a repumping laser power above 0.5 mW. When the 402-nm excitation power was reduced to $3\ \mu\text{W}$, the laser-induced fluorescence signal at 402 nm was enhanced only by up to a factor of four. If argon was used at the same pressure, the repumping excitation at 428 nm led to a maximum fluorescence enhancement of $g \approx 2$. On the other hand, only a negligible fluorescence enhancement was observed using nitrogen as a buffer gas. In contrast to helium, by using argon and nitrogen buffer gases a weak laser-induced fluorescence signal was also observed if the $^{232}\text{Th}^+$ ions were illuminated only by the 428-nm radiation without excitation at 402 nm. This observation indicates that the $1521_{5/2}$ level can be populated by $\text{Th}^+\text{-Ar}$ and $\text{Th}^+\text{-N}_2$ collisions since the energy of this level corresponds to only $\approx 0.19\ \text{eV}$.

We found a good agreement between the observed fluorescence enhancement factor g and the predictions of Eq. 4.4 with $\Gamma_2 = 20\ \text{s}^{-1}$ for helium. To obtain this value, we proceeded as follows: by using the experimental data for high and low 402-nm excitation power shown in Fig. 4.10 we fitted g , changing Γ_2 in Eq. 4.4 until a good agreement between the measured values and calculated dependencies was obtained. In addition, we used the calculated optical excitation rates and

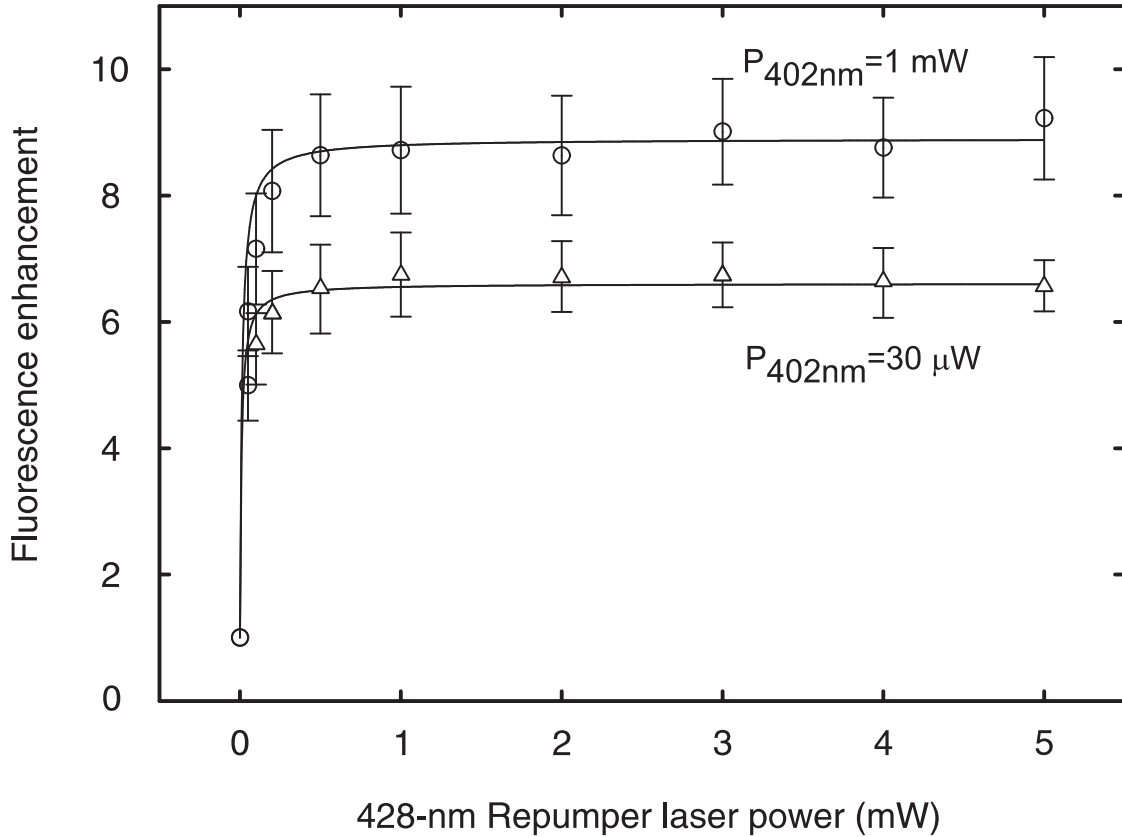


Figure 4.10: Laser-induced fluorescence signal of trapped $^{232}\text{Th}^+$ ions resulting from resonant laser excitation of the 402-nm $0_{3/2}-24874_{5/2}$ transition, showing the fluorescence enhancement due to repumping excitation at 428 nm for 1 mW (circles) and $30\ \mu\text{W}$ (triangles) of 402-nm excitation power. The data points are normalized to the fluorescence levels observed without 428-nm excitation. The dependencies (solid lines) correspond to solutions of Eq. 4.4 using excitation and quenching rate parameters corresponding to the conditions of the experiment.

the natural lifetime shown in Table 4.2 to obtain Γ_2 . The spontaneous-decay branching fractions of the $24874_{5/2}$ state were taken from Ref. [50]. In a similar way, we found quenching rates of the $1521_{5/2}$ level for argon ($\Gamma_2 = 1.5 \cdot 10^3\ \text{s}^{-1}$) and nitrogen ($\Gamma_2 = 5.0 \cdot 10^4\ \text{s}^{-1}$), at 0.2 Pa pressure for all gases. Table 4.3 summarizes the results. The value obtained from the Eq. 4.4 for helium is in agreement with the value measured using time-separated pulsed laser excitation (see Section 4.3.3).

Although the dipole polarizability for argon is higher than for helium ($\alpha_{\text{Ar}}/\alpha_{\text{He}}=8$), the factor of about 75 times in the quenching rates between them cannot be explained by the classical collisional model introduced by Langevin [79]. The diatomic

Table 4.3: Estimated (Eq. 4.4) and measured quenching rates Γ_2 for different buffer gases at 0.2 Pa pressure, and estimated population p_3 in the state $|3\rangle$ (see Fig 4.9) without and with repumping at 428 nm.

Buffer gas	Γ_2 (s^{-1})		p_3	
	estimated	measured	without 428 nm	with 428 nm
Helium	20	13(2)	$1.5 \cdot 10^{-5}$	$1.2 \cdot 10^{-4}$
Argon	$1.5 \cdot 10^3$		$5.0 \cdot 10^{-4}$	$1.0 \cdot 10^{-3}$
Nitrogen	$5.0 \cdot 10^4$		$5.0 \cdot 10^{-3}$	

buffer gas N_2 produces a much higher quenching efficiency than the noble gases. A similar behavior is known for the collisional quenching rates of the metastable D levels in alkali-like ions, see for example Refs. [77, 78]. We additionally investigate the pressure dependence of the fluorescence enhancement factor g for helium. It turns out that the observed variation of g with pressure points to a linear pressure dependence of the rate Γ_2 and to a less than proportional variation of Γ_m with pressure. At a lower buffer gas pressure of ≈ 0.02 Pa, the 428-nm repumping excitation enhances the laser-induced fluorescence signal by $g \sim 20$.

As was described before, the strength of the obtainable fluorescence signal is strongly affected by population trapping in metastable levels. To investigate this effect, we measure the saturation behavior for excitation of the 402-nm transition without radiation at 428 nm. The experimental data is shown in Fig. 4.11, for all the buffer gases studied here. It can be clearly seen that Eq. 4.4 accurately describes the observed saturation behavior for helium, argon and nitrogen. In the case of helium buffer gas, population of the $1521_{5/2}$ state reduces the effective saturation power for excitation of the 402-nm transition to a few microwatts corresponding to an intensity of ≈ 0.3 mW/cm². Bearing in mind that the saturation intensity for the two-level system $0_{3/2}$ - $24874_{5/2}$ is approximately 27.7 mW/cm², it follows that population trapping in the $1521_{5/2}$ state reduces the saturation intensity by two orders of magnitude.

4.5.2 Additional repumping schemes of the $0_{3/2}$ - $24874_{5/2}$ transition

With the purpose of finding conditions, which minimize the population of metastable levels and maximize the population of the $24874_{5/2}$ state, we also investigated extended repumping schemes by means of the fundamental radiation of the picosecond Ti:sapphire laser. In the latter schemes, the $1521_{5/2}$ level as well as higher-lying metastable levels were depleted by laser excitation.

The fundamental wavelength radiation of the picosecond Ti:sapphire laser was tuned to suitable repumping transitions for the six lowest metastable levels above

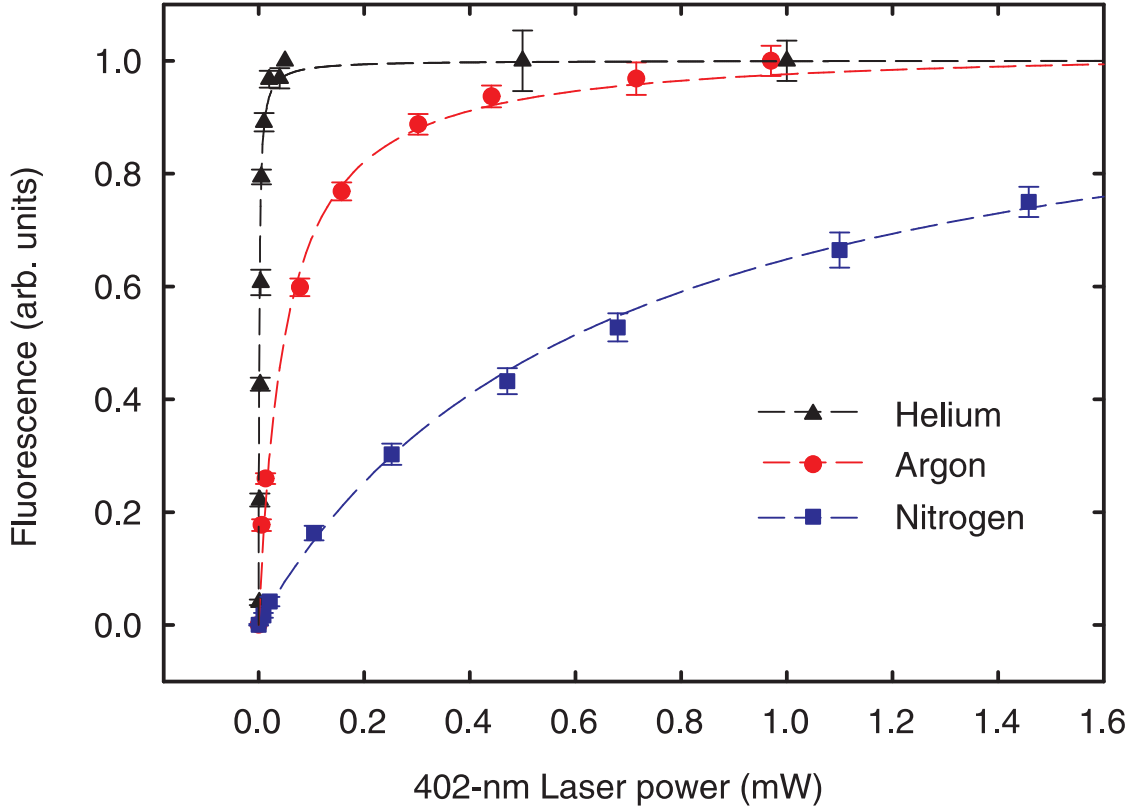


Figure 4.11: Variation of the laser-induced fluorescence signal of trapped $^{232}\text{Th}^+$ ions with laser power resulting from resonant laser excitation of the 402-nm $0_{3/2}$ – $24874_{5/2}$ transition in absence of 428-nm repumping excitation. The data points are normalized to the highest fluorescence levels observed with each separate buffer gas. The solid lines corresponds to the solution of Eq. 4.4.

the $1521_{5/2}$ level with *even* parity (see Fig. 2.3 for a comprehensive look of the electronic energy levels of Th^+). The latter mentioned six levels are populated by spontaneous decay from the $24874_{5/2}$ level. A fluorescence enhancement of approximately a factor of 3 and a factor of 1.5 was observed for excitation of the $4113_{5/2}$ – $17122_{3/2}$ and $4146_{7/2}$ – $16033_{5/2}$ transition, respectively. For these observations, helium was used as a buffer gas at 0.2 Pa. Table 4.4 shows the extended repumping excitations using the fundamental radiation of the picosecond Ti:sapphire laser. Excitation from higher-lying metastable levels, ranging from 5000 cm^{-1} to 7000 cm^{-1} , and excitation from metastable levels with *odd* parity does not lead to any significant increase in the laser-induced fluorescence signal in the $24874_{5/2}$ level. In total, the fundamental wavelength radiation was tuned to several suitable repumping transitions ranging from 750 nm to 840 nm. The depletion of the

1860_{3/2} level increased the laser-induced fluorescence signal in the 24874_{5/2} level only if there was no repumping excitation from the 1521_{5/2} level. This can be explained by a collision-induced population transfer between the 1521_{5/2} and 1860_{3/2} levels, whose energy difference (≈ 0.042 eV) is comparable to the kinetic energy of the buffer gas atoms at room temperature. Also these two metastable levels present a strong mixing in their electronic configuration, see Ref. [48]. In addition, the second-harmonic wavelength radiation of the picosecond Ti:sapphire laser was tuned from 395 nm to 415 nm for another six metastable levels (ranging from 6000 cm⁻¹ to 14 000 cm⁻¹) but no significant increase in the fluorescence signal in the 24874_{5/2} level was observed. With argon or nitrogen buffer gas, repumping from the energy levels above the 1521_{5/2} level does not result in any significant fluorescence enhancement, indicating that the quenching efficiency obtained with these gases is like than the realized laser repumping rate.

Table 4.4: Additional repumping transitions using the fundamental wavelength output of the picosecond Ti:sapphire laser. The depletion from the 1860_{3/2} level was efficient only if there was no repumping excitation from the 1521_{5/2} level. Helium was used as a buffer gas at a pressure of 0.2 Pa.

Lower level (cm ⁻¹)	Higher level (cm ⁻¹)	Wavelength (nm)	Fluorescence enhancement
1860	14 102	817	2
4113	17 122	769	3
4146	16 033	841	1.5

4.5.3 Population of the 24874_{5/2} level in continuous laser excitation

Table 4.3 shows the inferred effective quenching rates together with the calculated population probability of the 24874_{5/2} level under cw laser excitation for the three gases used in our investigations. For helium, additional repumping from the 4113_{5/2} level and the 4146_{7/2} level yielded a maximum population of $5.4 \cdot 10^{-4}$ in the 24874_{5/2} level. For all experimental conditions studied here, population trapping in low-lying metastable levels limits the obtainable population of the 24874_{5/2} state. In previous experiments with trapped Th⁺ ions, molecular hydrogen and helium buffer gases were compared, and hydrogen was found to produce ≈ 100 times higher fluorescence signal at the same pressure [58]. In our experiment, the diatomic buffer gas nitrogen shows an even stronger quenching efficiency. From the maximum fluorescence signal resulting from resonant laser excitation of the 402-nm 0_{3/2}-24874_{5/2} transition with nitrogen, we deduce that more than 100 photons/s

per ion are detected, thus providing efficient diagnostics of the trapped ions on the timescale expected for the decay of the ^{229}Th isomeric state [56]. While nitrogen produces the highest laser-induced fluorescence rate and most efficient collisional cooling, the noble gases offer the advantage that they can be purified more efficiently using getter materials and cryogenic traps and therefore enabling longer storage times for Th^+ .

In our experiment, we observe a considerable reduction of the storage times for Th^+ using the diatomic buffer gas nitrogen instead of the noble gases. In the next Chapter, most of the experiments are conducted using argon as a buffer gas in combination with the repumping laser at 428 nm. These conditions are chosen in order to achieve a compromise between the obtainable population of the $24874_{5/2}$ state and the storage times for Th^+ . Additionally, the quenching rates Γ_2 (Table 4.3) are of interest because they permit to select the suitable repetition rate in pulsed laser excitation. In the next Chapter, the latter excitation using the third-harmonic of a nanosecond Ti:sapphire laser in two-photon excitation will be used to investigate the electronic level structure of $^{232}\text{Th}^+$ in the energy range of the ^{229}Th isomeric state.

5 Two-photon laser excitation of trapped $^{232}\text{Th}^+$ ions

5.1 Introduction

This chapter describes two-photon laser excitation using two extended-cavity diode lasers on the $0_{3/2}$ – $24\,874_{5/2}$ transition at 402 nm and the $24\,874_{5/2}$ – $49\,960_{7/2}$ transition at 399 nm. The level at $49\,960_{7/2}$ is one of the highest-lying tabulated energy levels that can be excited by an electric-dipole transition from the $24\,874_{5/2}$ state. The energy of the $49\,960_{7/2}$ state corresponds to 6.2 eV, which is of interest as a test case for the search for higher-lying levels in the range above $60\,000\text{ cm}^{-1}$ (7.4 eV). Furthermore, in continuous excitation, we study the effect of co- and counterpropagating 402- and 399-nm excitation beams and the transferred population from the intermediate state ($24\,874_{5/2}$) to the excited state ($49\,960_{7/2}$). This shows that also, in the case of the complex level-structure of $^{232}\text{Th}^+$, cw two-photon excitation of highly excited states can be achieved.

In order to carry out a two-photon excitation of unknown higher-lying levels in $^{232}\text{Th}^+$, we study pulsed optical excitation by means of harmonic radiation of a pulsed nanosecond Ti:sapphire laser in combination with synchronized 402-nm ECDL pulses. Since the strength of the obtainable fluorescence signal is strongly affected by population trapping in metastable levels (see Section 4.3.2), here we make use of the advantage that in pulsed optical excitation a significantly higher population in the $24\,874_{5/2}$ level can be achieved to accomplish a two-photon excitation to the $49\,960_{7/2}$, $51\,268_{7/2}$ and to seven previously unknown higher-lying states. An additional favorable condition of the pulsed laser excitation is the peak power in the kilo-Watt range, useful for searching weak electric-dipole transitions from the $24\,874_{5/2}$ state to higher-lying states above $60\,000\text{ cm}^{-1}$.

The seven energy levels in Th^+ have not been previously reported and are in the energy range from $62\,849\text{ cm}^{-1}$ (7.79 eV) to $64\,874\text{ cm}^{-1}$ (8.04 eV). This investigation of the electronic level structure of Th^+ in the energy range of the ^{229}Th isomeric state is of importance because it enables the search for a resonant two-photon electronic bridge excitation of the ^{229}Th nucleus [13]. A comparison of the fluorescence signals observed with $^{229}\text{Th}^+$ and $^{229\text{m}}\text{Th}$ with $^{232}\text{Th}^+$ will indicate the population of the isomeric nuclear level in $^{229}\text{Th}^+$.

5.2 Two-photon laser excitation using ECDLs in continuous excitation

Here we show two-photon laser excitation using two extended-cavity diode lasers. For the first excitation step, we used the previous investigated strongest resonance line at 402 nm, and for the second excitation step, we used laser radiation at 399 nm to the state at $49\,960_{7/2}$. The level at $49\,960_{7/2}$ is one of the highest-lying tabulated energy levels that can be excited by an electric dipole transition from the $24\,874_{5/2}$ state and its radiative lifetime appears to be unknown. Apart from the direct decay channel from the $49\,960_{7/2}$ state at 399 nm to the $24\,874_{5/2}$ level, there are seventeen tabulated decay channels to other levels [48].

5.2.1 Lasers arrangement and partial level scheme

The laser system used to carry out optical excitation of $^{232}\text{Th}^+$ ions, consisted of three ECDLs emitting at 402 nm, 428 nm and 399 nm. The experimental apparatus is partially shown in Fig. 3.4, where the two ECDLs at 402 nm and 399 nm were used in continuous excitation. The average excitation power was 1 mW, 3 mW and 1.5 mW for the ECDL at 402 nm, 428 nm and 399 nm, respectively. Figure 5.1 shows the partial level scheme used in this section. The repumping radiation at 428 nm was tuned to the line center of the $1521_{5/2}$ – $24\,874_{5/2}$ transition and was overlapped copropagating with the 402-nm beam. Excitation to the $49\,960_{7/2}$ level was detected by monitoring the fluorescence emission in the wavelength range 240–320 nm, and the wavelength range around 400 nm was used to monitor the laser-induced fluorescence signal of the $24\,874_{5/2}$ state (see Section 3.6 for filter properties and PMT spectral sensitivities).

5.2.2 Experimental results

To carry out two-photon excitation of the $49\,960_{7/2}$ state, the frequency of the first excitation step at 402 nm was scanned across the $0_{3/2}$ – $24\,874_{5/2}$ transition, and, the second excitation step at 399 nm was tuned to the center of the $24\,874_{5/2}$ – $49\,960_{7/2}$ transition. Figure 5.2 shows Doppler broadened excitation spectra of $^{232}\text{Th}^+$ ions at 402 nm along with a Doppler-free fluorescence dip resulting from resonant excitation of the $24\,874_{5/2}$ – $49\,960_{7/2}$ transition. The measurements were performed using argon as a buffer gas at 0.2 Pa pressure. In this case, the fluorescence dip at the top of the Doppler-broadened spectrum shows that about 15 % of ions are transferred from the $0_{3/2}$ – $24\,874_{5/2}$ excitation cycle if the $24\,874_{5/2}$ – $49\,960_{7/2}$ transition is resonantly excited.

Figure 5.3 shows the excitation spectrum obtained when the first excitation step at 402 nm was tuned to the center of the $0_{3/2}$ – $24\,874_{5/2}$ transition and the frequency

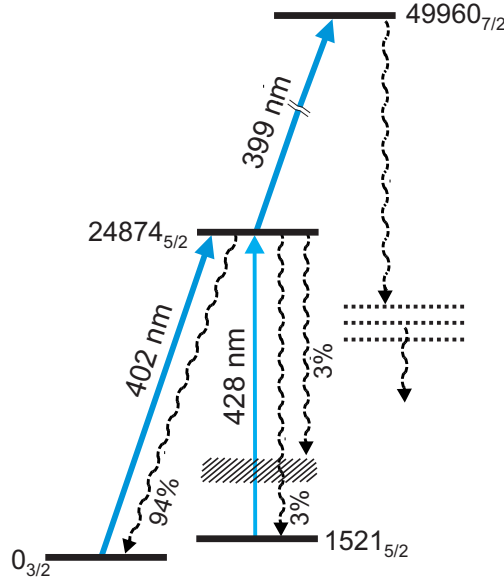


Figure 5.1: Relevant energy levels of the thorium ion Th^+ showing the main resonance transitions studied in this section and the lowest-lying metastable levels. The hatched area corresponds to a manifold of eleven metastable states. For the $24874_{5/2}$ level the spontaneous-decay branching fractions are indicated as given in Ref. [50].

of the second excitation step at 399 nm was scanned across the $24874_{5/2}$ – $49960_{7/2}$ transition. This two-photon excitation spectrum was observed for counterpropagating 402-nm and 399-nm excitation beams using helium buffer gas at 0.2 Pa pressure. The fluorescence signal observed in the 400-nm range, also shown in Fig. 5.3, indicates the population of the intermediate $24874_{5/2}$ level. The resonant reduction of this fluorescence shows that a substantial fraction of ions ($\approx 20\%$ for counterpropagating beams) is transferred from the $0_{3/2}$ – $24874_{5/2}$ excitation cycle if the $24874_{5/2}$ – $49960_{7/2}$ transition is resonantly excited. Taking into account the previously calculated population probability for the intermediate state (see Section 4.5.3), we estimate that less than 10^{-4} ions are excited to the upper state. The observed variation of the $49960_{7/2}$ level fluorescence strength with the excitation power of the 399-nm laser, points to a linear dependence in the range from $100\ \mu\text{W}$ to $2\ \text{mW}$ (in intensity: from $13\ \text{mW}/\text{cm}^2$ to $0.3\ \text{W}/\text{cm}^2$). This result indicates that we do not reach the saturation power of the $24874_{5/2}$ – $49960_{7/2}$ transition with the available laser power.

In our case, one expects that both, stepwise and direct two-photon excitation processes contribute to the population of the $49960_{7/2}$ level. The stepwise two-photon

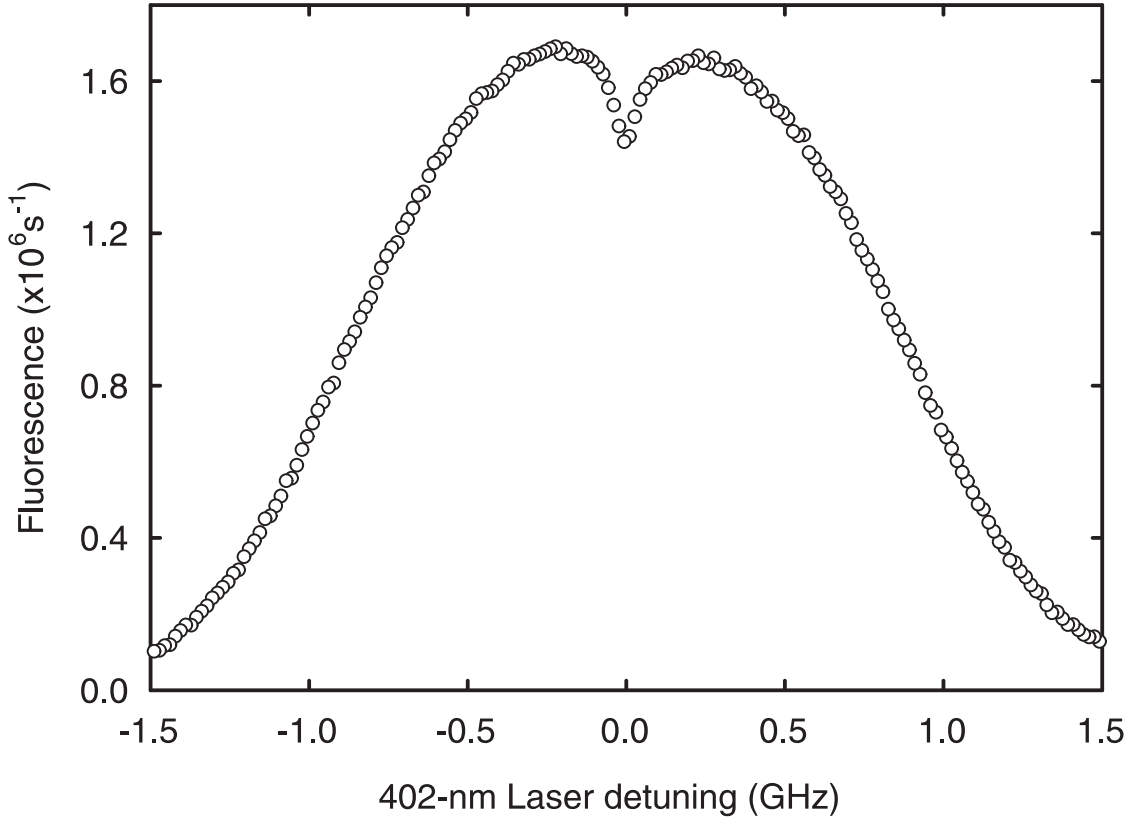


Figure 5.2: Laser excitation spectrum for counter-propagating laser beams, showing Doppler broadened excitation of the intermediate $24\,874_{5/2}$ state at 402 nm and Doppler free fluorescence dip resulting from two-photon excitation. Radiation at 399 nm is tuned to the line center of the $24\,874_{5/2}$ – $49\,960_{7/2}$ transition and 402 nm light is scanned in the range of the $0_{3/2}$ – $24\,874_{5/2}$ transition.

excitation is the population of the upper state via population of the intermediate state. It can be expressed as follows

$$\nu_{L1} = \nu_{12} \quad \nu_{L2} = \nu_{23} , \quad (5.1)$$

where ν_{L1} (ν_{L2}) is the frequency of the first (second) laser and ν_{12} (ν_{23}) is the frequency of the $0_{3/2}$ – $24\,874_{5/2}$ transition ($24\,874_{5/2}$ – $49\,960_{7/2}$ transition). On the other hand, direct two-photon excitation is obtained when the two-photon resonance condition is fulfilled by:

$$\nu_{L1} + \nu_{L2} = \nu_{13} , \quad (5.2)$$

where ν_{13} is the frequency of the $0_{3/2}$ – $49\,960_{7/2}$ transition.

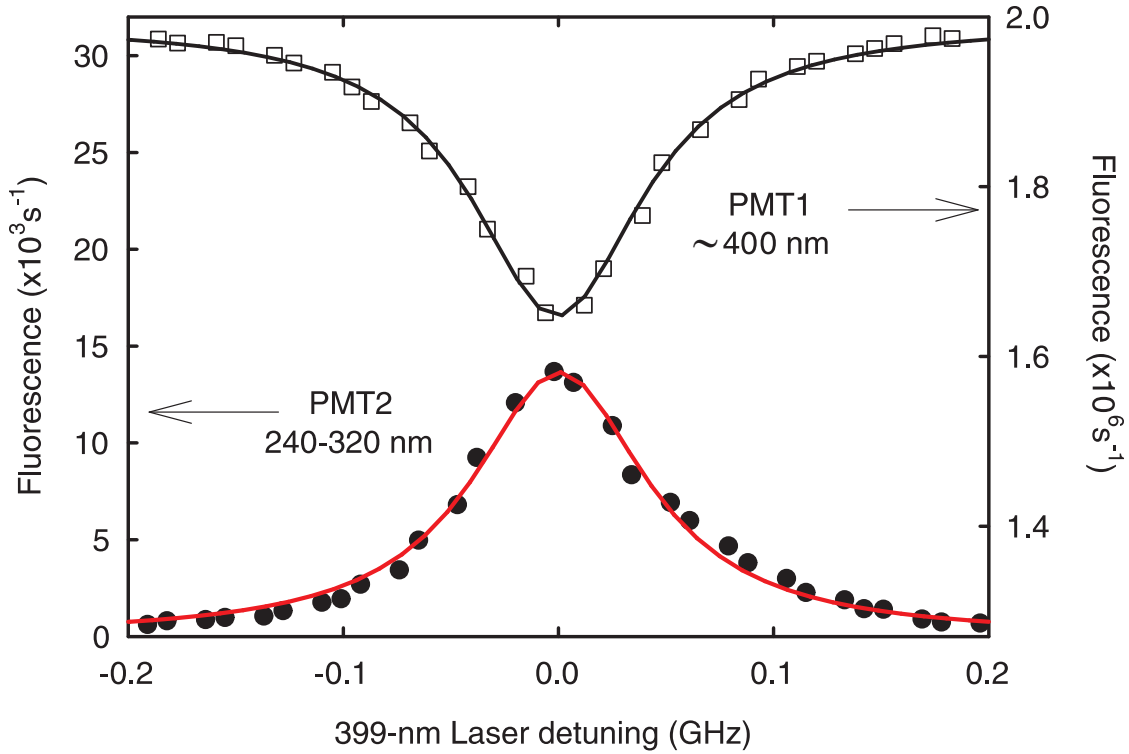


Figure 5.3: Two-photon laser excitation spectrum for counter-propagating laser beams, showing fluorescence signals from the upper $49960_{7/2}$ level (filled circles) and from the intermediate $24874_{7/2}$ state (open squares). Radiation at 402 nm is tuned to the line center of the $0_{3/2}$ – $24874_{5/2}$ transition and 399 nm light is scanned in the range of the $24874_{5/2}$ – $49960_{7/2}$ transition. The solid lines are fits to Lorentzian line shapes.

Figure 5.4 shows two-photon laser excitation spectra for co- and counterpropagating laser beams, depicting fluorescence signals from the upper $49960_{7/2}$ state. With counterpropagating beams, the width of the two-photon resonance is narrower and the fluorescence signal is approximately 1.5 times higher than with copropagating beams. In the copropagating case the sub-Doppler resonance populating the $49960_{7/2}$ level is formed predominantly by stepwise two-photon excitation, while in the counterpropagating case an additional contribution of direct two-photon excitation appears (see Ref. [80]). A similar feature was observed in a previous investigation on two-photon excitation between lower-lying energy levels ($0_{3/2}$ – $17121_{3/2}$ as a first excitation step and $17122_{3/2}$ – $34543_{5/2}$ as a second excitation step) of trapped Th^+ ions [58].

The calculated line shapes illustrated in Fig. 5.4 are based on the model presented in Ref. [81]. Here, we used the approximation in which the intermediate state

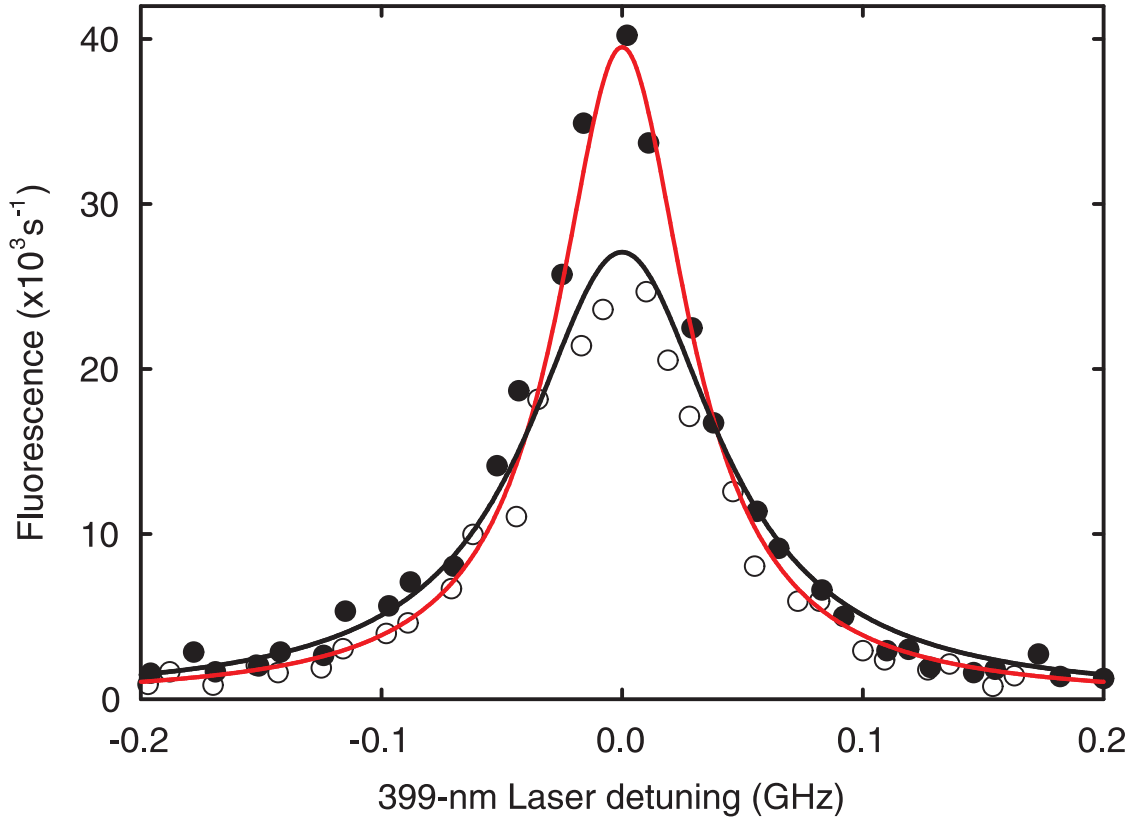


Figure 5.4: Laser-induced fluorescence signal of trapped $^{232}\text{Th}^+$ ions resulting from two-photon laser excitation of the $49\,960_{7/2}$ level. The spectra are detected by monitoring the fluorescence emission in the wavelength range 240–320 nm. Filled circles: counterpropagating beams; open circles: copropagating beams. The red (counterpropagating beams) and black (copropagating beams) solid lines correspond to calculations based on the model from Ref. [81].

is resonantly excited; for further details, see the theory developed in Ref. [81]. For our case, this occurs when the line center of the $0_{3/2}\text{--}24\,874_{5/2}$ transition is excited by cw radiation at 402 nm. For these calculations, we used the homogeneous width of the 402 nm transition, which was inferred from the Doppler-free saturation resonances of the transition at 402 nm (see Section 4.3.1). There, we observed a minimum width of 26(2) MHz. For the fitting of the two-photon lineshapes, good agreement with theory was obtained for a width of the $24\,874_{5/2}\text{--}49\,960_{7/2}$ resonance, which is approximately four times bigger than the width of the $24\,874_{5/2}$ resonance. This results in a radiative lifetime of $\tau \approx 6$ ns for the $49\,960_{7/2}$ state. The resulting linewidths for excitation with co- and counterpropagating laser beams

are 95 MHz (black solid line in Fig. 5.4) and 66 MHz (red solid line in Fig. 5.4), respectively.

In order to carry out low-resolution spectroscopy over extended wavelength ranges, we tried to use the second-harmonic radiation of a picosecond pulsed Ti:sapphire laser for the second excitation step from the $24\,874_{5/2}$ intermediate state. Unfortunately, using this laser did not allow us to observe the excitation of higher-lying states. One disadvantage of this laser system to accomplish two-photon excitation of unknown higher-lying levels above $60\,000\text{ cm}^{-1}$, is that the power in each longitudinal mode is in the order of a few microwatts only (assuming 50 mW in average power). Another disadvantage is that the broad spectrum, emitted by this laser, also excites several resonances from low-lying metastable levels simultaneously. In the case studied here (see partial level scheme in Fig. 5.1), we observed that the broad spectrum of the picosecond pulsed Ti:sapphire laser also excited the $1521_{5/2}$ – $26\,586_{3/2}$ transition at 398.9 nm and the $1860_{1/2}$ – $26\,965_{3/2}$ transition at 398.2 nm. The latter observation did not allow us to identify a fluorescence signal from the two-photon excitation of the $24\,874_{5/2}$ – $49\,960_{7/2}$ transition.

5.2.3 Conclusion

In conclusion, we have demonstrated two-photon excitation of $^{232}\text{Th}^+$ through the intermediate state at $24\,874_{5/2}$ by means of continuous laser excitation from two extended-cavity diode lasers. This shows that also in the case of the complex level-structure of Th^+ , two-photon excitation of highly excited states can be achieved. Since, in continuous excitation, only a small fraction of ions (less than 10^{-4}) are transferred to the excited state via the $24\,874_{5/2}$ state, we elaborate on nanosecond pulsed optical excitation for a two-photon excitation of the $49\,960_{7/2}$ and $51\,268_{7/2}$ states using the harmonic radiation of a pulsed nanosecond Ti:sapphire laser (with narrower linewidth in comparison with the picosecond pulsed Ti:sapphire laser) in combination with synchronized 402-nm ECDL pulses. In the following, this pulsed optical excitation will be used for searching for previously unknown transitions from the $24\,874_{5/2}$ state to higher-lying states above $60\,000\text{ cm}^{-1}$.

5.3 Two-photon laser excitation with nanosecond pulsed Ti:sapphire laser

This section illustrates two-photon excitation by means of harmonic radiation from a pulsed nanosecond Ti:sapphire laser in combination with synchronized 402-nm ECDL pulses. Henceforth, we take the advantage that in pulsed optical excitation a significantly higher population in the $24\,874_{5/2}$ level can be achieved (see Section 4.3.2). Here, we study two-photon laser excitation using pulsed laser excitation from the $0_{3/2}$ – $24\,874_{5/2}$ transition at 402 nm to the levels at: $49\,960_{7/2}$ and $51\,268_{7/2}$

by means of the second-harmonic of a pulsed nanosecond Ti:sapphire laser. The latter is of interest as a test case for the search for unknown higher-lying levels in the range above $60\,000\text{ cm}^{-1}$. Thus, after optimizing the detection parameters with energy levels reported in the literature for Th^+ , we carried out an investigation for unknown energy levels above $60\,000\text{ cm}^{-1}$ by means of third-harmonic radiation of the pulsed nanosecond Ti:sapphire laser.

5.3.1 Fluorescence detection in nanosecond pulsed laser excitation

In order to achieve a higher population in the intermediate state ($24\,874_{5/2}$ level at 402 nm), and consequently in the excited state, we elaborate on nanosecond pulsed laser excitation by modulating the 402 nm radiation. Additionally, these 402-nm pulses will be synchronized with a nanosecond pulsed Ti:sapphire laser for a two-photon excitation of unknown higher-lying states. The 402-nm radiation was amplitude-modulated to produce pulses using a fiber-coupled AOM with a rise time of approximately 9 ns. The fluorescence emission of the trapped $^{232}\text{Th}^+$ ions was detected with the use of a photomultiplier together with a fast gated integrator to record and to average the time-integrated fluorescence signal during the detection gate (see Fig. 5.5 and Fig. 5.6). The gated integrator normalized the average of the input signal by the gate width (through N pulses) to provide an output voltage. The latter was acquired with an analog interface for computer data acquisition. Fig. 5.5 shows the electronic and the optical setup for pulsed laser excitation, and Fig. 5.6 shows the complete time sequence for pulses used in our experiments.

The main time sequence was triggered by pulses from a generator at 1–4 kHz frequency (constrained by the repetition rate of the nanosecond Ti:sapphire laser). Then, with the delay generator 1 (in external rising edge trigger from the generator), we controlled the pulse delay of: the nanosecond Ti:sapphire laser, the 402-nm AOM, the gated integrators 1 and 2, and the AOM for the photodissociation picosecond Ti:sapphire laser. Also, with this delay generator, we regulated the pulse durations of the 402-nm and photodissociation picosecond Ti:sapphire lasers. With the delay generator 2 (in external rising edge trigger from the sequence former), the pulses to reset the gated integrators after each data acquisition were generated. In addition, with this generator, we produced the trigger for the photon counter (this was used for detection of high-energy photons from higher-lying states). The gated integrators were set to average the time-integrated signal over 300 pulses of the lasers. When the gated integrators recorded the previously described signal after 300 pulses, the sequence former sent a TTL output pulse to the data acquisition computer interface (in external falling edge trigger) and a single analog data is acquired. Afterward, the reset pulse erases the information in the gated

integrators and these are ready for a new measurement. The overall sequence time is approximately 0.32 s and is also shown in Fig. 5.6.

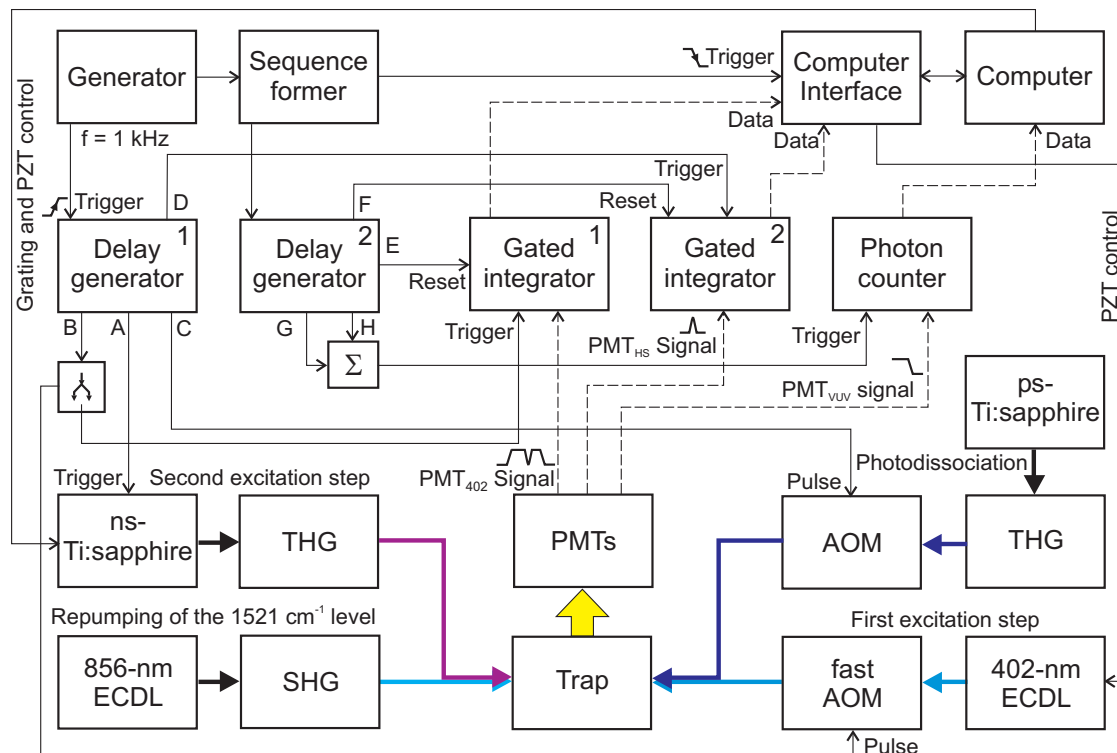


Figure 5.5: Electronic and optical setup for nanosecond pulsed laser excitation showing the data acquisition flow and pulsed control of the acoustic-optical modulators. The dashed lines correspond to the fluorescence signals from the photomultipliers. See Fig. 5.6 for the detailed time sequence of the used pulses.

5.3.2 Nanosecond pulsed laser excitation of the $24874_{5/2}$ level at 402 nm

The previously described time sequence and fast modulation for the 402-nm radiation was used to achieve a higher population in the $24874_{5/2}$ state. For this experiment, we used argon at 0.2 Pa pressure as a buffer gas and the ion production via photoablation was carried out with a pulsed Nd:YAG laser. The beam diameter for the 402-nm radiation in the trap was 1 mm. Figure 5.7 shows saturation of the laser-induced fluorescence signal for the $0_{3/2}-24874_{5/2}$ transition at 402 nm with (blue curve) and without (red curve) repumping excitation at 428 nm. Here, the 402-nm radiation was modulated to produce pulses of 35 ns duration and

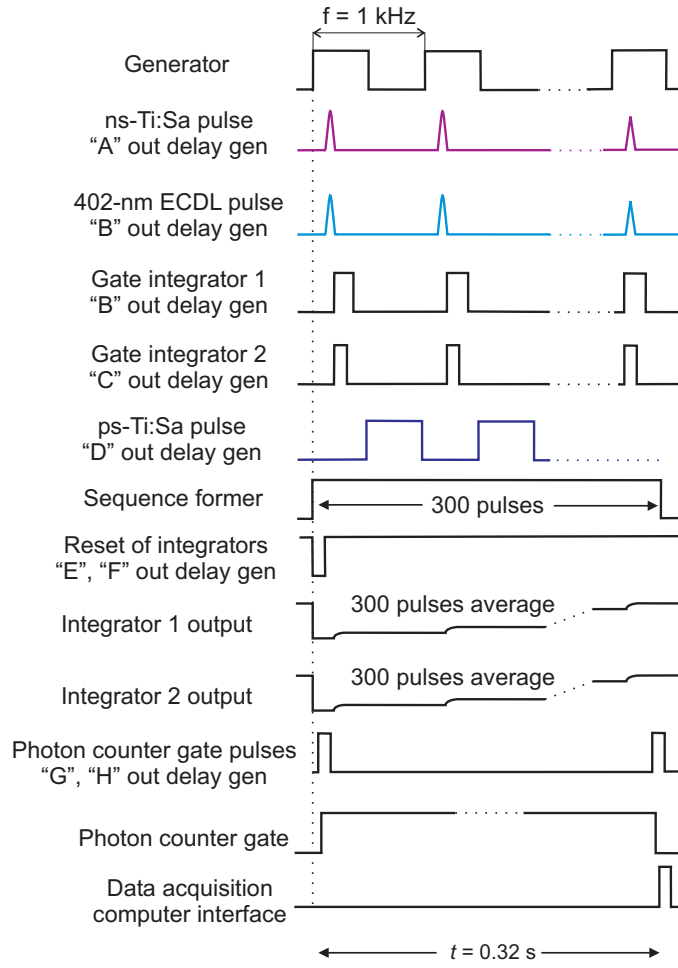


Figure 5.6: Time sequence for nanosecond pulsed laser excitation used for fluorescence detection and pulsed control of the acoustic-optical modulators.

the 428-nm light was used in cw mode. The detection window of the gated integrator was 100 ns, which yielded the maximum signal-to-noise ratio observed. In order to compensate variations in fluorescence strength caused by fluctuations of the number of loaded ions, the pulsed laser-induced fluorescence signal registered was normalized to the signal resulting from fixed conditions of cw excitation at 402 nm. In the data displayed in Fig. 5.7, we estimated a saturation pulse power of 1.9 mW and 1.5 mW with and without repumping excitation, respectively. The latter was obtained using the equation:

$$y_{sat} = C \frac{x/P_{sat}}{(1 + x/P_{sat})}, \quad (5.3)$$

where C is the maximum fluorescence signal and P_{sat} is the power when C reaches 50% of its value.

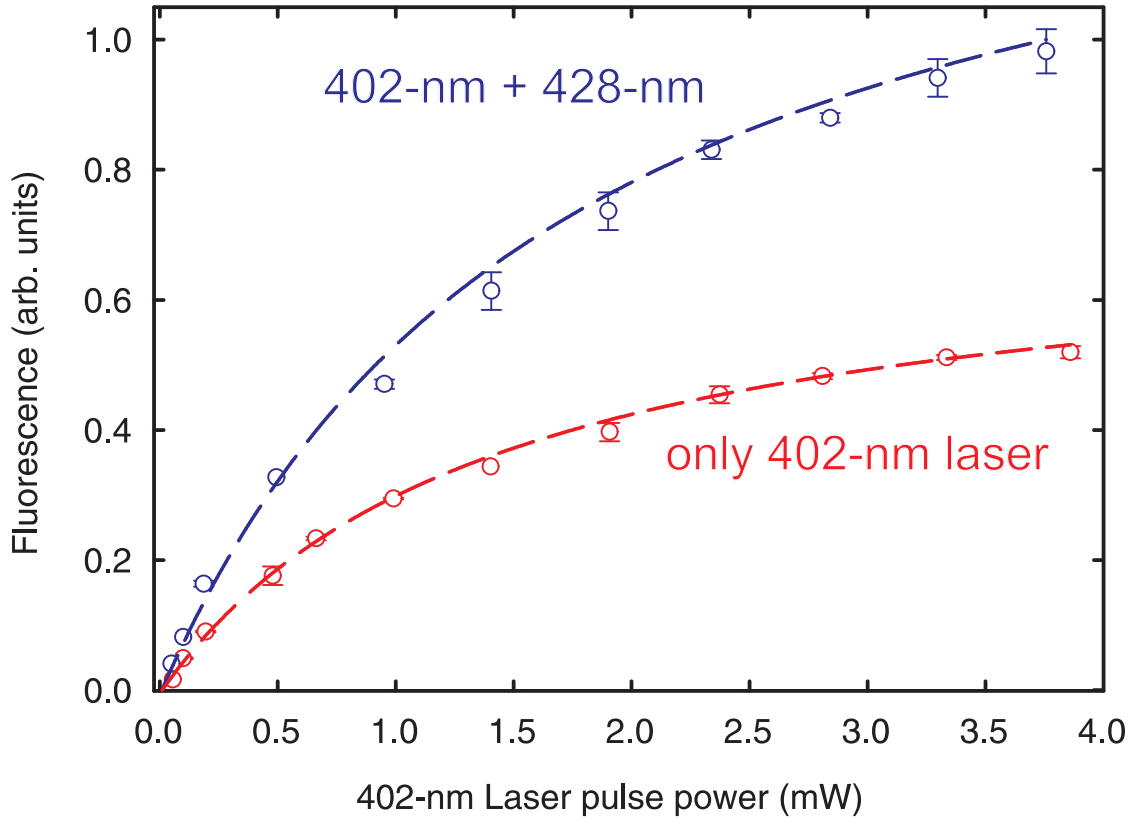


Figure 5.7: Saturation of the fluorescence signal of trapped $^{232}\text{Th}^+$ ions resulting from pulsed laser excitation of the $24874_{5/2}$ level with (blue curve) and without (red curve) repumping excitation at 428 nm. The dashed line is a fit to a saturation curve of the form of Eq. 5.3. The error bars reflect the fluctuations of the number of loaded ions.

The resulting saturation pulse intensity of $\approx 200 \text{ mW/cm}^2$ for the $0_{3/2}-24874_{5/2}$ transition at 402 nm is nearly 3 orders of magnitude higher than for cw excitation measured in Section 4.5.1 and is also about 1 order of magnitude higher than for a two-level system $0_{3/2}-24874_{5/2}$. A similar increase in the average population of the $24874_{5/2}$ level can be expected during the pulsed excitation. In Fig. 5.7 we did not observe characteristic Rabi oscillations since the duration of the 402-nm pulses is in the same order of magnitude as the natural lifetime of the $24874_{5/2}$ state and also because of the relative low pulse power used.

The quenching rate Γ_2 obtained in Section 4.5.1 for the $1521_{5/2}$ level was confirmed using 402-nm pulses of $\approx 35 \text{ ns}$ duration. In this situation, we could increase the repetition rate of the 402-nm pulses up to 5 kHz, using argon as a buffer gas, without any substantial reduction in the detected laser-induced fluorescence signal. This observation is in agreement with the quenching rate of $\Gamma_2 = 1.5 \cdot 10^3 \text{ s}^{-1}$

previously estimated. Based on these observations, 1 kHz of repetition rate and argon as a buffer gas were chosen, in order to maximize the population transfer to excited states for synchronized pulsed excitation.

5.3.3 Pulsed two-photon excitation to the levels at: 49 960_{7/2} and 51 268_{7/2}

In order to optimize the detection parameters and the laser pulses for nanosecond pulsed laser excitation, we carried out two-photon excitation of the 24 874_{5/2}–49 960_{7/2} transition at 399 nm as previously observed with ECDL excitation (see Section 5.2) and the 24 874_{5/2}–51 268_{7/2} transition at 379 nm. A beam of the second-harmonic radiation from the nanosecond Ti:sapphire laser, whose frequency was tuned to the line center of the 24 874_{5/2}–49 960_{7/2} transition or the 24 874_{5/2}–51 268_{7/2} transition, was overlapped copropagating with the 402-nm beam. Here, the 428-nm radiation was not employed. In Fig. 5.8 the timing used in these experiments for the pulses of the lasers and detection is presented. The maximum signal-to-noise ratio was found with the following detection window for τ_1 : 625 ns, 100 ns, and 100 ns for fluorescence signal from the 49 960_{7/2} state, depletion of the 24 874_{5/2} state, and fluorescence signal from the 51 268_{7/2}, respectively. See Section 3.6 for a complete description of the spectral filters, dichroic beam splitter and spectral sensitivity ranges of the PMT employed for fluorescence emissions associated with one- and two-step excitations.

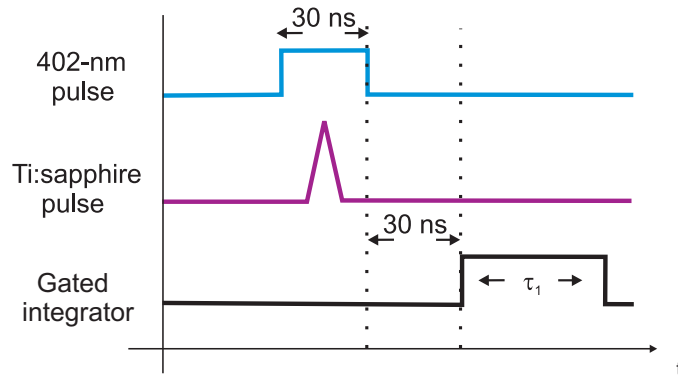


Figure 5.8: Timing used for the gated integrator, 402-nm laser, and nanosecond pulsed Ti:sapphire laser. The detection window τ_1 of the gated integrator depends on the excited state (see text).

Excitation to the 49 960_{7/2} level was detected by monitoring the fluorescence emission in the wavelength range below 320 nm, which was mostly fluorescence emission of the 49 960_{7/2} level to states at about 16 000 cm⁻¹. From the observed saturation of the laser-induced fluorescence signal for the 24 874_{5/2}–49 960_{7/2} tran-

sition, we could infer the saturation peak power of approximately 1.8 W corresponding to an intensity of $\approx 0.23 \text{ kW/cm}^{-2}$. Here, we observed a laser-induced fluorescence signal within a range of 8 GHz of scanning the Ti:sapphire laser across the $24\,874_{5/2}$ – $49\,960_{7/2}$ transition, clearly determined by the spectral distribution of the employed laser. Observation of the depletion signal from the $24\,874_{5/2}$ state at 402 nm was not possible for two-photon excitation at 399 nm, due to the stray light from the Ti:sapphire laser since the proximity of the two excitation wavelengths did not allow blocking of the latter by an optical filter.

In order to maximize the efficiency of fluorescence detection in the intermediate state (i.e. the depletion signal when 402-nm is selected), we investigated two-photon excitation on the $24\,874_{5/2}$ – $51\,268_{7/2}$ transition at 379 nm. The level at $51\,268_{7/2}$ is tabulated in Ref. [48] and its radiative lifetime appears to be unknown. The $24\,874_{5/2}$ – $51\,268_{7/2}$ transition at 379 nm in Th^+ had not been observed in the discharge spectra reported in Refs. [48, 49].

By monitoring the fluorescence emission in the wavelength range around 400 nm, we observed multiple depletion resonances in the Doppler-broadened spectrum showing that a fraction of ions is transferred from the $0_{3/2}$ – $24\,874_{5/2}$ excitation cycle if the $24\,874_{5/2}$ – $51\,268_{7/2}$ transition is resonantly excited. An explanation of this spectrum will be given in the next subsection, when we also show a similar spectrum obtained for a different excited state. We also observed this transition by monitoring the fluorescence emission in the wavelength range 240–320 nm, where from the observed saturation of the fluorescence signal, we could estimate the saturation peak power of approximately 1.7 W corresponding to an intensity of $\approx 0.22 \text{ kW/cm}^{-2}$.

5.3.4 First observation of high-lying states of Th^+ around 8 eV

In order to obtain information on the electronic level structure of the Th^+ ion in the previously unexplored region above $60\,000 \text{ cm}^{-1}$ (7.4 eV), we carried out a pulsed two-photon laser excitation to higher-lying levels in the range from $62\,849 \text{ cm}^{-1}$ (7.79 eV) to $64\,874 \text{ cm}^{-1}$ (8.04 eV) via the $24\,874_{5/2}$ intermediate state. This energy range is of interest since, as it was pointed out in Section 2.2.3, the higher the density of electronic energy states in Th^+ , the higher may be the probability for a pronounced resonance enhancement of inverse electronic bridge processes leading to excitation of the ^{229}Th nucleus [13].

In our experiment, a beam of the third-harmonic radiation from the nanosecond pulsed Ti:sapphire laser, was overlapped counterpropagating with the 402-nm beam and copropagating with the 428-nm radiation. Figure 5.9 shows the partial level scheme used for two-photon excitation, along with the wavelength ranges used to discriminate between the fluorescence emissions associated with depletion of the

intermediate state (PMT1) when the 402-nm signal is selected, and excitation of the upper state (PMT3) when the 402-nm signal is blocked.

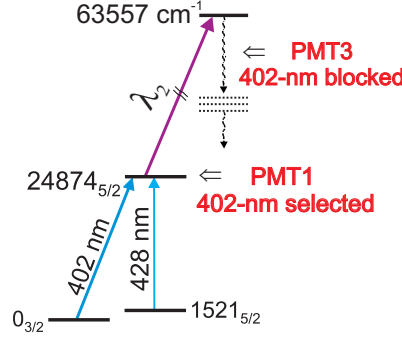


Figure 5.9: Relevant energy levels of the thorium ion Th⁺ showing an example of excitation of the 63 557.61 cm⁻¹ state, along with two PMT used for monitoring the fluorescence emission from the high-lying states (PMT3) when the 402-nm signal is blocked, and depletion signal of the intermediate state at 24 874_{5/2} (PMT1) when the 402-nm signal is selected. λ_2 corresponds to the frequency of the third-harmonic radiation from the Ti:sapphire laser tuned to the line center of the 24 874_{5/2}–63 557.61 cm⁻¹ transition at 258.5 nm.

Figure 5.10 displays the excitation spectrum of the 63 557.61 cm⁻¹ state observed by monitoring the fluorescence emission in the wavelength range around 400 nm. Here, we observed a Doppler-broadened laser excitation spectrum of the 402-nm transition with multiple fluorescence depletion signals resulting from two-photon excitation. This can be explained by the fact that the third-harmonic laser spectrum of the Ti:sapphire laser consists of ≈ 50 longitudinal modes distributed over the ≈ 30 GHz spectral range (see Section 3.4 for a detailed description). Therefore, we observed during the scanning of the 402-nm ECDL across the 0_{3/2}–24 874_{5/2} transition, excitations at fixed frequencies, which correspond to different velocity groups of atoms in resonance with longitudinal modes of the Ti:sapphire laser for excitation on the 24 874_{5/2}–63 557 cm⁻¹ transition. Hence, when the 24 874_{5/2}–63 557.61 cm⁻¹ transition is resonantly excited, a fraction of ions is transferred from the 0_{3/2}–24 874_{5/2} excitation and a fluorescence dip becomes noticeable. The contrast of the depletion signal depends on the 402-nm detection window τ_1 . The latter, which yielded the maximum signal-to-noise ratio, corresponds to approximately 100 ns (see Fig. 5.8 for timing of the pulses of the lasers and detection window).

Excitation to the 63 557.61 cm⁻¹ state was also detected by monitoring the fluorescence emission when the 402-nm signal was blocked (PMT3). Figure 5.11 shows the two-photon excitation spectrum observed for the 24 874_{5/2}–63 557 cm⁻¹ transition by means of the third-harmonic radiation of the Ti:sapphire laser at

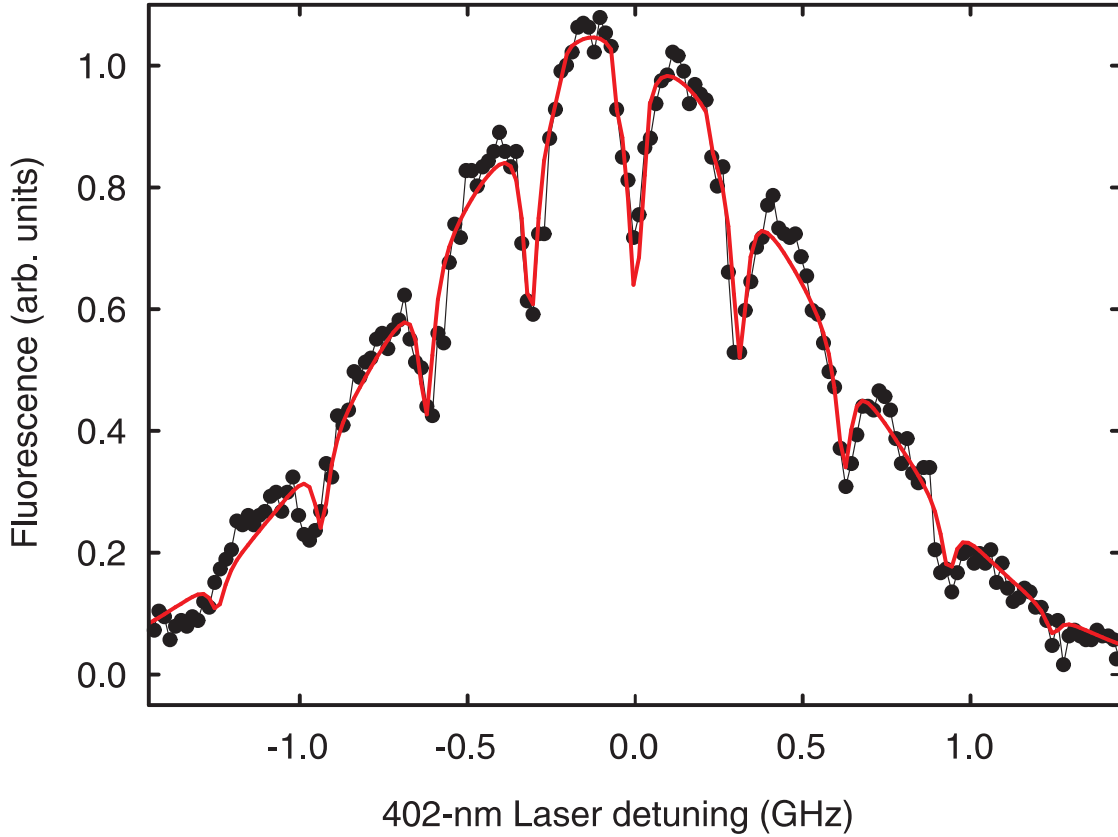


Figure 5.10: Doppler-broadened laser excitation spectrum of trapped $^{232}\text{Th}^+$ ions at 402 nm, showing multiple fluorescence depletion resonances resulting from excitation with the third-harmonic radiation of a pulsed Ti:sapphire laser tuned to the $24\,874_{5/2}-63\,557\text{ cm}^{-1}$ transition at $\lambda_2=258.5\text{ nm}$. The peak power of the third-harmonic radiation was $\approx 6\text{ W}$. The solid red line is a fit to a function described in the text with Eq. 5.5.

$\lambda_2=258.5\text{ nm}$. Here we used an additional gated integrator with a detection window of 50 ns synchronized as shown in Fig. 5.8. In this case, we subtracted the small background fluorescence signal induced from excitation of the $0_{3/2}-24\,874_{5/2}$ transition, which could not be blocked by the optical filter. The resolution of the fluorescence signal excited by each longitudinal mode, shown in Fig. 5.11, depends on the Ti:sapphire laser power. As a result one can see that the wings of the Lorentzian line-shape of the longitudinal modes overlap. The frequency separation of the several excitations in Fig. 5.11 observed in scanning the 402-nm laser is $\approx 350\text{ MHz}$, which is about 1.7 times smaller than the FSR of the Ti:sapphire laser. This can be explained by the fact that the velocity groups of atoms, in resonance with longitudinal modes of the Ti:sapphire laser, interact with a higher

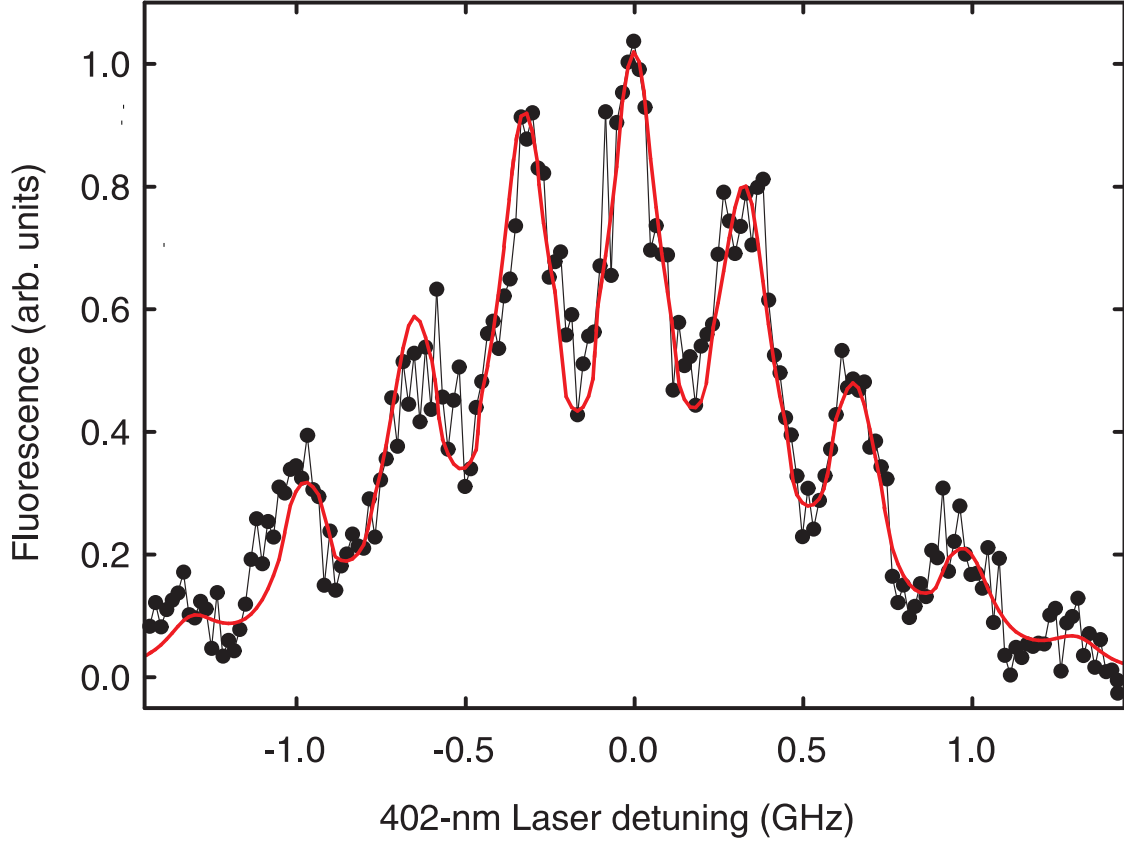


Figure 5.11: Fluorescence signal of trapped $^{232}\text{Th}^+$ ions resulting from two-photon laser excitation of the $63\,557\text{ cm}^{-1}$ level by means of the nanosecond Ti:sapphire laser tuned to $\lambda_2=258.5\text{ nm}$. The solid red line is a fit to a function described in the text with Eq. 5.5.

Doppler sensitivity for the second excitation step, resulting in a reduction by a factor $402\text{ nm}/\lambda_2 \approx 1.6$ of the frequency separation seen in the excited state.

In Fig. 5.10 and Fig. 5.11 the experimental data for laser excitation of the $63\,557.61\text{ cm}^{-1}$ state are plotted together with calculated line shapes based on the following model: We assume that the laser spectrum of the Ti:sapphire laser can be approximated with a Lorentzian line-shape for each longitudinal mode, and also, that the Doppler broadened spectrum of the 402-nm transition can be approximated with a Gaussian function, which can be respectively expressed as:

$$y_{\text{lorenz}}(x) = B \frac{\gamma^2}{(x - x_0)^2 + \gamma^2} \quad \text{and} \quad y_{\text{gauss}}(x) = A \times e^{-[x-x_0]^2/\sigma^2} + y_0, \quad (5.4)$$

where A, B is the height of the curve's peak, x_0 is the position of the center of the peak, σ is related to the FWHM of the curve, γ defines the HWHM of the curve, and y_0 is a y-axis offset.

The fitting of the Doppler broadened laser excitation spectrum with multiple fluorescence depletion signal in Fig. 5.10 and the two-photon line shapes shown in Fig. 5.11, was carried out by using:

$$y_{\text{gauss}}(x) \times [1 - \sum y_{\text{lorentz}}(x_i)] \quad \text{and} \quad y_{\text{gauss}}(x) \times \sum y_{\text{lorentz}}(x_i), \quad (5.5)$$

respectively, where $y_{\text{lorentz}}(x_i)$ was varied through the center of each longitudinal mode. As can be seen from the red solid lines in Fig. 5.10 and Fig. 5.11, this simple analytic description accurately describes the observed fluorescence signals for both cases. Thus, we used this model to derive the total amplitude of the fluorescence signal for measurements of power dependence and also for measurements of the width of the two-photon resonances.

Generally, one may expect that also spontaneous emission of VUV radiation from the excited state $63\,557.61\text{ cm}^{-1}$ to states close to the ground state can contribute to the depopulation of the excited state. We also carried out measurements with a VUV sensitive PMT. We used the detection by means of the gated integrator, described above, and also photon counting, as described in Fig. 5.6. With any of the two detection methods we could not observe high energy photons, whose energy was less than 200 nm, by evacuating the housing of the PMT to a pressure below 3 Pa. This observation is not surprising because spontaneous emission from a highly excited state is most likely to happen in a photon cascade in a dense electronic structure such as Th^+ . However, detection of VUV radiation may easily be spoiled by residual gas in the housing of the PMT or thin surface layers of water on the CaF_2 windows. In order to improve the detection probability, we are planning to heat the PMT housing along with the CaF_2 windows up to temperatures about 100°C and we will also incorporate a turbomolecular vacuum pump to reach pressures lower than 10^{-3} Pa. The detection of VUV radiation is critical since, as it was mentioned in Section 2.2.4, we envisage the detection of the “nuclear light” resulting from laser excitation of the isomer $^{229\text{g}}\text{Th} \leftrightarrow ^{229\text{m}}\text{Th}$ transition.

In scanning the third-harmonic radiation of the nanosecond Ti:sapphire laser, over the range of 250–264 nm, seven two-photon excitations to previously unknown levels were observed. Scanning could be performed at an average of 0.35 nm per day, and a full coverage of the tuning range of the third-harmonic output of the Ti:sapphire laser was not yet possible. The detected resonances showed comparable signal strengths (see below), and it is therefore assumed that they represent electric-dipole transitions originating from the $24\,874_{5/2}$ state. Consequently, it can be inferred that the identified levels are of even parity since for electric-dipole transitions the parity is preserved in such a way that $\pi_i\pi_f=-1$, with $\pi_{i,f}$ the parity of the initial, final state. Furthermore, for electric-dipole transitions the change in angular momentum between the initial and final states is given by $\Delta J=0,\pm 1$; therefore the possible values of the total angular momentum J for the observed states are $3/2 \leq J \leq 7/2$.

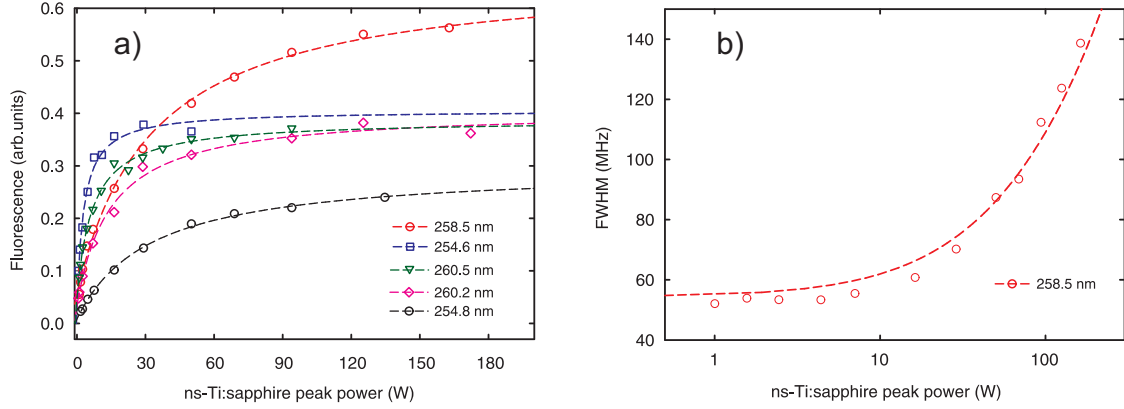


Figure 5.12: (a) saturation of the fluorescence signal resulting from pulsed laser excitation of the observed levels around 8 eV in Th^+ is presented. Here, the dashed lines show the results of the fit using the Eq. 5.3. The indicated wavelengths correspond to the second excitation step radiation of the Ti:sapphire laser, i.e. λ_2 in Fig. 5.9. (b) the width of the Lorentzian line-shape resulting from two-photon excitation on the $63\,557.61\text{ cm}^{-1}$ state as a function of the Ti:sapphire laser peak power is displayed. In this case, we fit the data points by means of the saturation broadening equation: $y_{width} = \eta_0 \sqrt{1 + x/P_{sat}}$, where η_0 is the natural linewidth of the atomic transition and P_{sat} is the saturation peak power.

Figure 5.12(a) shows saturation of the laser-induced fluorescence signal for five high-lying states of Th^+ around 8 eV. Each data point shows the results obtained by fitting Eq. 5.5 on each measured spectrum similar to Fig. 5.11 while varying the peak power on the second excitation step. For low excitation powers of the second excitation step, the signal-to-noise ratio of the fluorescence emission detected in PMT1 did not allow us to obtain reasonable data, hence we conducted the experiments using the PMT3 detection channel. The data points were normalized to the fluorescence signal observed in the $0_{3/2}-24\,874_{5/2}$ transition at 402 nm. It is worth noting in Fig. 5.12(a) the saturation of the fluorescence signal for the $64\,121.84\text{ cm}^{-1}$ state when the Ti:sapphire laser is tuned to $\lambda_2=254.8\text{ nm}$ with high saturation power but low fluorescence signal. This might reflect a high probability of branching to different metastable levels outside of the spectral sensitivity of the PMT3.

As it was pointed out in Section 2.2.2, we do not have information on the decay channels or branching ratios of electronic states above the energy $32\,957\text{ cm}^{-1}$ in Th^+ . Obviously, multiple photons are emitted from the excited state of which, we detect only in the wavelength range of $300\text{ nm} \leq \lambda \leq 400\text{ nm}$ and $410\text{ nm} \leq \lambda \leq 650\text{ nm}$. Therefore, fitting with the saturation law Eq. 5.3 is a simplification.

The data points in Fig. 5.12 (b) depict the Lorentzian width obtained from Eq. 5.5 resulting from two-photon excitation on the $63\,557.61\text{ cm}^{-1}$ state as a function of the peak power of the second excitation step laser. In this case, we obtained $\eta_0 \approx 52\text{ MHz}$, which results in a radiative lifetime of $\tau \approx 3.3\text{ ns}$. We also estimated η_0 by using the saturation peak power obtained from Fig. 5.12(a) resulting in good agreement with the previous value within 10% accuracy. This η_0 can not be directly associated with the radiative lifetime of the excited state because in addition to the power broadening, assuming that dominantly step-wise excitation populates the upper state (see Eq. 5.1), one has a contribution of the width of the $0_{3/2}-24\,874_{5/2}$ resonance and the linewidth of the longitudinal mode of the laser spectrum. We also investigated the exponential decay of the fluorescence signal from the $63\,557.61\text{ cm}^{-1}$ state as a function of time. Here, the detection window was fixed at 5 ns, and we monitored the fluorescence emission signal from the excited state as a function of time. Due to limitations in the response time of the electronics used, we inferred that the natural lifetime of this state is less than 20 ns.

Table 5.1 shows the total energy for the highly excited even-parity states around 8 eV in Th^+ , together with the J and calculated parameters α and β obtained from the saturation of the fluorescence signal by means of Eq. 5.3. As it was discussed in Section 3.4, we estimated the uncertainty of the total energy to be 0.07 cm^{-1} limited by the high fluctuations in the readout of the wavemeter induced by the pulsed laser. The total scanned energy range was from $62\,849\text{ cm}^{-1}$ (7.79 eV) to $64\,874\text{ cm}^{-1}$ (8.04 eV). In the experiment, we tuned the frequency of the third-harmonic radiation of the Ti:sapphire laser λ_2 from 250 nm to 263 nm in equidistant steps of $\approx 13\text{ GHz}$ ($1\text{ nm} \approx 4600\text{ GHz}$). The latter was chosen to cover any possible atomic transition since the observed continuous excitation of resonances over $\approx 24\text{ GHz}$ is clearly determined by the spectral distribution of the Ti:sapphire laser.

In the studied energy range, we also observed laser excitation of several transitions from the ground state to states around $40\,000\text{ cm}^{-1}$ and laser excitation of low-lying metastable levels to higher-lying states. The latter occur because spontaneous decay from the $24\,874_{5/2}$ level leads to a small accumulation of population in metastable levels. These laser excitations were detected by monitoring the fluorescence emission in the wavelength range below 300 nm, and the transitions were in agreement with the data tabulated in Ref [48]. In both cases, we did not observe the spectrum shown either in Fig. 5.10 or Fig. 5.11 since only for the two-photon excitation from the $24\,874_{5/2}$ state, the spectrum is characterized by the Doppler-free features produced by atoms in resonance with the intermediate and excited state transitions.

In order to determine the total angular momentum J of the excited state, we carried out a pulsed two-photon excitation of the previously described seven energy levels via the $0_{3/2}-25\,027_{1/2}$ ground state transition at 399.5 nm. As it can be seen, the J for the intermediate state is $J=1/2$. Therefore the excitation of

Table 5.1: Total excitation energy for the highly excited levels, total angular momentum J and vacuum wavelength for the second excitation step (λ_2) with its corresponding saturation peak power of the fluorescence signal (α) and maximum observed fluorescence emission signal (β).

Total excitation energy (cm ⁻¹)	J	λ_2 (nm)	α (W)	β (arb. units)
63 257.47		260.529	6.0	0.39
63 298.42		260.251	13.6	0.40
63 557.61		258.507	30.1	0.67
64 121.83		254.791	31.3	0.29
64 150.40	3/2	254.606	2.8	0.40
64 560.51	3/2	251.975	–	–
64 813.83		250.377	–	–

the high energy states will be observed only when its J is 3/2, the latter to meet the selection rules for the electric-dipole transitions. For the first excitation step at 399.5 nm a similar ECDL and modulation than the previously described was used (see Section 3.4 and Fig. 3.5). A typical average output power of this system was about 30 mW. This radiation was modulated to produce pulses of 70 ns duration and the detection window τ_1 used was ≈ 150 ns for the fluorescence signal when the 399.5-nm signal was blocked. According to our measurements reported in Section 4.2, the fluorescence signal observed for the excitation of the 399.5-nm $0_{3/2}$ – $24\,874_{5/2}$ transition was about 2.5 less than the fluorescence signal observed with excitation of the 402-nm $0_{3/2}$ – $24\,874_{5/2}$ transition. Nevertheless we could observe excitation of the $25\,027_{1/2}$ – $64\,150.40_{3/2}$ and $25\,027_{1/2}$ – $64\,560.51_{3/2}$ transitions. Table 5.1 also shows an unambiguously determination of the J for two levels and partial classification for other five levels. Therefore the J for the other states is limited to the range of $5/2 \leq J \leq 7/2$.

As it was mentioned in Section 2.2.3, in Ref. [56] the authors calculated the total energy of ten high-lying even-parity states with total angular momenta $J=3/2$ and $5/2$ which are not presented in experimental atomic spectra databases for Th⁺. Figure 5.13 shows the comparison between the calculated energy levels in Ref. [56] and the highly excited observed energy levels in our investigation. We also included in this figure additional energy levels below 7 eV measured in Ref. [48]. As can be seen from Fig. 5.13, the energy levels calculated in Ref. [56] have a systematic upward shift of ≈ 0.4 eV for the previously known levels.

The density of energy levels shown in Fig. 5.13 is comparable for the measured and the calculated levels in the scanned range. This is remarkable, since one can expect that our detection scheme allows us the observation of atomic transitions whose excitation is not too weak. For example in Ref. [56] the authors predict reso-

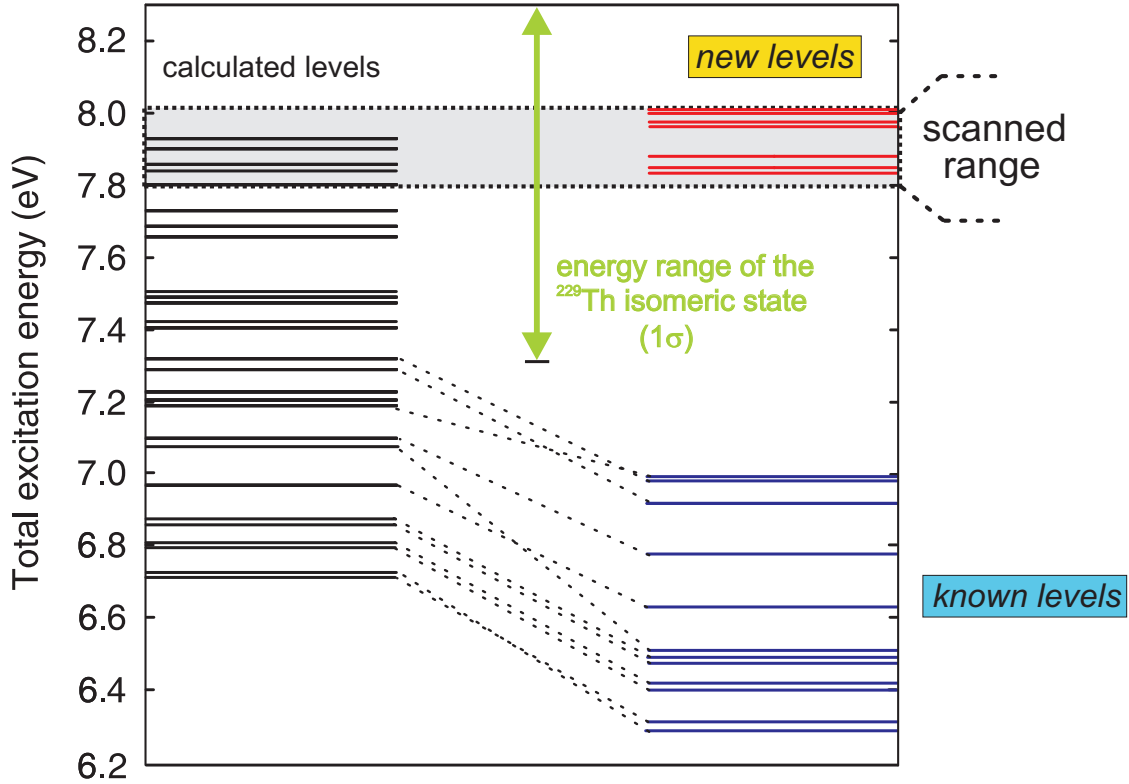


Figure 5.13: Comparison of the calculated levels in Ref. [56] (black horizontal lines) with those measured previously in Ref. [48] (blue horizontal lines) and the ones obtained in this work (red horizontal lines). The possible values of the total angular momentum J for the highly excited even-parity states are $3/2 \leq J \leq 7/2$. The green arrow indicates the present 1σ uncertainty range for the nuclear transition energy in ^{229}Th . The gray area is the total scanned energy in our investigation. The energy levels interlaced with a dashed line connects corresponding energy levels.

nances that vary by 4 orders of magnitude in strength, but our α values in Table 5.1 are within a range of 1 order of magnitude only. However, the amount of levels obtained by means of ab initio calculations in Ref. [56] can also be underestimated since the electron configurations in Th^+ are strongly mixed. Therefore, states that belong to a higher configuration that are not included in the calculations may appear in the investigated energy range. This mixing between configurations in a multi-level system such as Th^+ makes ab initio calculations difficult. Therefore, this coincidence in the density of states between our possibly limited detection scheme and the selection of electronic configurations made in the theoretical esti-

mation, suggests that the theoretical prediction for the density of strong transitions that will be relevant for electronic bridge excitation is realistic.

As it was pointed out by the authors in Ref. [56], the ab initio calculations can predict absolute energies only with a relative uncertainty of about 10% accuracy, hence a comparison of our measured energy levels with the calculated levels is not meaningful. Thus, the energy levels measured in this investigation can encourage future theoretical calculations in the complicated three-valence ion Th^+ for a better understanding of its atomic properties. This comprehensive investigation will also allow us the unambiguous identification of the signature of the unique nuclear structure of ^{229}Th since in a comparison of the fluorescence signals observed with $^{229}\text{Th}^+$ and $^{229\text{m}}\text{Th}^+$ with $^{232}\text{Th}^+$, the population of the isomeric nuclear level in $^{229}\text{Th}^+$ will be indicated.

5.4 Multi-photon ionization in trapped Th^+ ions

During our investigation of the previously described highly excited seven energy levels, we noticed a decay in the fluorescence signal observed at 402 nm when the third-harmonic radiation from the Ti:sapphire laser resonantly excited an upper state. For high powers of the second excitation step laser, this decay in fluorescence signal became up to 10 times faster than the typical decay due to the formation of molecular ions. As is well known, when atoms are exposed to a strong electromagnetic field, like from the nanosecond Ti:sapphire laser with peak intensities around 160 kW/cm^2 , they may undergo resonantly enhanced multi-photon ionization (see for example Refs. [82, 83] and references therein). Since the process that we observed depends strongly on the Ti:sapphire laser power (see below) and because the ionization energy for Th^+ is 11.9 eV (readily achievable with 1 photon at 402 nm $\approx 3.1 \text{ eV}$ and 2 photons at 260 nm $\approx 9.6 \text{ eV}$), we carried out experiments on identification of possible ionization of the Th^+ ensemble. We made use of the fact that their difference in the charge states makes the behavior of Th^+ and Th^{2+} in the ion trap significantly different.

The design of a similar experiment is described elsewhere [70]. Briefly, a channel electron multiplier (CEM)¹, operating at -2.4 kV , was mounted perpendicular to the trap axis at a distance of about 80 mm. A grid, with an open area of $\approx 88\%$, shielded the CEM and was switched to 1.1 kV with a fast commutator at the beginning of the sequence (see below). The field of the grid was used to accelerate the ions from the trap toward the CEM. For ion detection, the rf driving voltage was linearly decreased from an amplitude of $\approx 840 \text{ V}$ to 0 V within 100 ms until the potential of the grid was strong enough to extract the ions from the trap and accelerate them in the direction of the CEM. At the beginning of the sequence a multiscaler card was triggered, which measures the amount of ions detected by the

¹Burle, 5901 Magnum

CEM as a function of time. This setup operates as a miniature mass-to-charge ratio spectrometer: keeping the rf driving frequency constant while decreasing the rf driving voltage, decreases the pseudopotential depth for the trap. The latter varies for particles with different mass-to-charge ratios.

The motion of the ions is treated as a motion in a pseudopotential established by the time-averaged quadrupole potential [69]. The depth of this pseudopotential in the radial direction could be stated as the energy required to move an ion from the center of the trap to the surface of the electrode and is given by $d_r = m \cdot \omega_{ps}^2 \cdot r_0^2 / 2$, where m is the mass of the ion, ω_{ps} is the secular frequency of the ions and r_0 is the radial distance from the trap center to the end of the middle electrode. For a better picture, it is better to express d_r in the following way: $d_r \propto Q^2 / m U_{\text{rf}}$, where Q is the charge of the ion and U_{rf} is the amplitude of the rf voltage (at angular frequency Ω). Therefore, d_r / Q is the required potential that can be applied to two opposite middle electrodes before ejecting the ions from the interrogation zone.

Figure 5.14 shows the appearance of Th^{2+} ions after illuminating the ion cloud with the Ti:sapphire laser, when the $24\,874_{5/2} - 64\,150.40_{3/2}$ transition is resonantly excited at 254.6 nm. As it was described in Section 3.1, the q parameter used throughout all experimental investigations is ≈ 0.35 (it is therefore 0.7 for Th^{2+}). Hence, for these trap parameters, one can expect the coexistence of the two charge states in the linear Paul trap. The Th^+ ions arriving around 84 ms (at higher rf amplitude) are those with higher energy that are first extracted from the trap by the grid field. The last Th^+ ions arriving around 88 ms are ejected from the trap because they reached the border of the (a, q) stability diagram [69], that scales like $U_{\text{rf}} \propto \sqrt{m/Q}$. Since both parameters d_r and (a, q) depend on the mass-to-charge ratio, two distinct peaks appear in in Fig. 5.14 for Th^+ and Th^{2+} .

In our experiment, we observed that Th^+ ions were released from the trap at the trap potential depth of $d_r \approx 0.7$ eV and at the Mathieu q parameter of ≈ 0.05 . After approximately 5 ms of decreasing the rf driving voltage with the described ramp, we observed that Th^{2+} ions were released at the trap potential depth of $d_r \approx 1.1$ eV and $q \approx 0.06$. The latter values of the trap potential depth are estimates based on our trap parameters. The a value estimated in these experiments was $\approx 10^{-4}$, which is determined by the static voltage that is applied to all electrodes of the two outer sections for the axial confinement. We found a good agreement between this a value and the scaling of the q for the values mentioned above.

The observation described in Fig. 5.14 indicates that, most likely, a photon with energy of ≈ 3.1 eV from the ECDL at 402 nm and two photons with total energy of ≈ 9.5 eV from the Ti:sapphire laser provide enough energy to ionize the Th^+ ions. In order to obtain the signal displayed in Fig. 5.14, we monitored the fluorescence emission signal from the $0_{3/2} - 24\,874_{5/2}$ transition at 402 nm with the Ti:sapphire laser tuned to the $24\,874_{5/2} - 64\,150.40_{3/2}$ transition at 254.6 nm. Then, when the fluorescence signal at 402 nm decayed to 10% of its initial value, we decreased the rf driving voltage and triggered the grid as described before. We did not observe

any Th^{2+} CEM signal when the Ti:sapphire laser peak power was below ≈ 200 W. For Fig. 5.14 the used peak excitation power of the third-harmonic radiation was about 630 W.

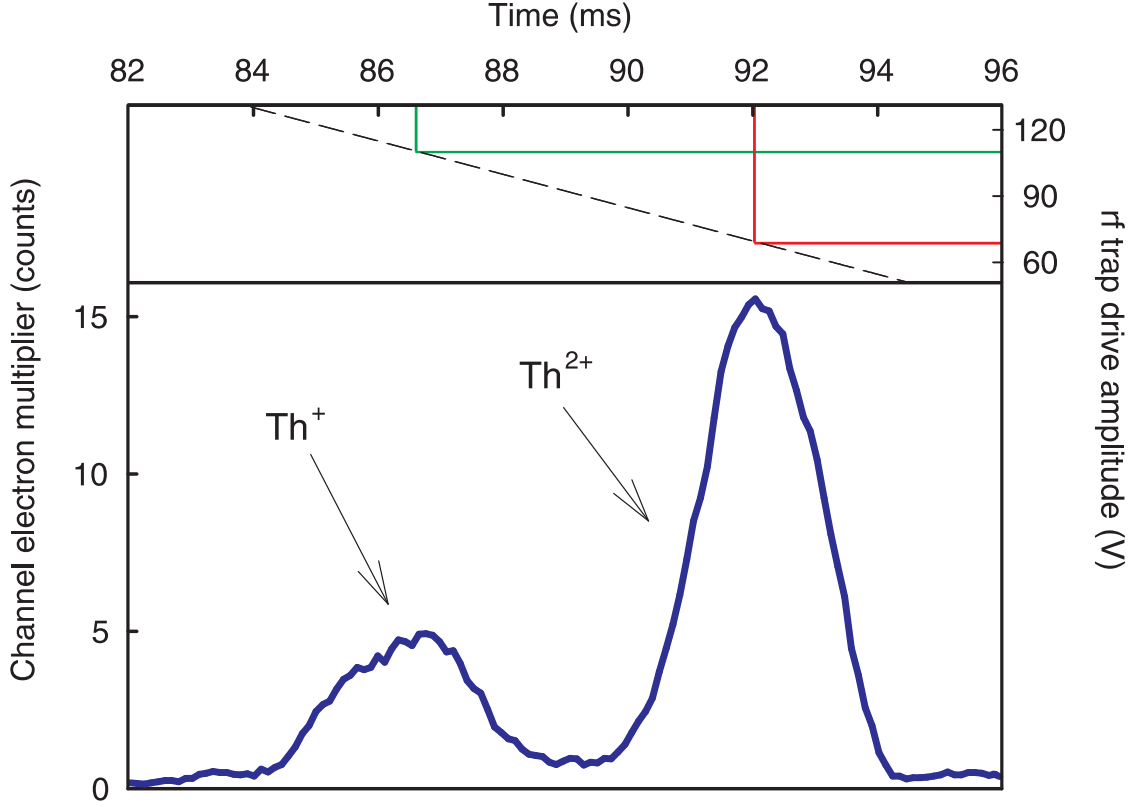


Figure 5.14: Channel electron multiplier (CEM) signal resulting from ionization of Th^+ ions by means of the third-harmonic radiation of Ti:sapphire laser tuned to the $24874_{5/2}-64150.40_{3/2}$ transition at 254.6 nm. The measurements were performed using argon as a buffer gas at $8 \cdot 10^{-3}$ Pa pressure. The q for Th^+ is ≈ 0.35 , therefore 0.7 for Th^{2+} . Above the ion signal is shown the decreasing of the rf driving voltage described in the text.

The data points in Fig. 5.15 show the laser power dependence of the ionization rate for the Ti:sapphire laser being resonant with different upper states. The $24874_{5/2}-64150.40_{3/2}$ transition at 254.6 nm (blue curve in Fig. 5.15) and the $24874_{5/2}-63557.61$ cm^{-1} transition at 258.5 nm (red curve in Fig. 5.15) were chosen because of their relative difference of about 10 times in saturation peak power α . The α for the red curve in Fig. 5.15 is 30.1 W and for the blue curve is 2.8 W. In the experiment, we measured the decay of the 402-nm fluorescence signal as a function of time and afterward, we fitted the experimental data points with an exponential decay curve and extracted the decay rate.

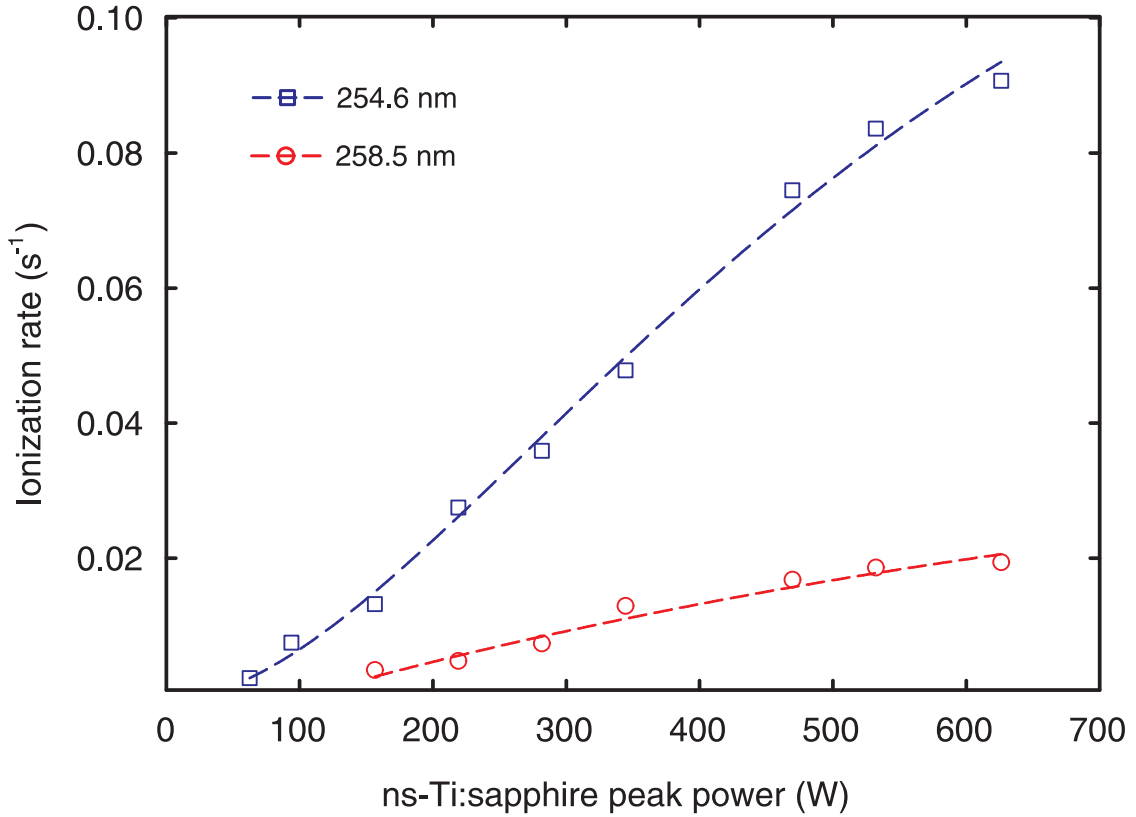


Figure 5.15: Ionization $\text{Th}^+ \rightarrow \text{Th}^{2+}$ rates as a function of the Ti:sapphire peak power for excitation of two different upper states. Argon at 0.2 Pa pressure was used as a buffer gas. The dash lines are fits to a function described in the text.

In Fig. 5.15 the experimental data for the ionization rates are plotted together with fit lines based on the model presented in Ref. [82], where the solutions for rate equations are established for a three level ladder scheme assuming a two resonant fields for the process. Unfortunately, we could not extract information such as multi-photon ionization cross sections from this approximation since presently we have no information on the radiative lifetime and decay channels of the excited state. As it can be seen in Fig. 5.15, the ionization process $\text{Th}^+ \rightarrow \text{Th}^{2+}$ depends on the saturation power α , i.e. depends on the population in the excited state. For example, for the data points shown in Fig. 5.15 we observed for the $24874_{5/2} - 64150.40_{3/2}$ transition faster population of the excited state than for the $24874_{5/2} - 63557.61 \text{ cm}^{-1}$ transition by means of increasing the laser power. Consequently, we observed that in the former the ionization process initialized earlier than in the latter, and also that the ionization rate is about 5 times higher at 630 W peak power. As the saturation peak powers α listed in Table 5.1 are in the same

range (2.8 W–31.3 W) of those presented in Fig. 5.15, one can expect that in our experiment the laser peak power for which the ionization of Th^+ ions become significant are between 50 W and 200 W.

The previous described observations of multi-photon ionization $\text{Th}^+ \rightarrow \text{Th}^{2+}$ are very critical for the search for a resonant two-photon electronic bridge excitation of the ^{229}Th nucleus. In this case, the trapping efficiency and the ion storage time must be fully optimized, since when working with the radioactive isotope ^{229}Th we will have a limited amount of opportunities to load the trap from a limited amount of thorium. Therefore, during the comprehensive investigation of the electronic level structure of $^{229}\text{Th}^+$ in the energy range of the $^{229\text{m}}\text{Th}$ isomeric state special care should be taken by using low peak power of the second excitation step laser nearby resonances to electronic highly states. In Chapter 6 we will describe further interactions of the radiation from the Ti:sapphire laser with the ensemble of Th^+ ions, where another ion loss mechanism is mitigated using high laser peak powers, but which is different from the multi-photon ionization described in this section.

6 Formation and photodissociation of molecular ions with Th^+

6.1 Chemical reactions of trapped Th^+ ions

In our first observations of fluorescence emission from the strongest tabulated line of the Th^+ emission spectrum at 402 nm in Section 4.3, the ions would remain in the linear Paul trap for only a few tens of seconds. This experimental observation goes with the fact that thorium ions are quite reactive with water, oxygen, methane, and carbon dioxide molecules present as residual gases in the vacuum chamber (see Refs. [58, 84, 85] and references therein). Therefore, improved vacuum conditions (e.g. to reduce the partial pressure of water vapor via long-term baking of the vacuum apparatus) and higher purity of the buffer gas employed are required to extend the storage times of the Th^+ ions in the trap for cyclic laser excitation.

In order to investigate the effect of molecular ions formation with buffer gas cooled Th^+ ions, we measured the time-dependent laser-induced fluorescence signal in continuous excitation with an ECDL tuned to the $0_{3/2}-24874_{5/2}$ transition at 402 nm. Figure 6.1 shows a typical decay-curve of laser-induced fluorescence signal due to the formation of molecular ions in reactions with the background gas. A similar curve was also obtained when the ion cloud was illuminated with 402-nm radiation briefly every 100 s, showing that the ion loss is independent of the laser excitation. The maximum exponential-decay time constant observed was approximately 1000 s, after baking the buffer gas system and the vacuum chamber during three weeks up to a maximum temperature of 180 °C, using a big buffer gas purifier¹, and improved connections between the buffer gas system and the vacuum chamber. When the buffer gas system was not sufficiently purified, we observed a strong dependence on the ion loss with the buffer gas flux. In this case, we achieved storage times lower than 100 s. Above this range, reactions of Th^+ ions with background gas present in the vacuum system seem to be the dominant mechanism.

This limited storage times observed in Th^+ ions possess a significant challenge in time-intensive experiments such as measuring the hyperfine structure and search-

¹Pure Gas Products, MC190-902F

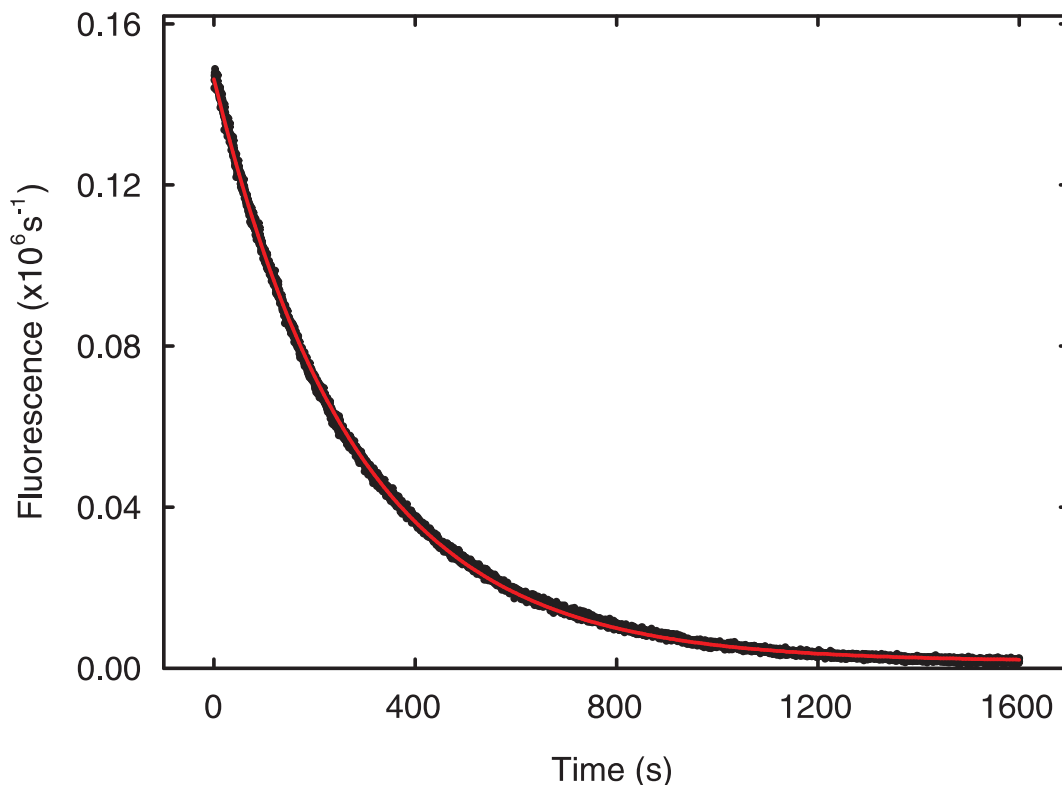
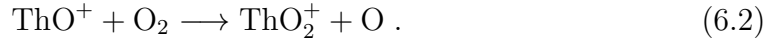


Figure 6.1: Typical fluorescence decay-curve due to the formation of molecular ions with $^{232}\text{Th}^+$ ions resulting from continuous laser excitation tuned to the $0_{3/2}-24874_{5/2}$ transition at 402 nm. The red solid line is fit to an exponential decay with a time constant of $\tau_R = 1/\Gamma_R \approx 300$ s.

ing for the nuclear isomer transition $^{229g}\text{Th} \leftrightarrow ^{229m}\text{Th}$ in the $^{229}\text{Th}^+$ ion. Reactions of actinide ions with molecules have attracted significant attention because a possible contribution of the $5f$ electrons to the chemical reaction might be of interest since the $5f$ electrons are relatively high in energy and are spatially extended (see Refs. [84, 86–88] and references therein). In all these extensive studies, it was also confirmed that Th^+ is among the most reactive ions of the group of the actinides [89]. For example, Th^+ ions are able to activate the O–H bonds in water, O–O bonds in oxygen, CO–O bonds in carbon dioxide, and C–H and C–C bonds in hydrocarbons. The latter might be due to fact that a minimum of two non- f valence electrons in the electronic ground state is required for the activation of C–H or C–C bonds [88, 90], which are already available in the case of Th^+ (i.e. $6d^27s$ for the $0_{3/2}$ ground state, $1521_{5/2}$ and $1860_{3/2}$ lower-lying metastable states, and $6d7s^2$ for the $4113_{5/2}$ state [48]).

The major product of the reactions of Th^+ ions with water, oxygen and carbon dioxide is the thorium oxide molecular ion (ThO^+), which has an estimated bond

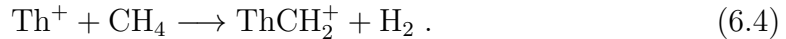
dissociation energy of approximately 9.1 eV [88]. In a previous study with Th^+ , the authors in Ref [91] found that oxidation occurs by means of the following sequential reactions



In the case of the reactions of Th^+ ions with water, the ThO^+ product corresponds to a branching ratio of 65 % [90] and an additional reaction is given by



which has an estimated branching ratio of 35 % [90]. On the other hand, when Th^+ reacts with hydrocarbons, the bond dissociation energies range from 1.1 eV up to 4.7 eV [92]. In this case the following reaction for methane was found



In our experimental observations, the presence of high concentrations of water and hydrocarbons has been measured using a residual gas analyzer (RGA). However, a quantitative analysis of the actual molecules while using high pressures (0.2 Pa) of buffer gas for collisional cooling of $^{232}\text{Th}^+$ ions and quenching of lower-lying metastable states has not been possible by means of RGA detection.

6.2 Photodissociation of molecular ions with Th^+

Contrary to expectations based on the high ThO^+ binding energy and fast reaction rate of Th^+ with oxygen, we have discovered several wavelength ranges where the formation of molecular ions with Th^+ could be suppressed by laser irradiation of the ion cloud. The latter was observed in an investigation of high-lying states in Th^+ above the energy range of $60\,000\text{ cm}^{-1}$ (described in Section 5.3.4) using the third-harmonic radiation of a nanosecond pulsed Ti:sapphire laser. This observation indicates that the strong peak power of UV photons of the Ti:sapphire laser can break the chemical compound formed in Th^+ , in the photodissociation process. If the $^{232}\text{Th}^+$ ions are illuminated by the UV radiation, we observe that the detected fluorescence signal at 402 nm recovers by up to approximately 95 % depending on the peak power of the Ti:sapphire laser.

Figure 6.2 shows molecular formation with Th^+ and photodissociation of molecular ions by means of the Ti:sapphire laser at 258.5 nm. Here, the observation of the fluorescence signal at 402 nm was started at $t=0\text{ s}$ after the photoablation laser pulse, with an initial ion number in the order of 10^6 . The data points shown in Fig. 6.2 were obtained using 402-nm ECDL pulses of 30 ns duration in combination with delayed ($\approx 200\text{ ns}$) Ti:sapphire laser pulses of 30 ns duration. The detailed

schematic of pulsed laser excitation and detection was described previously in Section 5.3.2. In the displayed Fig. 6.2, a beam of 258.5-nm light with a diameter of ≈ 0.7 mm was switched on at 250 s. Before the Ti:sapphire laser was turned on, the Th^+ fluorescence signal decreased exponentially because of the formation of molecular ions (see above and Fig. 6.1). After the ion cloud was illuminated with the Ti:sapphire radiation, the detected fluorescence signal at 402 nm rapidly increased up to $\approx 88\%$ of the initial signal, showing photodissociation of molecular ions with Th^+ . The data were obtained for two settings of Ti:sapphire laser peak power which differ by a factor of three. In the photodissociation regime, at the higher Ti:sapphire peak power we observed that the 402-nm fluorescence signal decays only by $\approx 10\%$ in several hours of continuous measurements.

In order to obtain a simple analytic description of the photodissociation of molecular ions with Th^+ , we approximate this process in a simple differential equation with ions and molecules, where $A(t)$ is the amount of trapped Th^+ ions as a function of time, and $(1-A(t))$ is the molecular fraction. The time-dependent variation of the amount of ions can be expressed as:

$$\frac{dA(t)}{dt} = -A(t)\Gamma_R + [1 - A(t)]\Gamma_D, \quad (6.5)$$

where Γ_R is the molecule formation rate and Γ_D is the photodissociation rate. In the steady state condition, i.e. $\frac{dA(t)}{dt}=0$, the Th^+ ion population is given by $A = \frac{1}{1+\Gamma_R/\Gamma_D}$ and the time constant is given by $\tau=1/(\Gamma_D + \Gamma_R)$.

Using the experimental data shown in Fig. 6.2, we found a good agreement between the observed fluorescence signal and the predictions of Eq. 6.5 with the photodissociation rate $\Gamma_D \approx 5.8 \cdot \Gamma_R$, which results in a time constant of $\tau \approx 8.5$ s when the Ti:sapphire peak power was 450 W (see red curve in Fig. 6.2). When the peak power of the Ti:sapphire laser was reduced to 150 W, we obtained $\Gamma_D \approx 0.7 \cdot \Gamma_R$ and $\tau \approx 34$ s (see cyan curve in Fig. 6.2). For the above cases, Γ_R was in the order of $\approx 0.02 \text{ s}^{-1}$. Under conditions of efficient photodissociation, the time constant (8.5 s) is very fast and the steady state ion population approaches 100 % (see the ion population A above) of the initial ion population. The dashed lines of Fig. 6.2 show that the simple model described with Eq. 6.5 accurately describes the observed photodissociation mechanism.

Figure 6.3 shows the increase of the photodissociation rate as a function of the Ti:sapphire laser peak power based on the results of the model with Eq. 6.5. The photodissociation rate becomes small for peak powers lower than 90 W corresponding to an intensity of approximately 20 kW/cm^2 . The photodissociation rate observed in the peak power range of Fig. 6.3 corresponds to an steady state ion population A within 10–95 % of the initial ion population. The high non-linear behavior shown in Fig. 6.3 can be explained by a multi-photon process, where several photons from the Ti:sapphire laser interact with the ion cloud to break the chemical compound formed in Th^+ . Next, we make use of the recovered Th^+ fluo-

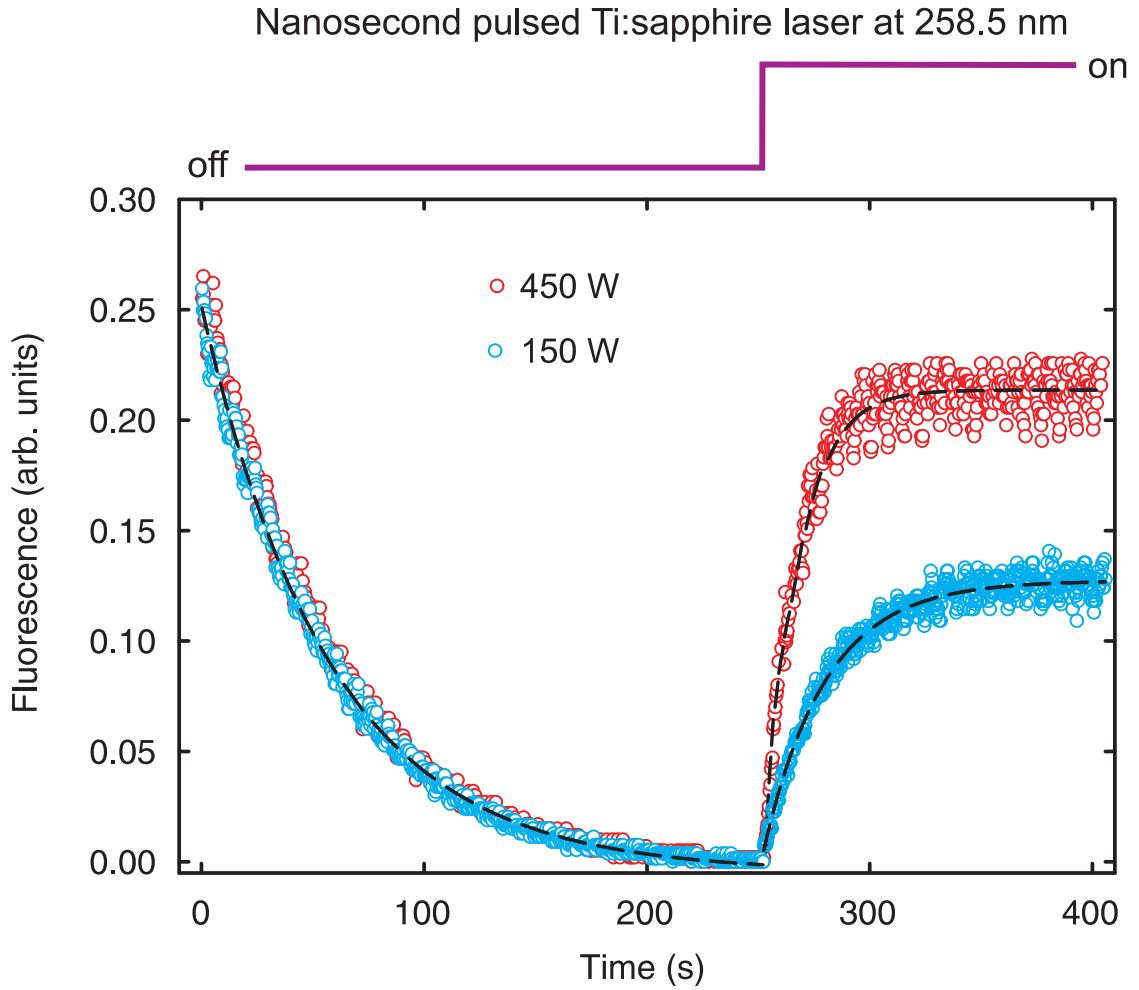


Figure 6.2: Fluorescence signal of trapped $^{232}\text{Th}^+$ ions resulting from laser excitation tuned to the $0_{3/2}-24\,874_{5/2}$ transition at 402 nm, showing the formation ($t \leq 250$ s) and the photodissociation of molecular ions with Th^+ induced by UV photons of the Ti:sapphire laser for two settings of Ti:sapphire laser peak power. The dashed lines correspond to solutions of Eq. 6.5.

rescence signal obtained after irradiating the ion cloud with the Ti:sapphire laser, in order to identify the molecules that are formed in our trap by means of secular frequency excitation.

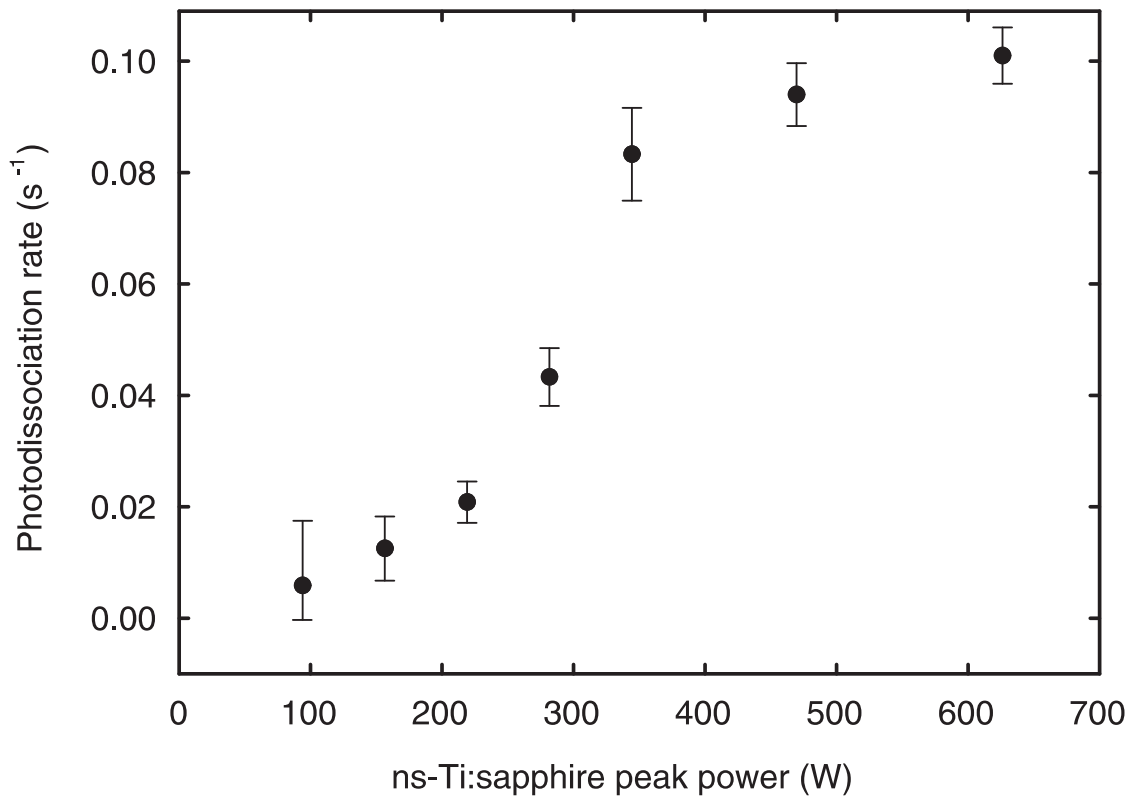


Figure 6.3: Photodissociation rates of molecular ions with Th^+ as a function of the nanosecond pulsed Ti:sapphire laser peak power. The third-harmonic radiation was fixed at ≈ 258.5 nm. The rates were calculated by means of the model described in the text with Eq. 6.5. The error bars correspond to the standard deviation of the measurements performed in each laser power.

6.3 Secular frequency excitation of molecular ions

In order to determine which molecule is responsible for reacting chemically with Th^+ and thus form molecular ions, we carried out an experiment when the molecular ions were ejected from our linear Paul trap by means of resonant excitation of its characteristic secular frequency. The advantage of this resonant excitation via secular frequency is that it allows us to measure indirectly the mass of the species present in our trap. Although this technique is destructive, i.e. we lost completely the ions for further interrogations, for this case it is well suited because at this moment we are not working with the radioactive isotope ^{229}Th .

In a quadrupole linear Paul trap the ion cloud oscillates with a secular frequency in the trap given by

$$f_{ps} = \frac{\omega_{ps}}{2\pi} = \frac{1}{2\pi} \frac{e U_{\text{rf}}}{\sqrt{2} m \Omega r_0^2}, \quad (6.6)$$

where m and e are the mass and the charge of the ion, respectively, U_{rf} is the amplitude of the rf voltage (at angular frequency Ω), and r_0 is the radial distance from the trap center to the end of the middle electrode. Therefore an energy transfer to the ensemble of ions can be done by resonantly exciting an ion by applying an oscillating electric field to the middle section dc electrodes (see drawing of the linear Paul trap in Fig 3.1). When the resonance character is obtained, the ion's amplitude of oscillation will increase until it finally is lost from the trapping region, thus also for cyclic laser excitation.

In order to determine the mass of the possible molecular ions that are photodissociated by means of laser irradiation of the ion cloud, we carried out secular frequency excitation of molecular ions described below. From the described measurements in Section 6.2, we understood the photodissociation rate and the steady state ion population at which this process takes place in the trap. By knowing this, one can expect a change in the number of recovered Th^+ ions when the molecular ions, coexisting with the Th^+ ions, are resonantly ejected from the trap with their characteristic f_{ps} . Hence, we measured the number of recovered Th^+ ions at fixed Ti:sapphire peak power (630 W) as a function of the frequency f_{ps} . The f_{ps} was kept at the electrode for a time of 1 s at ≈ 1 V amplitude, enough to enable the resonant transfer of the energy to eject more than 70 % of the ions from the trap. The total frequency was scanned from 200 kHz to 300 kHz in equidistant steps of 3 kHz. The resonant frequency f_{ps} for $^{232}\text{Th}^+$ ions was found to be 269(1) kHz for our experimental conditions. We carried out several measurements of this frequency for Th^+ through all these experimental investigations, to control possible temporal fluctuations resulting from drifts of the trap driving voltage or frequency.

We observed a well defined frequency range f_{ps} where the number of recovered Th^+ ions was negligible. The range was $f_{ps}=245(2)$ kHz, which might correspond to the calculated masses: $(232+17)$ amu $\rightarrow f_{ps}=250(2)$ kHz, $(232+16)$ amu $\rightarrow f_{ps}=251(2)$ kHz or $(232+14)$ amu $\rightarrow f_{ps}=253(2)$ kHz by using Eq. 6.6. As it can be seen from the ion products of the reactions described in Eq. 6.1, Eq. 6.3 and Eq. 6.4, the molecular ions can either be ThO^+ , ThOH^+ or ThCH_2^+ . In this case, we do not have the experimental resolution needed to distinguish between these three molecular ions. Data points in Fig. 6.4 show the increase in the fluorescence signal at 402 nm, which results from illuminating the trapped ion cloud with output of the Ti:sapphire laser at ≈ 400 s after resonantly excited different species of molecular ions with f_{ps} . Here the f_{ps} were applied during 5 s right before switching on the Ti:sapphire laser.

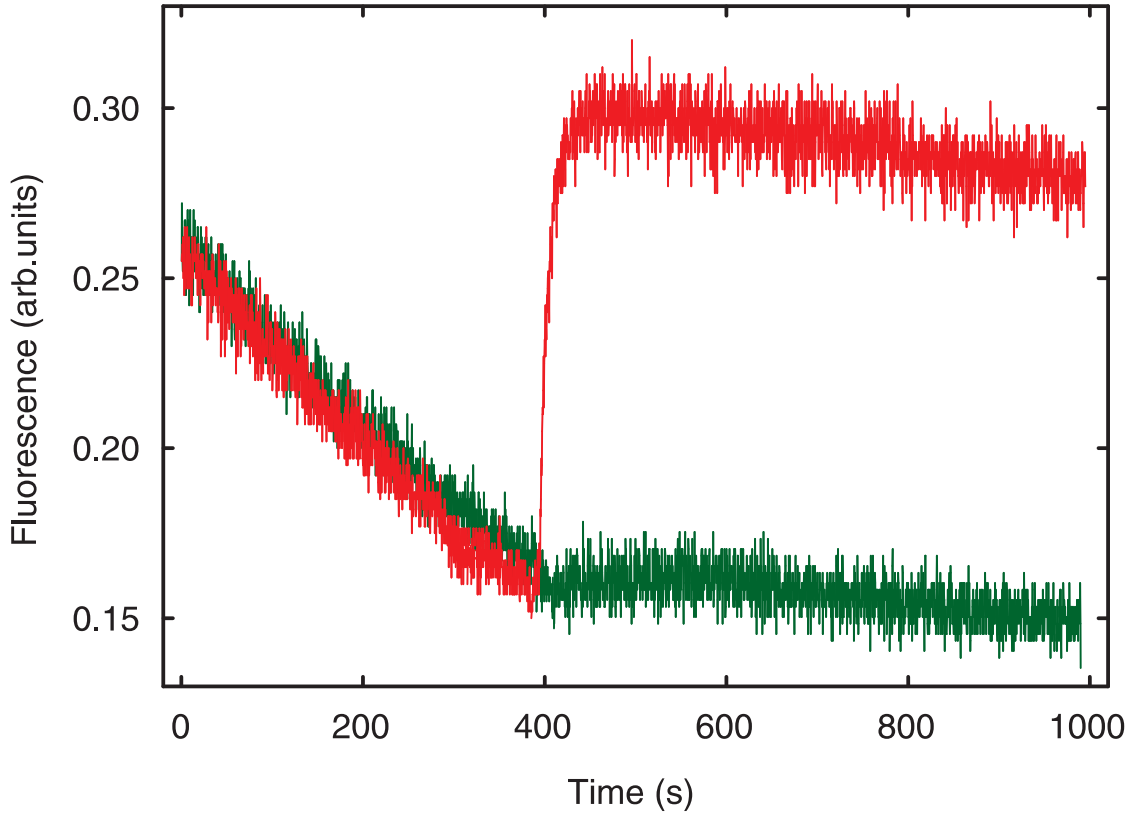


Figure 6.4: Fluorescence signal of trapped Th^+ ions resulting from resonant laser excitation of the 402-nm $0_{3/2}-24\ 874_{5/2}$ transition, showing formation and photodissociation of molecular ions when the ion cloud was illuminated with the Ti:sapphire laser at ≈ 400 s after applying different f_{ps} . The red curve was obtained when we ejected from the trap the molecular ions with $f_{ps}=200-240$ kHz. The green curve was obtained by ejecting the molecular ions with $f_{ps}=245(2)$ kHz.

Figure 6.4 clearly shows that mainly the molecular ions that are photodissociated with the Ti:sapphire laser are in the range $f_{ps}=245(2)$ kHz or atomic masses within $(232+14)-(232+17)$ amu. A similar curve than the red one in Fig. 6.4 was obtained when no resonant frequency f_{ps} was applied to the trap.

Unfortunately, we could not discriminate between the molecular ions ThOH^+ , ThCH_2^+ or ThO^+ since only 3 amu separates their difference in mass. We also tried to resolve these molecular ions by means of channel electron multiplier (CEM) detection, described in Section 5.4. We unsuccessfully attempted to measure the evolution in time of the molecular ions when the decay-curve of 402-nm fluorescence signal changes. Here also the experimental resolution did not allow us to observe any difference between the Th^+ ions and its formation of molecular ions.

To conclude, we would like to emphasize that although our measurements did not allow us a complete identification of the molecular ions that are photodissociated, they indeed allowed us to shrink the range for the atomic mass of possible molecular ions present in our ion trap experiment. The chemical reactions found in our research are in agreement with previous investigations on trapped buffer gas cooled Th³⁺ ions [85]. Therefore it is expected that our finding of photodissociation of molecular ions may be very useful for future experiments on the search for the isomeric state transition in the ²²⁹Th nucleus, either in our system with Th⁺ or using the other approach with Th³⁺ [9].

7 Conclusion and outlook

In this thesis we have demonstrated two-photon excitation of trapped, buffer gas cooled $^{232}\text{Th}^+$ ions through the intermediate state at $24\,874_{5/2}$. In order to achieve a high population in the intermediate state, and consequently in the excited state, we have used pulsed laser excitation with a nanosecond Ti:sapphire laser in combination with synchronized 402-nm ECDL pulses. Our investigation showed two efficient detection methods for laser excitation of 8-eV electronic states in Th^+ ions. We have reported laser excitation of seven previously unknown levels in the range from $62\,849\text{ cm}^{-1}$ (7.79 eV) to $64\,874\text{ cm}^{-1}$ (8.04 eV) via the $24\,874_{5/2}$ intermediate state. The Th^+ ion seems to be well suited for an inverse electronic bridge process because both, theory and experimental results, agree on the density of strong transitions in the expected range of the nuclear resonance.

In Chapter 5 we demonstrated the identification of seven highly excited electronic states of even-parity and the classification of two of them via the total angular momentum $J=3/2$. In order to unambiguously determine J for the remaining five upper excited states, we propose to carry out a pulsed two-photon laser excitation of those levels through the transition $0_{3/2}-25\,188_{3/2}$ at 397.0 nm. This transition can also be easily driven with a semiconductor diode laser. By selecting three intermediate states with different J , i.e. $J = 1/2, 3/2, 5/2$, we could unambiguously establish the J for the 8-eV electronic states, since for electric-dipole-allowed transitions the change in angular momentum between the initial and final states is given by $\Delta J=0, \pm 1$. The information about the total angular momentum along with the total excitation energy of the highly excited states can encourage future theoretical calculations in the complicated three-valence ion Th^+ for a better understanding of its atomic properties.

All the investigations mentioned in this thesis were performed with the naturally occurring isotope ^{232}Th . A critical step in the experiment is to apply them to the more radioactive isotope ^{229}Th , where it will be necessary to minimize the amount of thorium used for trap loading. In this case, the trapping efficiency and the ion storage time must be fully optimized. When working with the radioactive isotope ^{229}Th , we will have a limited amount of substance of $\approx 10^{14}$ nuclei (≈ 1 kBq activity) before requiring more stringent radiation safety procedures. Contrary to expectations based on the high ThO^+ binding energy, we discovered photodissociation of molecular ions with Th^+ . The latter was caused by the interaction of the high peak intensity of UV radiation with the ion cloud resulting in continuous hours of laser interrogation of the Th^+ ensemble. This will benefit the future work

with the radioactive isotope and mitigates the problem caused by the high chemical reaction rate of thorium with residual gases present in the vacuum apparatus. Furthermore, the chemical reactions found in our research with Th^+ are similar as those in previous investigations on trapped buffer gas cooled Th^{3+} ions [85]. Therefore it is expected that our finding of photodissociation of molecular ions with Th^+ may set the ground for a comprehensive investigation on the search for the isomeric state transition in the ^{229}Th nucleus, either in our system with Th^+ or using the other approach with Th^{3+} [9].

Another interesting effect activated by the interaction of the Ti:sapphire laser with the ensemble of Th^+ ions is the resonantly enhanced multi-photon ionization $\text{Th}^+ \rightarrow \text{Th}^{2+}$. The latter is induced by the high peak intensities of the Ti:sapphire laser when a two-photon excitation of a highly excited state is obtained. This Th^+ ion loss mechanism by means of ionization $\text{Th}^+ \rightarrow \text{Th}^{2+}$ is also critical for future experiments with the radioactive isotope ^{229}Th . As explained above, the amount of substance will be limited and therefore we have to minimize the unwanted loss, such as this ionization. For that reason, during the scanning of the electronic level structure of $^{229}\text{Th}^+$ in the energy range of the $^{229\text{m}}\text{Th}$ isomeric state, special care should be taken to use low peak power for the second excitation step when the laser is near resonant with an upper state.

Finally, we also envision another method for loading our linear Paul trap in order to increase the ion production and the trapping efficiency of Th^+ ions. For future investigations with the radioactive isotope ^{229}Th we are developing a new trap, which will have the advantage of allowing degassing of the trap electrodes by electron beam heating. Also an additional production of $^{229}\text{Th}^+$ ions via a heated filament will be done. We found the motivation in this approach from previous experiments with trapped $^{229}\text{Th}^+$ ions in Refs. [57,58]. With an improved ion production efficiency and with the know-how described above, we are ready to search for a direct observation of the $^{229\text{g}}\text{Th} \leftrightarrow ^{229\text{m}}\text{Th}$ transition in the ^{229}Th nucleus and figure out the mystery of the lowest energy forbidden optical transition of a nuclear state known so far.

Acknowledgment

Growing in a small and humble town in Costa Rica one of my biggest childhood dreams was to be a scientist and study in Germany. Till this day I still remember the anxiety I felt after asking Ekkehard for his support as my future advisor. At that time I was not fully aware of the project ahead of me, its challenges as well as its achievements. I am very grateful to Ekkehard for opening me the doors to his project, as well as for believing in me. Thank you for making this experience possible, for being always available, a good listener, and being open minded regarding my ideas. Your presence as my advisor exceeded my expectations and from the inside of my heart I will always have a place for everything that happened during this time.

I would like to thank my Russian battle comrade, Maxim, who spent most of his time with me in the lab, taught me many of his tricks and turned out to be a real friend. I will always be grateful to you. This thesis contains many of the great ideas he had in the pursuit of the answers for the questions that arose during our investigation. Hopefully someday we will find an answer to all the after-lunch non-scientific discussions...and maybe even the perfect job.

I want to show my gratitude to Kai, who collaborated with me at the beginning of this investigation, and to Nils, who participated at the end of the work reported here. Without your help this work would not be possible. Also discussions and different ideas from Christian were very appreciated. I am also grateful to Dieter, Thomas, Sven, Burghard, Andreas and Mr. Kremling, who contributed to the development of this project.

Finally, to the person who was with me during this time, listening, supporting and giving me all kind of advices, I will be eternally grateful. This adventure would have never been this way without you. I do not have the right words to express what I feel for you, but I do not worry because we certainly are going to have more adventures around this world listening to each other. For giving me what I needed at the right time, to my wife: Tatiana.

Bibliography

- [1] M. Skłodowska-Curie. “Rayons émis par les composés de l’uranium et du thorium. Présenté par M. Lippmann. Séance du Mardi 12 Avril 1898”. Paris, Gauthier-Villars, 1898. In: Comptes Rendus Hebdomadaires des Séances de L’Academie des Sciences, volume 126, No 15.
- [2] J. J. Thomson. “Cathode Rays”, *The Electrician* 39, 104 (1897).
- [3] H. Geiger, E. Marsden. “On a Diffuse Reflection of the α -Particles”, *Proceedings of the Royal Society, Series A* 82: 495500 (1909).
- [4] E. Rutherford. “The Scattering of α and β Particles by Matter and the Structure of the Atom”. *Philosophical Magazine, Series 6* **21**: 669688 (1911).
- [5] L. A. Kroger, C. W. Reich, *Nuclear Physics A* **259**, 29 (1976).
- [6] B. R. Beck, J. A. Becker, P. Beiersdorfer, G. V. Brown, K. J. Moody, J. B. Wilhelmy, F. S. Porter, C. A. Kilbourne, R. L. Kelley, *Phys. Rev. Lett.* **98**, 14250 (2007).
- [7] B. R. Beck, J. A. Becker, P. Beiersdorfer, G. V. Brown, K. J. Moody, C. Y. Wu, J. B. Wilhelmy, F. S. Porter, C. A. Kilbourne, R. L. Kelley, Lawrence Livermore National Laboratory, Internal Report **LLNL-PROC-415170**, 2009.
- [8] E. Peik, Chr. Tamm, *Europhys. Lett.* **61**, 181 (2003).
- [9] C. J. Campbell, A. G. Radnaev, A. Kuzmich, *Phys. Rev. Lett.* **106**, 223001 (2011).
- [10] E. Peik, K. Zimmermann, M. Okhapkin, Chr. Tamm, in *Proceedings of the 7th Symposium on Frequency Standards and Metrology, 5-11 October 2008* (World Scientific Publishing Co., Singapore, 2009).
- [11] W. G. Rellergert, D. DeMille, R. R. Greco, M. P. Hehlen, J. R. Torgerson, Eric R. Hudson, *Phys. Rev. Lett.* **104**, 200802 (2010).
- [12] G. A. Kazakov, A. N. Litvinov, V. I. Romanenko, L. P. Yatsenko, A. V. Romanenko, M. Schreitl, G. Winkler, T. Schumm, arXiv 1204:3268.

- [13] S. G. Porsev, V. V. Flambaum, E. Peik, Chr. Tamm, Phys. Rev. Lett. **105**, 182501 (2010).
- [14] C. W. Reich, R. G. Helmer, Phys. Rev. Lett. **64**, 271 (1990).
- [15] D. G. Burke, P. E. Garrett, T. Qu, R. A. Naumann, Phys. Rev. C **42**, R499 (1990).
- [16] R. G. Helmer, C. W. Reich, Phys. Rev. C **49**, 1845 (1994).
- [17] K. Gulda, W. Kurcewicz, A. J. Aas, M.J.G. Borge, D.G. Burkard, B. Fogelberg, I. S. Grant, E. Hagebø, N. Kaffrell, J. Kvasil, G. Løvhøiden, H. Mach, A. Macková, T. Martinez, G. Nymank, B. Rubio, J. L. Tainj, O. Tengblad, T. F. Thorsteinsen, ISOLDE collaboration, Nuclear Physics A **703**, 45-69 (2002).
- [18] V. Barci, G. Ardisson, G. Barci-Funel, B. Weiss, O. El Samad, R. K. Sheline, Phys. Rev. C **68**, 034329 (2003).
- [19] E. Ruchowska, W. A. Płóciennik, and J. Żylicz, H. Mach, J. Kvasil, A. Algora, N. Amzal, T. Bäck, M. G. Borge, R. Boutami, P. A. Butler, J. Cederkäll, B. Cederwall, B. Fogelberg, L. M. Fraile, H. O. U. Fynbo, E. Hagebø, P. Hoff, H. Gausemel, A. Jungclaus, R. Kaczarowski, A. Kerek, W. Kurcewicz, K. Lagergren, E. Nacher, B. Rubio, A. Syntfeld, O. Tengblad, A. A. Wasilewski, L. Weissman, Phys. Rev. C **73**, 044326 (2006).
- [20] Y. Izawa, C. Yamanaka, Phys. Lett. B **88**, 59 (1979).
- [21] B. R. Mottelson, S. G. Nilsson, Kongelige Danske Videnskabernes Selskab, Matematisk-fysiske Meddelelser, **29**(16), 1955.
- [22] A. M. Dykhne, E. V. Tkalya, JETP Letters **67**, 251 (1998).
- [23] C. J. Campbell, A. G. Radnaev, A. Kuzmich, V. A. Dzuba, V. V. Flambaum, A. Derevianko, Phys. Rev. Lett. **108**, 120802 (2012).
- [24] S. Matinyan, Phys. Rep. **298**, 199 (1998).
- [25] E. V. Tkalya, Phys. Usp. **46**, 315 (2003).
- [26] G. M. Irwin, K. H. Kim, Phys. Rev. Lett. **79**, 990 (1997).
- [27] D. S. Richardson, D. M. Benton, D. E. Evans, J. A. R. Griffith, G. Tungate, Phys. Rev. Lett. **80**, 3206 (1998).
- [28] S. B. Utter, P. Beiersdorfer, A. Barnes, R. W. Lougheed, J. R. Crespo López-Urrutia, J. A. Becker, M. S. Weiss, Phys. Rev. Lett. **82**, 505 (1999).

-
- [29] R. W. Shaw, J. P. Young, S. P. Cooper, O. F. Webb, *Phys. Rev. Lett.* **82**, 1109 (1999).
- [30] V. F. Strizhov, E. V. Tkalya, *Soviet Physics JETP*, **72**, 387 (1991).
- [31] E. V. Tkalya, A. N. Zherikhin, V. I. Zhudov. *Phys. Rev. C*, **61**, 064308, (2000).
- [32] E. V. Tkalya, *JETP Lett.* **71**, 311 (2000).
- [33] C. J. Campbell, A.V. Steele, L. R. Churchill, M.V. DePalatis, D. E. Naylor, D. N. Matsukevich, A. Kuzmich, M. S. Chapman, *Phys. Rev. Lett.* **102**, 233004 (2009).
- [34] U. I. Safronova, W. R. Johnson, M. S. Safronova, *Phys. Rev. A* **74**, 042511 (2006).
- [35] V. N. Egorov, *Opt. Spektrosk.* **16**(4), 549-554 (1964).
- [36] S. Gerstenkorn, P. Luc, J. Verges, D. W. Englekemeir, J. E. Gindler and F. S. Tomkins, *J. Phys. (Paris)* **35**, 483 (1974).
- [37] C. E. Bemis, F. K. McGowan, J. L. C. Ford Jr, W. T. Milner, R. L. Robinson, P. H. Stelson, G. A. Leander, C. W. Reich, *Phys. Scr.* **38**, 657 (1988).
- [38] S. Raeder, V. Sonnenschein, T. Gottwald, I. D. Moore, M. Reponen, S. Rothe, N. Trautmann, K. Wendt, *J. Phys. B: At. Mol. Opt. Phys.* **44** 165005 (2011).
- [39] V. Sonnenschein, S. Raeder, A. Hakimi, I. D. Moore, K. Wendt, *J. Phys. B: At. Mol. Opt. Phys.* **45** 165005 (2012).
- [40] V. Sonnenschein, I. D. Moore, S. Raeder, A. Hakimi, A. Popov, K. Wendt, *The European Physical Journal A* **48**, 52 (2012).
- [41] G. Musiol, J. Ranft, R. Reif, D. Seeliger. *Kern- und Elementarteilchenphysik*. VCH Verlagsgesellschaft, Weinheim, 1988.
- [42] P. F. A. Klinkenberg, *Physica* **16**, 618 (1950).
- [43] J. F. Wyart, V. Kaufman, *Physica Scripta*, **24**, 941-952 (1981).
- [44] S. G. Porsev, V. V. Flambaum, *Phys. Rev. A* **81**, 032504 (2010).
- [45] P. F. A. Klinkenberg, *Physica C*, **151**, 552 (1988).
- [46] P. F. A. Klinkenberg, R. J. Lang, *Physica* **15**, 774 (1949).

- [47] J. Blaise, J. F. Wyart, in *International Tables of Selected Constants*, Vol. 20, 1 (Centre National de la Recherche Scientifique, Paris, 1992), [<http://www.lac.u-psud.fr/Database/Tab-energy/Thorium/Th-tables/Th2o.html>].
- [48] R. Zalubas, C. H. Corliss, *Journal of research of the National Bureau of Standards. Section A. Physics and chemistry* **78A**, 163 (1974), [<http://nistdigitalarchives.contentdm.oclc.org/cdm/ref/collection/p13011coll6/id/63425>].
- [49] B. A. Palmer, R. Engleman, Jr., *Atlas of the Thorium Spectrum* (Los Alamos National Laboratory, Los Alamos, 1983).
- [50] H. Nilsson, Z. G. Zhang, H. Lundberg, S. Johansson, B. Nordström, *Astron. Astrophys.* **382**, 368 (2002).
- [51] V. A. Dzuba, V. V. Flambaum, *Phys. Rev. Lett.* **104**, 213002 (2010).
- [52] V. A. Krutov and V. N. Fomenko, *Ann. Phys. (Leipzig)* **476**, 291 (1968).
- [53] M. Morita, *Prog. Theor. Phys.* **49**, 1574 (1973).
- [54] D. Kekez, A. Ljubičić, K. Pisk, B. A. Logan, *Phys. Rev. Lett.* **55**, 1366-1368 (1985).
- [55] S. Kishimoto, Y. Yoda, M. Seto, Y. Kobayashi, S. Kitao, R. Haruki, T. Kawauchi, K. Fukutani, T. Okano, *Phys. Rev. Lett.* **85**, 1831 (2000).
- [56] S. G. Porsev, V. V. Flambaum, *Phys. Rev. A* **81**, 042516 (2010).
- [57] W. Kälber, J. Rink, K. Bekk, W. Faubel, S. Göring, G. Meisel, H. Rebel, R. C. Thompson, *Zeitschrift für Physik A: Atomic Nuclei* **334**, 103 (1989).
- [58] W. Kälber, G. Meisel, J. Rink, R. C. Thompson, *J. Mod. Opt.* **39**, 335 (1992).
- [59] H. G. Dehmelt. *IEEE Transactions on Instrumentation and Measurement*, 31, 8387 (1982).
- [60] J. C. Bergquist, W. M. Itano, D. J. Wineland, *Phys. Rev. A* **36**, 428 (1987).
- [61] A. A. Madej, J. E. Bernard. *Frequency measurement and control - advanced techniques and future trends*. Springer, Berlin, 2001.
- [62] O. A. Herrera-Sancho, M. V. Okhapkin, K. Zimmermann, Chr. Tamm, E. Peik, A. V. Taichenachev, V. I. Yudin, P. Głowacki, *Phys. Rev. A* **85**, 033402 (2012).

-
- [63] V. V. Flambaum, Phys. Rev. Lett. **97**, 092502 (2006).
- [64] X. T. He and Z. Z. Ren, Nucl. Phys. **A806**, 117 (2008).
- [65] V. V. Flambaum, N. Auerbach, and V. F. Dmitriev, Europhys. Lett. **85**, 50005 (2009).
- [66] E. V. Tkalya, Phys. Rev. Lett. **106**, 162501 (2011).
- [67] A. Cingöz, D. C. Yost, T. K. Allison, A. Ruehl, M. E. Fermann, I. Hartl, J. Ye, Nature **482**, 68-71 (2012).
- [68] D. R. Denison, Journal of Vacuum Science and Technology **8**, 266–269 (1971).
- [69] W. Paul, Rev. Mod. Phys. **62**, 531 (1990).
- [70] K. Zimmermann. *Experiments Towards Optical Nuclear Spectroscopy With Thorium-229*. PhD thesis, Mathematik und Physik, Gottfried Wilhelm Leibniz Universität Hannover, Hannover, Germany, 2010.
- [71] B. N. Chichkov, C. Momma, S. Nolte, F. von Alvensleben, A. Tünnermann, Appl. Phys. A **63**, 109 (1996).
- [72] K. Zimmermann, M. V. Okhapkin, O. A. Herrera-Sancho, E. Peik, Appl. Phys. B **107**, 883-889 (2012).
- [73] Mark B. Morris, Thomas J. McIlrath, James J. Snyder, Appl. Opt. **23** (21), 3862 (1984).
- [74] H. Simonsen, T. Worm, P. Jessen, and O. Poulsen, Phys. Scr. **38**, 370 (1998).
- [75] F. G. Major and H. G. Dehmelt, Phys. Rev. **170**, 91–107 (1968).
- [76] Y. Moriwaki, M. Tachikawa, Y. Maeno, and T. Shimizu, Japanese Journal of Applied Physics Part 2-Letters, 31(11B):L1640–L1643, (1992).
- [77] A. A. Madej, J. D. Sankey, Phys. Rev. A **41**, 2621 (1990).
- [78] M. Knoop, M. Vedel, F. Vedel, Phys. Rev. A **58**, 264 (1998).
- [79] P. Langevin, Annales De Chimie Et De Physique **28**, 433 (1903).
- [80] J. E. Bjorkholm, P. F. Liao, Phys. Rev. Lett. **33**, 128 (1974).
- [81] J. E. Bjorkholm, P. F. Liao, Phys. Rev. A **14**, 751 (1976).
- [82] V. S. Letokhov, Laser Photoionization Spectroscopy (Academic, London, 1987).

-
- [83] B. Witzel, C. J. G. J. Uiterwaal, H. Schröder, D. Charalambidis, K. L. Kompa, *Phys. Rev. A* **58**, 3836 (1998).
- [84] J. Zhou, H. B. Schlegel, *J. Phys. Chem. A* **114**, 8613-8617 (2010).
- [85] L. R. Churchill, M. V. DePalatis, M. S. Chapman, *Phys. Rev. A* **83**, 012710 (2011).
- [86] J. K. Gibson, R. G. Haire, J. Marçalo, M. Santos, J. P. Leal, A. Pires de Matos, R. Tyagi, M. K. Mrozik, R. M. Pitzer, B. E. Bursten, *Eur. Phys. J. D* **45**, 133138 (2007).
- [87] J. K. Gibson, J. Marçalo, *J. Coord. Chem. Rev.* **250**, 776783, (2006).
- [88] H. H. Cornehl, R. Wesendrup, M. Diefenbach, H. Schwarz, *Chem. Eur. J.* **3**, 1083-1090, (1997).
- [89] J. K. Gibson, R. G. Haire, *Radiochim. Acta* **91**, 441448, (2003).
- [90] H. H. Cornehl, C. Heinemann, D. Schroder, H. Schwarz, *Organometallics* **14**, 992-999 (1995).
- [91] R. Johnsen, F. R. Castell, and M. A. Biondi, *J. Chem. Phys.* **61**, 5404 (1974).
- [92] J. Marçalo, J. P. Leal, A. P. de Matos, *Int. J. Mass Spectrom.* **157**, 265-274 (1996).
- [93] J. K. Gibson, R. G. Haire, M. Santos, J. Marçalo, A. Pires de Matos, *J. Chem. Phys. A* **109**, 2768 (2005).

Scientific publications

- O. A. Herrera-Sancho, M. V. Okhapkin, K. Zimmermann, Chr. Tamm, E. Peik, A. V. Taichenachev, V. I. Yudin, P. Głowacki, Two-photon laser excitation of trapped $^{232}\text{Th}^+$ ions via the 402 nm resonance line. *Phys. Rev. A* **85**, 033402 (2012)
- K. Zimmermann, M. V. Okhapkin, O. A. Herrera-Sancho, E. Peik, Laser ablation loading of a radiofrequency ion trap. *Appl. Phys. B* **107**, 883-889 (2012)
- O. A. Herrera-Sancho, D. Castro-González, J. A. Araya-Pochet, W. E. Vargas-Castro, Ultra thin films of gadolinium deposited by evaporation in ultra high vacuum conditions: Composition, growth and morphology. *Applied Surface Science* **257**, 3510 (2011)

Curriculum Vitae

Name: Óscar-Andrey Herrera-Sancho
Date of birth: 31st August 1979
Place of birth: San José, Costa Rica
Nationality: Costa Rican

- 1999 – 2003 University of Costa Rica, San José, Costa Rica
–B. Sc. in Physics
- 2004 – 2008 University of Costa Rica, Center for Research on Materials
Science and Engineering, San José, Costa Rica
–M. Sc. in Physics
–Thesis: Ultra thin films of gadolinium deposited by evapo-
ration in ultra high vacuum conditions
- 2004 – 2006 University of Costa Rica, San José, Costa Rica
–Researcher and lecturer
- 2005 – 2007 National Metrology Institute of Costa Rica, San José, Costa
Rica
–Metrologist
–Head of the Physical Metrology Department
- 2008 – 2009 Costa Rican Institute of Technology, Cartago, Costa Rica
–Researcher and lecturer
- 2008 – Present Costa Rican Accreditation Entity, San José, Costa Rica
–Technical expert
- 2009 – Present Physikalisch-Technische Bundesanstalt, Braunschweig, Ger-
many
–Research assistant